CRANFIELD UNIVERSITY

Shixian Guo

# Kinematic Simulation and Structure Analysis of a Morphing Flap

SCHOOL OF ENGINEERING
MSc by research

MSc THESIS
Academic Year: 2012 - 2013

Supervisor: Dr S.Guo
December 2013

CRANFIELD UNIVERSITY

SCHOOL OF ENGINEERING
MSc by research

MSc THESIS

Academic Year 2012 - 2013

Shixian Guo

# Kinematic Simulation and Structure Analysis of a Morphing Flap

Supervisor: Dr S.Guo
December 2013

This thesis is submitted in partial fulfilment of the requirements for the degree of Master of Science

# ABSTRACT

This thesis presents a study on the design and analysis of a morphing flap structure integrated with actuation mechanism for potential application to large aircraft. Unlike the conventional rigid flap mounted on the wing trailing edge, the morphing flap is designed as a unitized structural system integrated with three primary components: the upper and lower flexible skins reinforced by stringers, an eccentric beam actuation mechanism (EBAM) with discs fixed on it, and the connection of the discs with the stringers. Based on the EBAM concept proposed by Dr Guo in previous research [1], the current study has been focused on the EBAM design and optimization, kinematic simulation and structural modelling of the morphing flap.

Although a lot of efforts have been made to develop the morphing flap in previous research, it is lack of detailed design of the disc-skin linkage and clear view on the mechanism optimization in relation to the shape requirement. The main objective of this research is to meet the morphing shape requirements and calculate the actuation torque for a specified morphing flap. Firstly effort was made to design and optimize the disc shape and locations in the EBAM for the best matching of the specified morphing shape with minimum actuation torque demand. It is found that minimum three discs are required and their locations have little effect on the actuation torque. Secondly attention was focused on designs of the disc and a C-linkage with the stringers. To ensure that the C-linkage works in practice, a twisted stringer flange design was proposed. Thirdly the actuation mechanism was integrated with the stiffened skin to play the role of an active rib in the flap structure. Based on the design, FE modelling and analysis of the morphing flap structure was carried out. The behaviour of the morphing flap under the internal actuation and external aerodynamic load was applied for stress analysis and detailed design of the structures. Finally the kinematics of the integrated morphing flap was simulated by using CATIA to demonstrate the feasibility and the effectiveness of the improved design.

Keywords:

Morphing flap; Eccentric beam actuation mechanism, twisted disc, optimization, simulation

# ACKNOWLEDGEMENTS

The author wishes to thank his supervisor Dr.S Guo for his kindly technical advice, guidance, time and consideration.

He thanks also Ying Liu and Juita Saleh, whose help were always appreciated.

# TABLE OF CONTENTS

# LIST OF FIGURES

# LIST OF TABLES

# LIST OF EQUATIONS

# LIST OF ABBREVIATIONS

| | |
|---|---|
| FE | Finite Element |
| EBAM | Eccentric Beam Actuation Mechanism |
| FP7 | Seventh Framework Programme of the EC |
| OEW | Operating Empty Weight |
| MTOW | Maximum Take Off Weight |
| SAW | seamless aeroelastic wing |
| UAV | Unmanned Air Vehicle |
| $W_{vep}$ | Vertical extreme point |
| $W_{fup}$ | Fixed point on upper skin |
| $W_{flw}$ | Fixed point on lower skin |
| ° | Degree |
| $F_{ty}$ | Yield strength in Tension, |
| $C_p$ | Pressure coefficient |
| DOC | Direct Operation Costs |
| SADE | Smart High Lift Devices for Next Generation Wings |
| DARPA | The Defence Advanced Research Projects Agency |
| STOL | short take-off and landing |

# 1 Introduction

## 1.1 General

In this modern age, airline companies have to balance the soaring fuel price while operating satisfactorily in a very competitive market. Therefore, they are always looking for improvements from the aircraft manufacturers. Not only do they want to reduce the Direct Operation Costs (DOC) but also improve the operational flexibility of their fleets. In the past 50 years, however, only limited changes have been made to the wing geometry. Most of the current research is concentrated on conventional wing design but not so much work is focused on the morphing technology. There is thus room for investigation into the design and efficiency of the morphing structure. But due to the low level of technologies available in the past, morphing structure are now only used in small UAVs, and are unsuitable for commercial aircraft. Because for small vehicles, it is relatively easy to obtain a change in shape due to the reduced dimension of the wings, because a small structure requires low energy to perform morphing. New morphing configuration will radically change the way we design wings. After that pilots will be able to control, and manage the position of morphing structure at different flight conditions (cruise, take-off and landing). Morphing technology will improve the performance of the aircraft, as pilots will be able to reduce the drag and noise during the flight, hence reduce the fuel consumption.

It has been found that some work [1,2,3,4] has been done in the past regarding the study of morphing flap mechanism design but less attention has been given to kinematic simulation, optimization of mechanism for shape requirements and the actuation system.

## 1.2 Research Background

The feasibility of morphing wing concept has been demonstrated in the technology development for small aircraft. In a research project supervised by Dr.Guo funded by EPSRC and UK aerospace industry, a seamless aeroelastic wing [1] and a rudderless morphing fin [2] suitable for UAV have been developed. The design concept has been extended to the development of smart high lift devices for next generation wings in an EU FP7 project SADE. A morphing flap trailing edge has been designed and an experimental model has been built in previous research projects [3].

The current research builds on work done by other people. But none of them studied the kinematic simulation and optimization of the actuation system in particular. Lemoine [4] developed a design methodology applied to morphing flaps integrated with the eccentric beam actuation system but not much work was done on the optimal position of the disc, detail structural connections and kinematic simulation. Precedent work by Di Matteo, Natalia [5] on the optimization of a morphing flap structure developed a concept to optimize the shape, but not many details were given and it is not a mature technique so this concept still needs to be validated.

## 1.3 Research Objectives

The kinematics of the integrated morphing flap will be demonstrated by numerical simulation using the 'Digital Mock-Up kinematic' module in CATIA. Based on the model, the analysis of the structural behaviour of the morphing flap under the internal actuation and external dynamic load will be carried out to demonstrate the feasibility and the effectiveness of the improved design. Detailed research tasks for this project are given below:

1. Design of curve beam, twisted discs and twisted stringers to meet the requirement of the EBAM. Design the connections between flexible skins and the eccentric beam.

2. Optimize the discs positions to meet the shape requirement of the morphing flap and calculate the torque needed for actuation system.

3. After the design work of the eccentric beam system, structure model will be built, and then working with CATIA, connections between the moving parts will be defined and simulation integrated with actuation mechanism will be carried out.

4. Given the structural model, material property, boundary conditions and aerodynamic load, finite element analysis will be conducted.

## 1.4 Research Method

### 1.4.1 Review of Existing Mechanisms and Methodologies

The research starts with an extensive review of conventional high lift devices and existing trailing edge morphing design and design of other morphing structure. This includes the different design approaches and the different technologies available. There is also a short description of the advantages and disadvantages of each high lift device and its application.

### 1.4.2 Develop a Design Methodology

The methodology for the design of morphing flap is to use an eccentric beam actuation mechanism. It covers concept design, geometrical design, structural analysis and mechanism design. For this methodology, a powerful design and analysis tool CATIA V5 has been used to shorten the design and analysis time. Design of eccentric beam would be calculated by applying tapered distributed pressure to create continuous deflection, and the curve will be drawn by CATIA. The twisted discs will be built by a step by step procedure. Optimization of the discs position will be carried out by beam bending theory, applying different number of loads at different positions to meet the shape requirement of the morphing flap and calculate the torque needed for actuation system. Design the connection between flexible skins and the eccentric beam is mostly through creative idea about the mechanism and by kinematic simulation. After the design work of the eccentric beam system, structure model will be built, and then working with CATIA, connections between moving parts will be defined and simulation integrated with actuation mechanism will be carried out. Finally, given the structural model, material property, boundary conditions and aerodynamic loads, work with Patran-Nastran software, the static analysis will be conducted to validate the design.

# 2 Literature Review

This chapter presents a review of the current technologies and future trends in aircraft design and provides an introduction to the study of morphing structures. At the beginning, the current status of the aviation industry is stated and ambitious targets set for the next few years are presented. The high lift devices mounted on the conventional modern wings are presented in Section 2.2. In Section 2.3, morphing technologies are introduced as a very promising solution for the development of the next generation aircraft structures. Finally, Eccentric beam actuation mechanism design concept is illustrated.

## 2.1 Historical Developments and Future Trends in Aircraft Design

As shown in [6], air travel is continuing to experience the fastest growth among all kinds of transport. Increasing total fuel consumption and the potential impacts of aircraft engine emissions on the global atmosphere (polluting emissions, noise…) have motivated the industry, scientific community, and international governments to look for solutions to reduce emissions. Airlines and aircraft manufacturing companies are pushed to deliver aircraft characterised by high performance, high efficiency, low costs, and at the same time, low impact on the environment, in order to reduce the fuel consumption and to achieve low production and operative costs. The Vision 2020 report [6], by the European Commission for Research, specifies stringent requirements, which include a consistent reduction of carbon dioxide and nitrogen oxides emissions, as well as of the noise caused by the aircraft, to be achieved in the next few years.

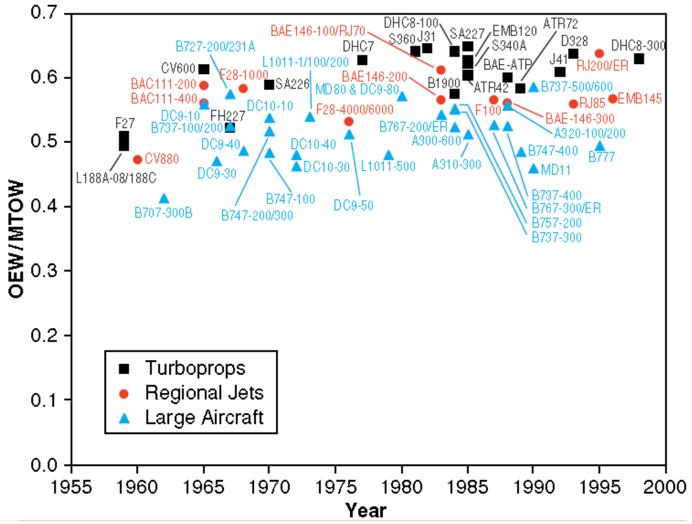


**Figure 2-1 Historical trends in structural efficiency [6]**

There has been a continuous increase in aircraft performance and capabilities over past decades [6]. Despite the gradual and continuous improvements, however, modern airliners are, in general, still very similar to the older aircraft decades ago. The ratio between the Operating Empty Weight (OEW) and the Maximum Take Off Weight (MTOW) is taken as an index of the structural efficiency of the aircraft, Babikian et al. in [7] shows the graph in Figure 2-1. He points out this parameter has not changed much over the past 50 years. (The reference from 2000 up to date is not available in published references.) Moreover, after a lot of research work, the conventional design concepts and methodologies are almost fully optimised and have reached their maximum potential. For these reasons, the current technologies cannot meet the ambitious high performances and the stringent requirements set for the next few decades.

An innovative and very promising solution is morphing technologies. Morphing can be defined as an aircraft with the capability to achieve a continuous shape change upon a specific actuation. The employment of morphing technology could allow the wing to vary its shape smoothly, to achieve near-optimal lift and drag profiles throughout different phases of the flight. The main advantages of this would be reduced fuel consumption, a higher aerodynamic efficiency and noise reduction. Extra benefits come from morphing could be an improvement of aircraft control during flight and a better air load distribution over the wing.

## 2.2 High Lift Devices

High-lift devices are moving surfaces intended to increase lift during certain flight conditions. They include devices, for example, flaps and slats, as well as less common features such as leading edge extensions and blown flaps. Aircraft designs include compromises intended to maximize performance for a particular role. One of the most fundamental of these is the size of the wing. In fact, a bigger wing planform will generate more lift and reduce take-off and landing distance, but also generate more drag during cruising flight and hence causes more fuel consumption. High-lift devices are employed to trade off the different requirements in various flight phases, allowing the purpose of an efficient cruise, and lift increasing during take-off and landing. They improve the aircraft flying capabilities so much that they have become indispensable component of aircraft and routinely mounted on almost any modern air vehicle.

Leading and trailing edge devices both require a change of the original shape of the wing. The Increase of aircraft cruise speed and innovative powerful engine have changed development of high lift devices. The original basic high lift designs have been developed into complex geometries in order to keep up with the demanding requirement for high performance aircraft.

### 2.2.1 Traditional High Lift Devices for the Leading Edge

**Fixed Slot**

The fixed slot (Figure 2-2) has been successfully applied on air vehicles with low cruise speeds and short take-off and landing (STOL). However, the high drag generated by the device, makes it unacceptable for commercial subsonic aircrafts.

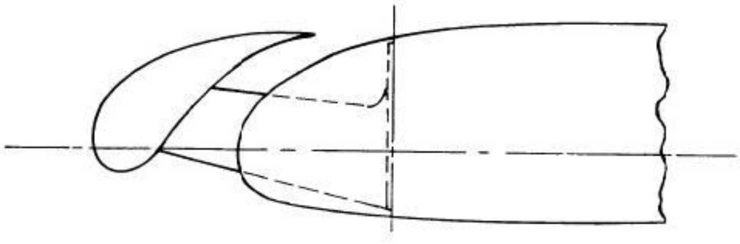

**Figure 2-2  Fixed slot** [8]

### Hinged leading edge (droop nose)

The droop nose is employed by rotating the leading edge structure around a hinge positioned close to the front spar.  This mechanism cannot be found on a commercial subsonic aircraft, but it is proposed for future supersonic fighter airplanes [8].  The main disadvantage of the droop nose is that the radiuses of curvature on the upper wing surface is too tight and trigger flow separation, which make it unacceptable for a commercial aircraft.  However it is not a problem for a supersonic airplane, where a much higher leading edge sweep angle generate a stable vortex on the upper surface, which provides lift, and eliminates the negative effects of flow separation.

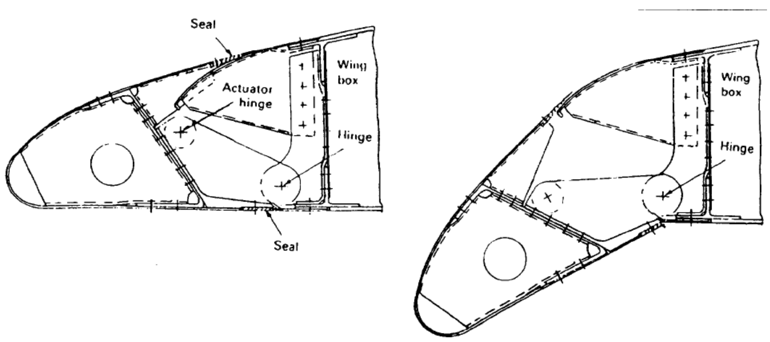


**Figure 2-3  Hinged leading edge** [8]

### Simple Krueger Flap

The simple Krueger flap consists of a panel hinged on the lower side of the wing leading edge, shown in Figure 2-4.  This panel can rigidly rotate downward and forward for up to an angle of 60° to 80°.  It offers adequate high-lift performance for inboard wing section, however, its drawback lies in its inability to adapt to varying angles of attack.  This device is one of the simplest leading edge devices used on modern commercial aircraft.

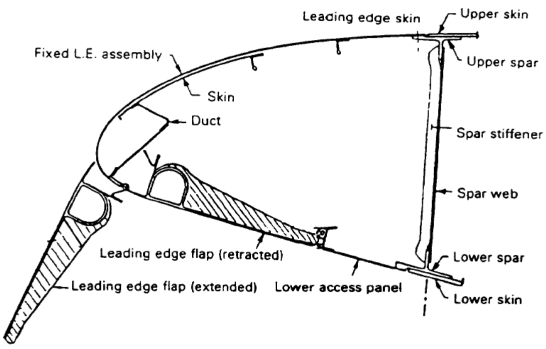


**Figure 2-4  Simple Krueger Flap** [8]

### Folding, bull-nose (rigid) Krueger

The folding Krueger flap is a modification of the simple Krueger flap by adding a folding bull nose.  The nose, having a D-shaped cross section, connected with a slave linkage to deploy the bull nose as the main Krueger panel deploys.  Due to the rounded bull nose, the bull-nose changes the flow on the upper surface, hence improves the performance of the simple Krueger flap to a wider range of angles of attack.

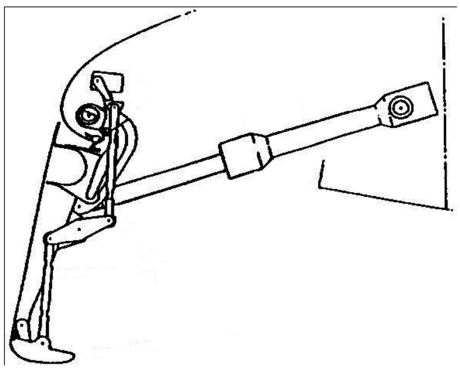

**Figure 2-5  Boeing 727 folding, bull-nose Krueger** [8]

## 2.2.2 Traditional High Lift Devices for the Trailing Edge

The flaps are usually mounted on the trailing edge of the wing.  During take-off, the use of flaps reduces the runway distance and the climb rate required.

During landing, when the flaps are typically fully extended, the additional drag generated contributes to a shorter landing.

### Split Flap

At the wing trailing edge, part of the lower surface was hinged to the main structure and was able to rotate downwards, while the upper surface remained still. The split flap was used on military airplanes in earlier days as a speed brake, able to generate drag without losing lift. Since it does not allow significant lift increase, the split flap is not found on any modern airliner.

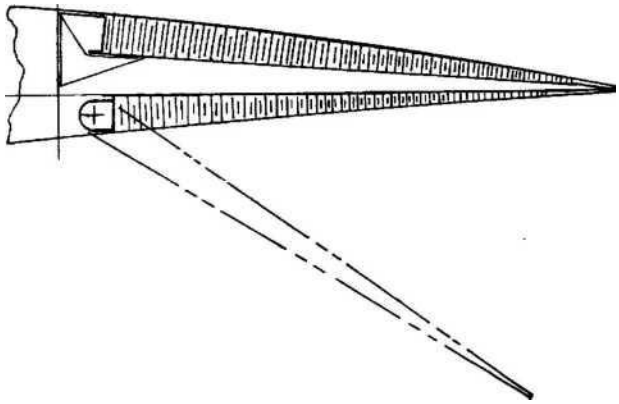

**Figure 2-6 Split Flap** [8]

### Plain Flap

The plain flap, with a rounded leading edge, can deploy by downward rotation without open a slot. It can be deflected up to a maximum of about 20°, beyond this, flow separation on the upper surface would occur, hence reducing its capability to increase lift. Plain flaps are planned for a future supersonic transport airplane.

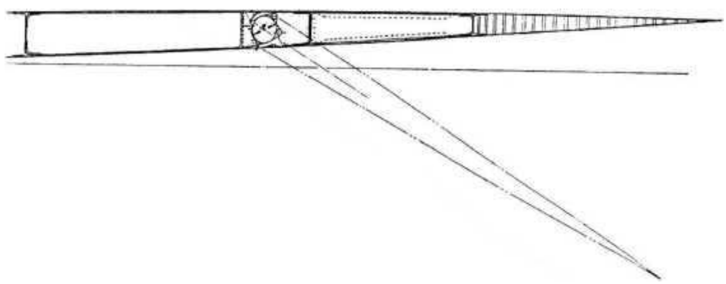

**Figure 2-7 Plain Flap** [8]

### Simple Slotted Flap

In this design the flap is mounted on pivots below the lower wing surface and is able to deflect about 30° to 35°.  During the deployment, a gap between the flap and the wing is created and high pressure air from below the wing is forced over the flap, contributing to maintain the airflow attached to the flap.  The slotted flap generates a significant lift increase due to the high-speed air go through the leading edge of the flap, which increases the velocity of the air around the aerofoil.  The principle can be extended to have multiple slots to further increase the lift.

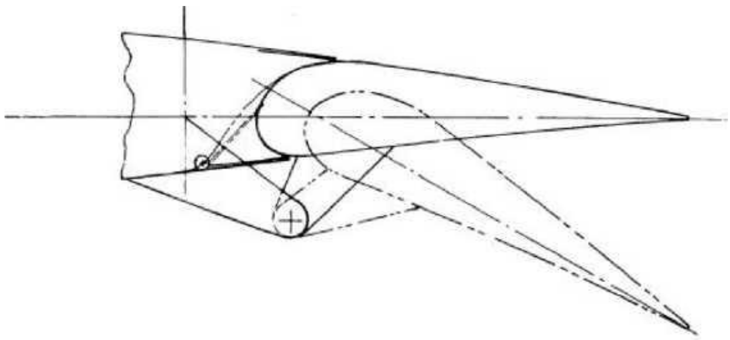

**Figure 2-8  Simple slotted flap** [8]

### Single Slotted Fowler Flap

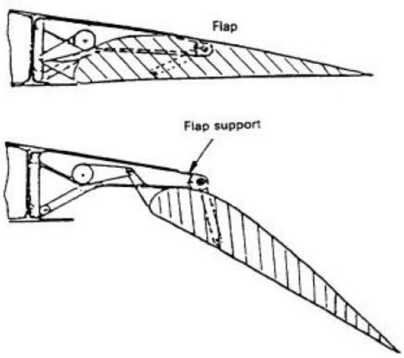


**Figure 2-9  Single Slotted Fowler Flap** [8]

This flap is similar to a simple slotted flap, with an important overlap between the flap and trailing edge panel from the main wing structure (as shown in Figure 2-9).  When the flap is in fully deployed position, the overlap is converted in a chord wise movement of the flap, called Fowler motion.  The additional benefit of a Fowler flap is represented by the increase in the wing planform because of the motion. Slotted Fowler Flaps are widely adopted on commercial airplane due to their good performance and medium level of complexity.

## 2.3 Morphing Concepts

The design of morphing structures has to satisfy several challenges due to the conflicting requirements. From a structural point of view, morphing wings should have high flexibility to enable shape changes, but also be stiff enough to withstand the aerodynamic loads. A careful analysis of the trade-off between these two is very important to ensure a good design. The requirement for both flexibility and strength is only one of the many possible issues that need to be deal with in the study of morphing technologies.

Nowadays, however, the concept "morphing wings" has been referred to more significant transformations of the wing shape. As shown in [9], a morphing wing can be defined as 'one which has the ability to either alters its shape in a continuous change along the chord or spar or to change its shape in a drastic manner'. The Defence Advanced Research Projects Agency (DARPA) has provided a technical definition of morphing referred to a wing as "the capability to perform either a 200% change in aspect ratio, a 50% change in wing area, a 5% change in wing twist or a 20° change in wing sweep" [9].

**Table 2-1 Possible classification of morphing concepts [5]**

| Type of Morphing | MAVs | UAVs | Commercial Aircraft |
|---|---|---|---|
| **Mechanical** | Wing folding | Telescopic spar | Variable sweep |
| | Tail folding | Wing folding | |
| **Elastic** | Piezoelectric | Piezoelectric | Eccentric beam |
| | SMAs | SMAs | Active flexible rib |
| | Wing twisting | Wing twisting | Rotating rib |
| | Stiffness tailoring | Stiffness tailoring | Vertebrae like rib |

As can be seen from Table 2-1, a summary of the main morphing concepts are summarized and a possible classification is offered. Two main characteristics of the concepts are considered: the type of morphing pursued, either mechanical or elastic deformation, and which kind of air vehicles the concept can be applied to. Many concepts are at a theoretical stage and their feasibility has not yet been demonstrated [10; 11]. Moreover, morphing techniques that have proved to be successful for small vehicles cannot be transferred directly to large aircrafts [5]. For small vehicles, it is relatively easy to obtain a change in shape due to the reduced dimension of the wings, because a small structure requires low energy to perform morphing. Other design can be used on large aircraft such as variable sweep, eccentric beam, active flexible rib, rotating rib and vertebrae like rib, which will be discussed later.

**Morphing by Mechanical Actuation**

Morphing through mechanical devices include wing sweep variation, variable span performed by using telescopic wings, wings with moving spars and wings or tail folding.

**Morphing by Elastic Deformation**

'Morphing by elastic deformation' is still achieved by using some moving components, but the change of shape is primarily due to considerable elastic deformation. Typically, the moving parts provide the actuation needed to deflect the structural components [5].

### 2.3.1 Morphing Leading Edge Devices

#### Dornier Droop Nose

The Dornier Company developed and patented a concept for the droop nose of a transport aircraft [12]. The internal actuation mechanism consists of three bars connected to both upper and lower skins and set into rotation by an arm connected to the front spar. Three bars are for transmitting the actuator force into flexible panels for shape adaptation and transmitting the aerodynamic loads into front spar. Some disadvantages are found regarding the requirements for a new leading edge high lift system with high quality surface:

- Rigid parts in between the flexible panels
- Guided deformation by the four-bar linkage system for achieving the desired droop angle.

A loss in surface quality probably is caused by a discrete connection of the skin panels, although the design of bars and of flexible skin panels is better for load introduction.  However the rigid parts and the linkage mechanism enforce the skin to a constraint kinematical movement which constricts the natural deformation behaviour.  This will lead to high stresses and strains at locations were the skin is attached to rigid parts and the kinematics.

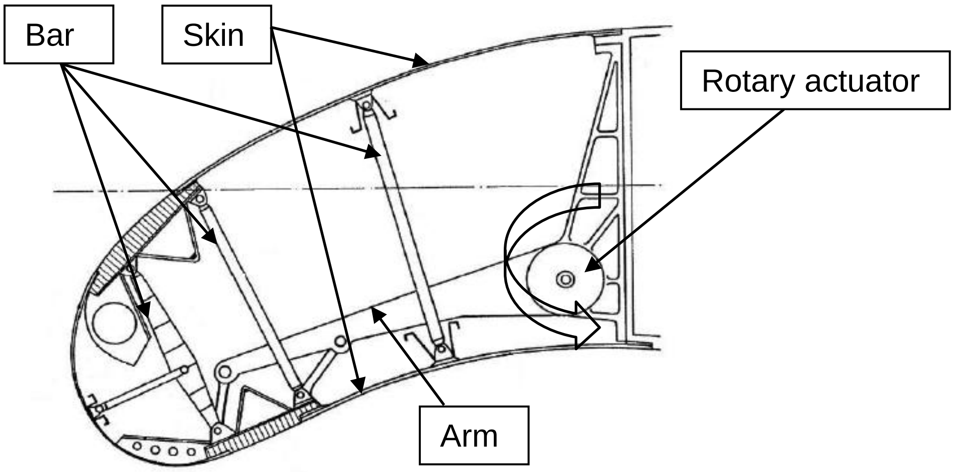


**Figure 2-10  the Dornier Droop Nose [12]**

### Boeing Discontinuous Droop Nose

In 1982, Boeing Company patented the design concept for a deflecting leading edge characterized by a discontinuous lower surface [12].  This concept was able to reduce the high strains in the leading edge skin associated with the deflection, but it reduced the structural stiffness of the nose and it required a complex internal kinematic mechanism to be actuated.

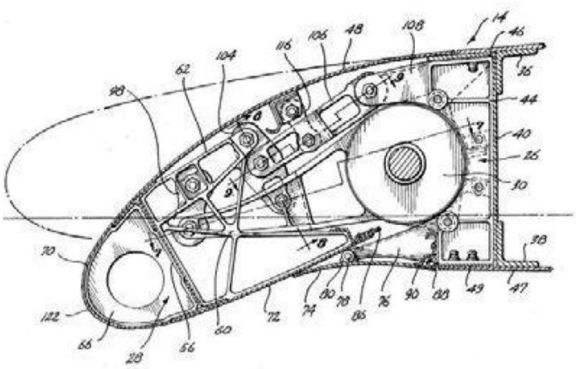

**Figure 2-11  Discontinuous Droop Nose proposed by Boeing [12]**

## 2.3.2 Morphing Trailing Edge Devices

As reported by Monner [13; 14], achieving a camber variation at the trailing edge maximizes the efficiency of the shape change from a structural and aerodynamic point of view [5]. In fact, in order to improve control efficiency, “distributed control surfaces should be used in the regions where the effect of the surfaces is likely to be reversed in the speed envelope considered” [15].

### Morphing by multi-hinge internal actuation

The first group belongs to the active flexible rib [14; 16], the rotating rib [17]. They are all characterised by moving elements capable of transferring the motion from one to another. In fact, these concepts allow large deflection and can be applied on large vehicles. However, a mass of moving parts reduces the reliability, increases the overall weight of the structure and also maintenance costs. Moreover, the skins have to be highly flexible to follow the deformation of the inner parts.

### Active flexible rib

The active flexible rib concept allows a smooth chord wise as well as span wise differential camber. As shown in Figure 2-12, the common fixed rib was replaced by movable separate plates connected to each other with revolute and prismatic joints. An actuator makes the rotation of the plates and the motion is then transferred gradually from one to another. Linear slide bearings ensure the connection between the rib segments with the upper and lower skins.

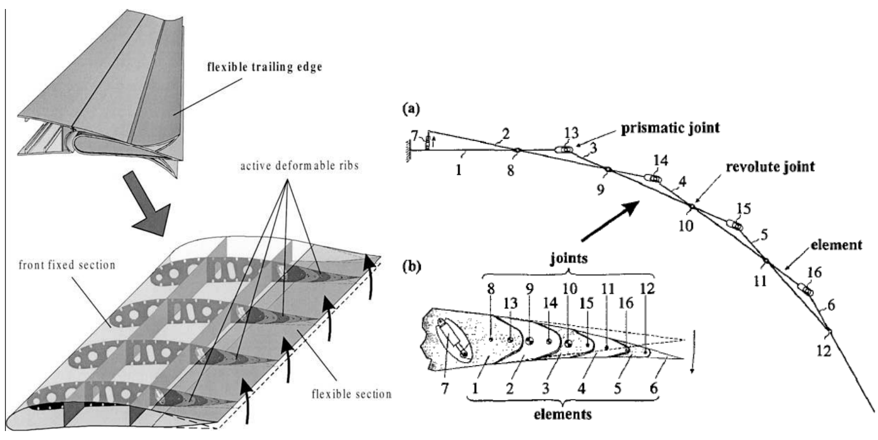


**Figure 2-12 Active flexible wing concept** [14; 16]

### Rotating rib

The concept is demonstrated in Figure 2-13: At the trailing edge, upper and lower skins are not rigidly connected and they are allowed to glide along a slide bearing. The movable rib can rotate around a hinge axis mounted on wing structure and slide along the upper and lower skins by rib contours. However, slow actuation velocity, little camber variation and frictions between rib and skins have limited its application.

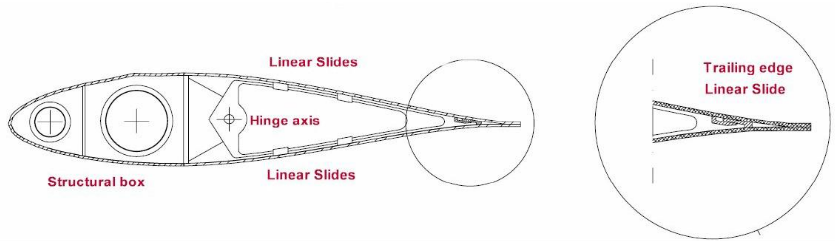


**Figure 2-13 the rotating rib concept** [17]

### Morphing by eccentric actuation

The eccentuator is a bent beam capable to transform a rotary input motion into a vertical and lateral translation at the output end. The beam is assembled to several rectangular webs which connected to the skins and when rotated it can push the skin up or down and deflect the skins to the desired shape, as shown by Bartley-Cho et al in [7; 18]. Figure 2-14 illustrates an example of trailing edge actuated by eccentuator and its operating principle.

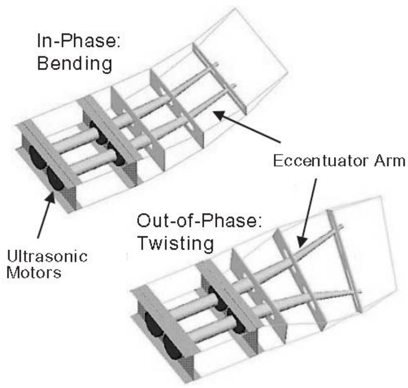


**Figure 2-14 Morphing by eccentric actuation** [18-20]

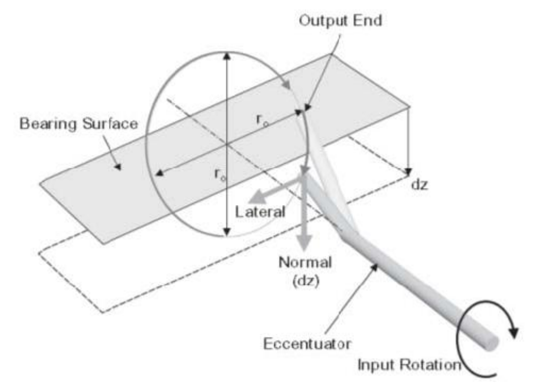


**Figure 2-15 Eccentric beam actuation**

Perera and Guo in [16] also use the eccentric beam concept to develop a small seamless aeroelastic wing (SAW) structure for a light weight UAV (Unmanned Air Vehicle).

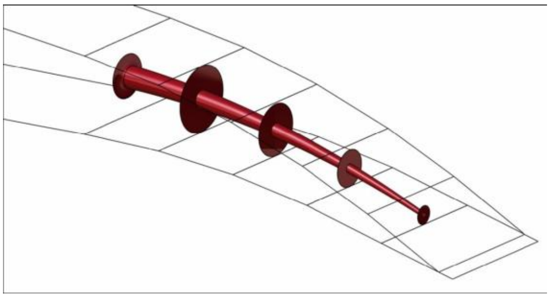

**Figure 2-16 Eccentric beam actuation mechanism** [16]

Due to eccentric beam actuation mechanism is relatively simple and reliable, with large load carry capability and low energy requirements, without too much friction and many parts, it is chosen for this study.

## 2.4 Eccentric Beam Design Concept

### 2.4.1 The Curved Beam

This design is kind of morphing by elastic deformation. The eccentric beam concept which consists of using a curved beam had already been proposed by a member of the SAW project [16].

The concept consists of a curved beam positioned horizontally inside the trailing edge of the SAW and rotated by a rotary actuator. Because it would be connected to both the upper and lower surfaces of the flap, its rotation would allow the corresponding morphing of the flap. Figure 2-17 shows what the curved beam looks like, and its position at 0° and 90° from both left side view and top view.

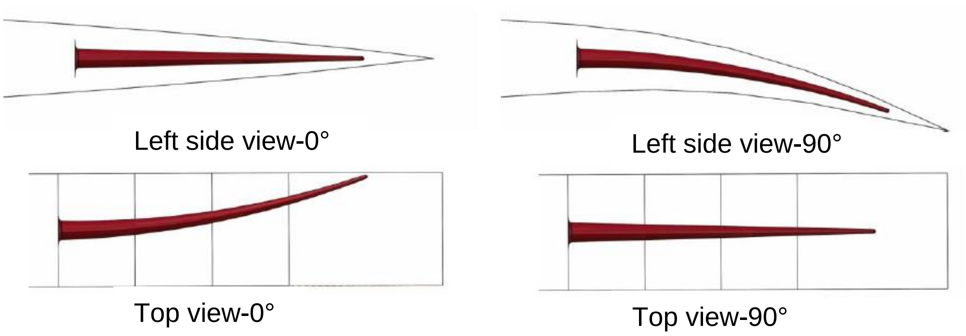


**Figure 2-17 the eccentric beam concept** [4]

### 2.4.2 Connection Discs and Problem Definition

It is a design purpose that the desired deflected shape of the flap will follow the beam curvature. So a link between the curved beam and the skins are required. Circular discs appear to be proper considering that the movement of the beam is rotational. Several of them have been positioned along the beam, their number depends on many parameters like the length of the trailing edge and the thickness of the chosen profile.

The figure 2-16 illustrates the beam-disc concept. When the beam is rotated, the discs fixed on it roll on the skins and push them up or down.

This concept may seem very simple; however a major issue is encountered when trying to make it working properly. That comes from the relative movement between the discs and the morphing skins. Take one disc for example: the contact point with the wing surface during the rotation remains the $W_{vep}$ of this disc. During the rotation, except its vertical motion, it also has a horizontal movement induced by the beam curvature ‘increasing’.

This happens where the disc planes are set perpendicular to the beam curve, as shown in Figure 2-18. The brown beam and disc indicate the 0° rotation, and the green line is the radius of the disc which goes through the vertical extreme point. The yellow beam and disc indicate the 90° rotation, the yellow line is the radius of the disc which goes through the vertical extreme point, it can be seen that the $W_{vep}$ move backward on the upper part, move forward on the lower part.

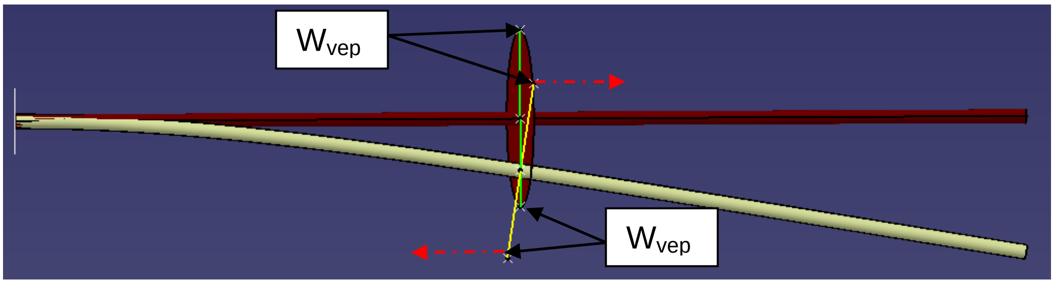


**Figure 2-18 Movements of the $W_{vep}$** [4]

For small deflection, the points on the skins can be approximated seen as rotating around a trailing edge point at the rear spar. The pink curves in the figure 2-19 are the aerofoil shape before morphing, the green one are the aerofoil shape after morphing, and the white curves are the track of the points at the rear part. The upper pink curve rotates around the point A, while the pink curve rotates around the point B. As can be seen from the figure 2-19, the upper and lower skins both move forward, but the upper skin moves further than the lower skin. Therefore, when the skins are in a downward deflection, a fixed point on the upper skin $W_{fup}$ will move forward while the one on the lower surface $W_{flw}$ will move backward relatively.

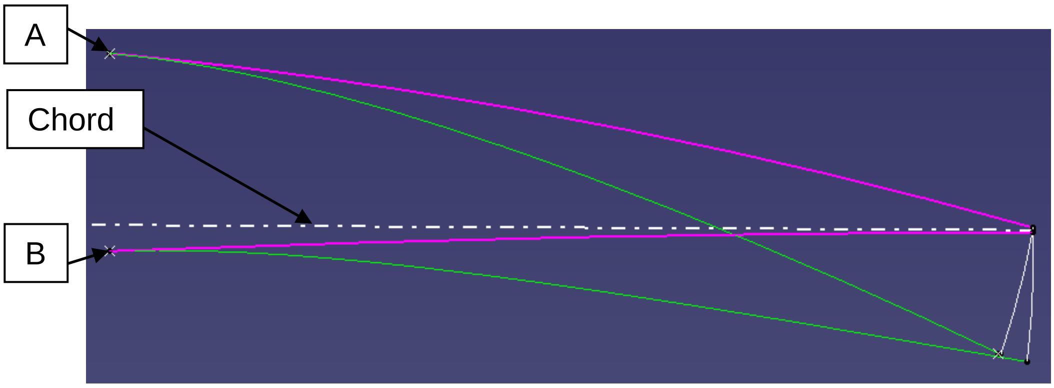


**Figure 2-19 Movements of points on the flap surfaces**

For this reason, the disc sets normal to the beam curve would lead to a sliding between the discs and the skins. The following design is proposed as potential solution to the issue.

**Disc at a setting angle:**

In order to synchronize the motion of skins and discs, the disc is rotated along the vertical axis so that the movement of $W_{vep}$ during the beam rotation changes its direction or move slower. The disc remains planar but in a new plane which is set at a certain angle to the normal plane as shown in Figure 2-20.

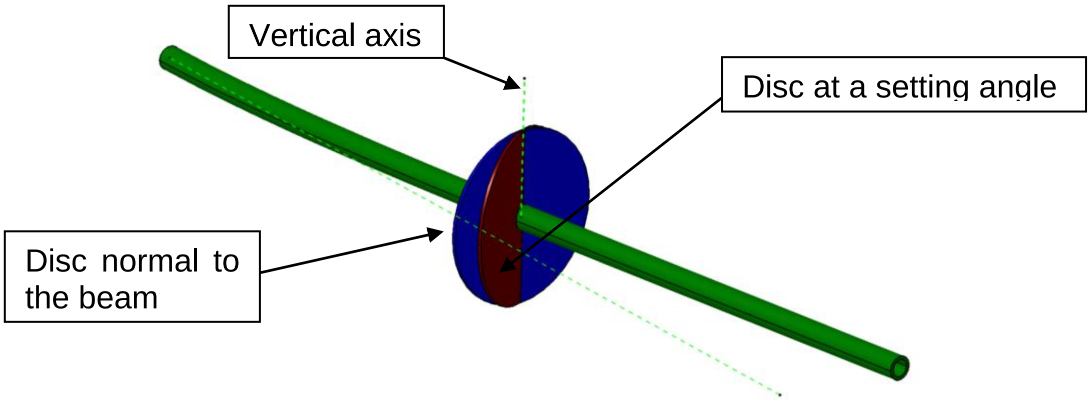


**Figure 2-20 Setting angle concept**

The setting angle of the plane should be calculated in order to minimize the gap between the two motions (disc and skin). For a skin with small horizontal movement, it is a good way to simplify the design. However, when horizontal movement of the skin increases, there will be a bigger gap between the skin and the disc.

**Twisted disc concept**

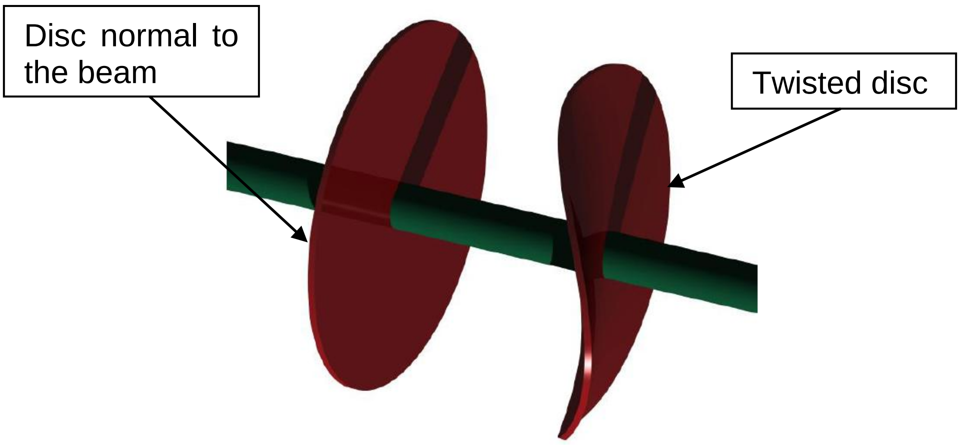


**Figure 2-21 Twisted disc concept**

Keeping the disc perpendicular to the stringer axis, this design proposes to twist it so that at each time, the disc should follow exactly the path of the stringer.

There is a need to twist only half of the disc considering that a complete rotation of the beam is only ± 90°. The Figure 2-21 above shows what the twisted disc would look like compared to a circular disc.

A challenge of this design is to find out the correct shape for the twisted disc, so that its radii can normal to the stringer axis at any rotation angle. It could be determined by combining both the horizontal movement (chord wise) of the wing and the lateral motion (span wise) of the disc during the beam rotation. The resulting 2D curve should then be winded round the beam in order to obtain a 3D twisted disk.

The difficulty of this concept is not only to create a twisted disc, but also to connect the disc together with stringers while allowing its lateral sliding. However it would be interesting to develop it more in details, considering that this concept seems relatively simple and efficient.

# 3 Actuation Mechanism Design

## 3.1 Input Parameters

From a geometrical point of view, the twisted disc design is a relatively complex issue. It is a question of a twisted disc which fixes on the eccentric beam and rotates around an axis. The disc radii are always normal to the stringer axis, which have to be designed accurately. Besides that, the movement of the flap trailing edge surfaces must be considered in order to make sure the rolling of the discs on these surfaces while avoiding their relative chord wise sliding.

To start with the geometrical analysis, some parameters are needed. In this thesis, the author takes the aerofoil NACA 4412 for study, the geometry parameters of the trailing edge was used. The following parameters were then fixed for all the following design:

For the CAD model, the aerofoil (NACA4412) was created from a list of coordinates imported into CATIA (Refer to Appendix G). The chord is 1200mm length, the span is 500mm width and the thickness of the skin is 2mm.

**Table 3-1 Geometrical parameters**

| Name | Symbol | Value |
|---|---|---|
| Profile | NACA | 4412 |
| Chord length | C | 1200mm |
| Beam start | - | 50% of C |
| Beam length | L | 600mm |
| Span | S | 500mm |
| Maximum deflection angle | $\theta_{max}$ | 10° |
| Position of disc | $L_1$ | 50% of L |
| Thickness of skins | $t_s$ | 2mm |

## 3.2 Equation of the Curved Beam

The first step of the design process is to determine the curvature of the beam. It is design intent that the movement of the skin will follow the beam, so that the disc radii will change its dimension and direction slowly. It is the key part of the mechanism and all the following calculations depend on its curvature. To do so, one parameter is used, and one assumption is required:

- Flap trailing edge maximum deflection $\theta_{max}$ equal to 10°.(Maximum deflection is about 7% of chord length, which is normal for a morphing flap)

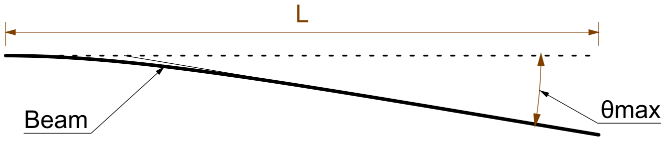


**Figure 3-1 Beam maximum deflection $\theta_{max}$**

- Equation of the curve matching to the displacement of a cantilever beam under tapered distributed pressure, which is similar to the aerodynamic load distribution over a morphing flap trailing edge, and generate continuous and smooth deflection.

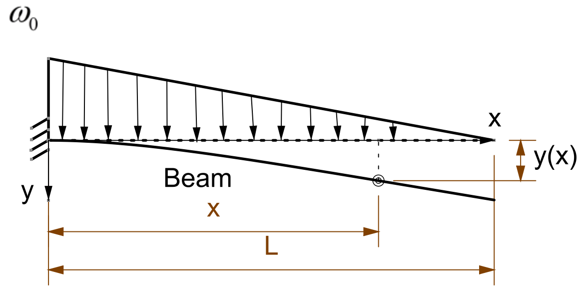


**Figure 3-2 Beam under tapered distributed pressure**

As a result, the following equation can be found (Refer to APPENDIX A for all the details of hand calculation):

$$y(x) = \frac{\omega_0}{EI}\frac{1}{L}[\frac{L^3x^2}{12} - \frac{x^5}{120} - \frac{L^2x^3}{12} + \frac{Lx^4}{24}] \quad \textbf{(3-1)}$$

To determine the ratio $\frac{\omega_0}{EI}$ :

Where $\omega_0$ is the aerodynamic load, E is elasticity modulus, I is flexural rigidity.

The max deflection angle is used considering:

y'(L)=10° and L=0.6m

Hence it comes:

$$y'(x) = \frac{\omega_0}{EI}\frac{1}{L}[\frac{L^3x}{6} - \frac{x^4}{24} - \frac{L^2x^2}{4} + \frac{Lx^3}{6}] \quad \textbf{(3-2)}$$

$$\mathrm{y}'(\mathrm{L}) = \frac{\omega_0}{EI}\frac{1}{L}\left[\frac{L^4}{6} - \frac{L^4}{24} - \frac{L^4}{4} + \frac{L^4}{6}\right] = \frac{\omega_0}{EI}\frac{L^3}{24} \tag{3-3}$$

$$\frac{\omega_0}{EI} = \frac{y'(L) \times 24}{L^3} = \frac{10/180 \times pi \times 24}{0.6^3} = 19.3925m^{-3} \tag{3-4}$$

The equation for the curve beam is then:

$$\mathrm{y}(\mathrm{x}) = \frac{19.3925}{L}[\frac{L^3x^2}{12} - \frac{x^5}{120} - \frac{L^2x^3}{12} + \frac{Lx^4}{24}] \tag{3-5}$$

$$= -0.2693x^5 + 0.808x^4 - 0.9696x^3 + 0.5818x^2$$

$$\mathrm{y}(L) = \frac{19.3925}{L} \times \frac{L^5}{30} = 0.0838 \tag{3-6}$$

$$\mathrm{y}'(\mathrm{x}) = \frac{19.3925}{L}\left[\frac{L^3x}{6} - \frac{x^4}{24} - \frac{L^2x^2}{4} + \frac{Lx^3}{6}\right] \tag{3-7}$$

$$= -1.3467x^4 + 3.2321x^3 - 2.9089x^2 + 1.1635x$$

## 3.3 The Beam Rotation Axis

The beam rotation axis is the rotation centre of the eccentric beam. Normally, for a symmetric aerofoil, the rotating axis is set at the chord of the aerofoil, in order to have a better structural arrangement. In this thesis, the aerofoil NACA 4412 is an asymmetric aerofoil, the axis is created by connecting the front point and rear point of the mean chord of a morphing part. The reason for this arrangement is that at the rear part of the trailing edge, the chord is close to the lower skin, the space for the disc is quite small, and it will be difficult to design the connection between the disc and the skin.

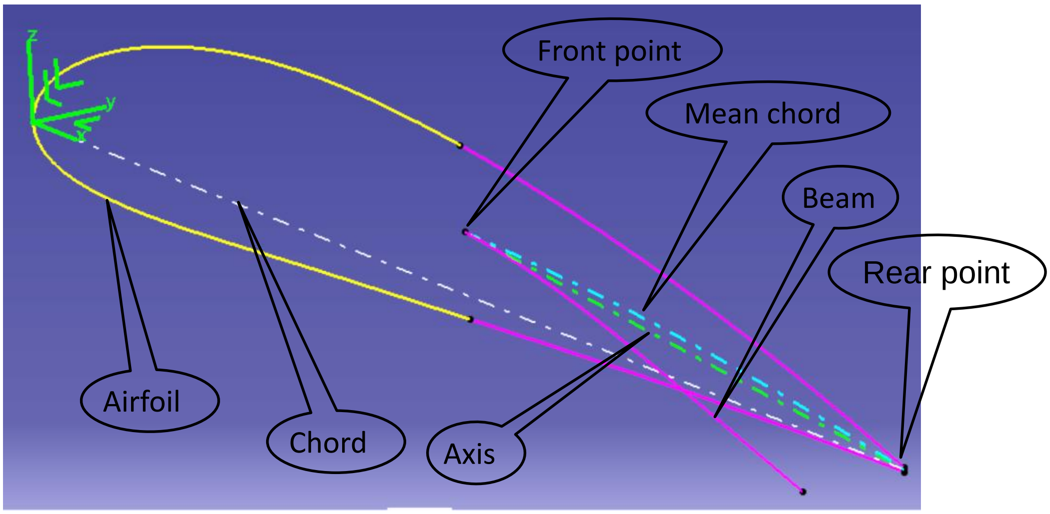


**Figure 3-3 the rotational axis**

In the Figure 3-3 an axis system has been established. The x axis corresponds to the direction of the chord, the y axis to the span wise and the z axis to the vertical. The axis system will be used later.

## 3.4 Eccentric Beam

Using the beam rotation axis and a plane created from the y direction and the rotation axis as a reference, the code for the curve equation is the following:

$$`y`=1000*19.3925/0.6*(0.6^{5}*`x`^{2}/12-0.6^{5}*`x`^{5}/120-0.6^{5}*`x`^{3}/12 + 0.6^{5}*`x`^{4}/24) \qquad \textbf{(3-8)}$$

In the CATIA law, 'x' and 'y' are created with parameter of type real, and 'x'**2=$x^2$. 'x'=[0,1], so it should be multiplied by 0.6 to make it equal to L([0,0.6]).

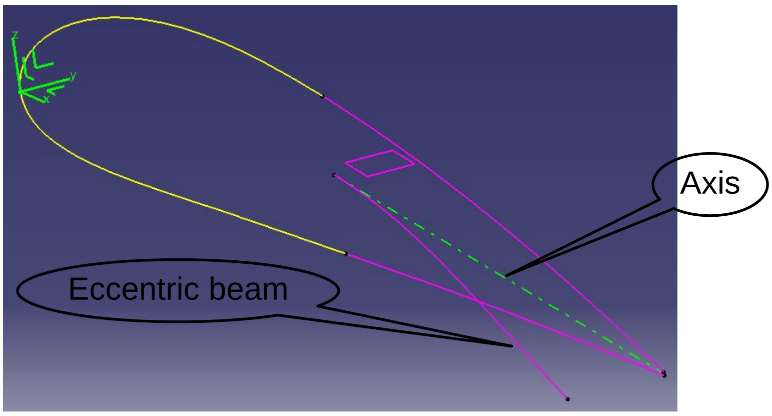


**Figure 3-4 Beam generated by using CATIA**

After creating the eccentric beam, upper and lower radii of disc are not the same, because the eccentric beam is at a symmetric position. For a relatively narrow trailing edge, this will lead to difficulty in structure design, because space is needed for some moving parts to actuate the skin. The author tries to make a more symmetric disc by combining the mean chord with the eccentric curve, to have a balance space distribution to arrange both the upper and lower structure. But because combing two curves increases the radius of the beam, the distance between the skin and the beam becomes bigger during rotation, and this is proved to be not realistic.

For example: The morphing of the skin at the middle of the beam is 30mm, and the radius of the disc ‘r’ is equal to the morphing of the skin. The distance between mean chord and the rotation axis is ‘a’, the distance between the skin and the eccentric beam is ‘L’; O is the rotation axis, R is the radius combining the initial r and a, and is rotated from OA to OC. The connection between the skin and the disc is CD at 90° rotation, considering the beam rotate back form 90° to 80°, CD is rotated around O to EF, K is the initial position of the beam without combining with a, G is the intersection between CD and OK, θ is the angle between OG and OD, the vertical movement of the disc is calculated as follow:

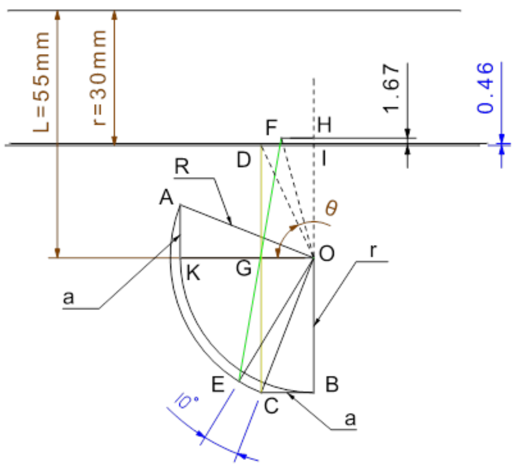


**Figure 3-5  Middle cross section**

$$\tan\theta = \frac{DG}{OG} = \frac{L\text{-}r}{a} \qquad \textbf{(3-9)}$$

$$\theta = \arctan(\frac{L-r}{a}) = 64.7327\deg \qquad \textbf{(3-10)}$$

a=11.8mm; r=30mm; L=55mm;

OD=$\sqrt{\mathrm{DG}^2 + \mathrm{OG}^2} = \sqrt{(\mathrm{CD}-\mathrm{CG})^2 + \mathrm{OG}^2}$=$\sqrt{(L-r)^2 + a^2}$

The vertical movement of the disc:

$\mathrm{HI} = \mathrm{OH} - \mathrm{OI} = \sqrt{(L-r)^2 + a^2} \times (\sin(\theta + 10°) - \sin(\theta)) = 1.67$mm.

The vertical movement of the skin:

30×(sin(90°)-sin(80°))=0.4558mm;

This means that the design intent is not achieved at 80° rotation. Other rotating situation can be checked by the same method. Although this calculation is for the 2-Dimension situation, due to the motion of x direction is quite small compare to the length of the disc, it can explain the problem. So although the medium status of the skins and beams are not strictly required, it is advised that their relative morphing motion should not have too much difference (about 5%) in case of clash. It should always be checked after design.

Another method to create the beam is as follow:

Figure 3-6 shows the cross section at $x_0$ position, $y_0$ is the deflection at $x_0$. O is the rotate centre of the beam; d equals the distance between rotate centre and the mean chord at $x_0$; A is the initial position of the beam, B is the position of the beam after morphing; C is the new position of the A; D is the position of C after morphing. F is the point on the mean chord at $x_0$. In order to have the same disc radius of upper and lower part, the A is repositioned at C. The angle between OC and OF is θ. The movement of the point C along OB direction during the beam rotation is the same as point A. The movement of C along OB direction can be represented as OF+OG.

OB=OF+OG **(3-11)**

$$y_0=OF+OG \tag{3-12}$$

$$OF=OC \times \cos\theta \tag{3-13}$$

$$OG=OD \times \sin\theta \tag{3-14}$$

$$OD=OC=OF/\cos\theta=d/\cos\theta \tag{3-15}$$

$$y_0=OF+OG=OC \times \cos\theta +OD \times \sin\theta$$

$$=OC \times (\sin\theta +\cos\theta)$$

$$=d/\cos\theta \times (\sin\theta +\cos\theta) \tag{3-16}$$

$$=d \times (\tan\theta+1)$$

$$\theta=\mathrm{atan}(y_0/d-1) \tag{3-17}$$

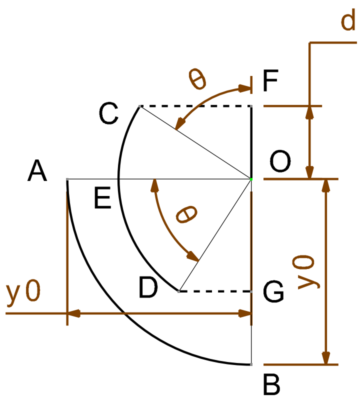


**Figure 3-6 Cross section at $x_0$**

When the ratio of $y_0/d$ is different, the angle θ will be different, and when the beam rotates, the skin will follow the motion of the disc, so for a morphing part not strictly follow a sine function, this method can be applied.

In this thesis, the morphing of the skin follows a sine function to obtain a continuous deflection, so it is abandoned.

Different status of the beam during the rotation can be obtained by , in this case, from 0° to 90° rotation with increment of 10°.

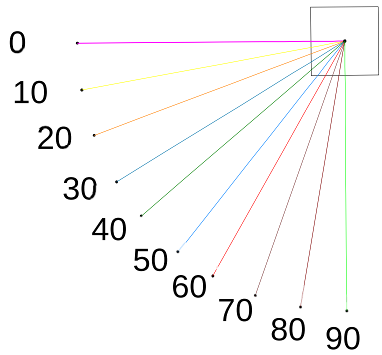


**Figure 3-7 View from x direction**

## 3.5 The Motion of the Skins

For a more precise design, in this case, the rotational motion of the beam corresponds to the motion of the morphing skin, so the author makes some medium status of the skins (mainly due to aerodynamic consideration), in order to precisely control the motion of the skin during the rotation. The motion of the skins follows a sine function according to the curvature of the beam in order to follow the motion of the beam rotation.

The next step consists of morphing the upper and lower skin with different morphing status. Since the skins follow exactly the motion of the beam, start from the plane offset 600mm from the trailing edge, the upper and lower skins are deflected corresponding to the rotation of the beam. The skins motion followed a status of beam rotating from 0° to 90°, by increment of 10°. Creating new laws base on the previous one, by multiplying sin (θ°) (θ belongs to [0°, 90°]), 10 new laws can be obtained:

$$`y`=(1000*19.3925/0.6*(0.6^5*`x`^2/12-0.6^5*`x`^5/120-0.6^5*`x`^3/12 + 0.6^5*`x`^4/24))*\sin(\theta); \quad (\theta=10°, 20°\ldots 90°)$$

And 10 curves are created by 'Parallel Curve' using laws in CATIA. Then, ten curves of skins are created as follows:

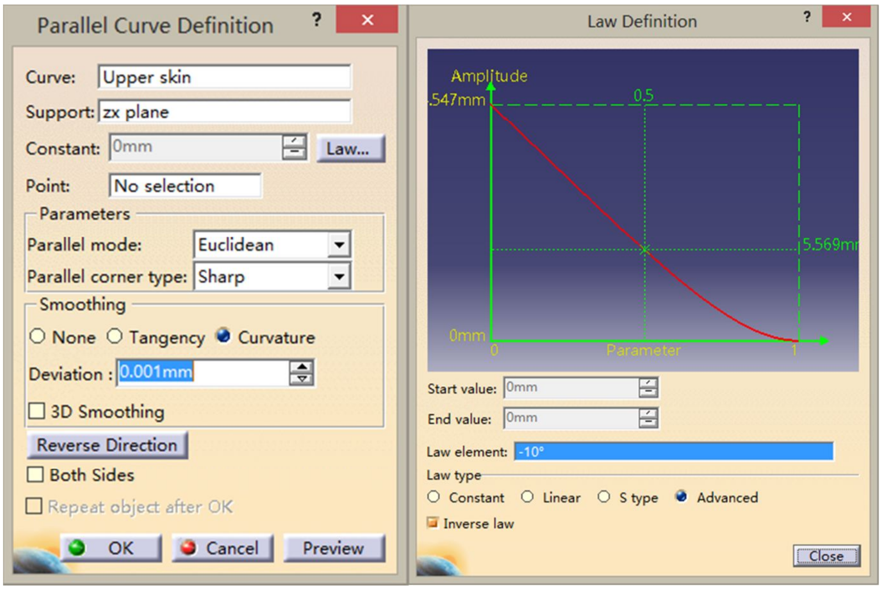


**Figure 3-8 CATIA interface for creating curve from law**

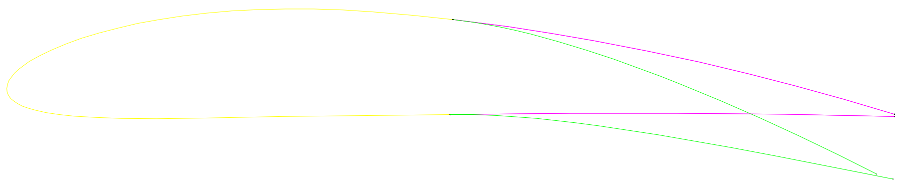

**Figure 3-9 Flap before and after morphing**

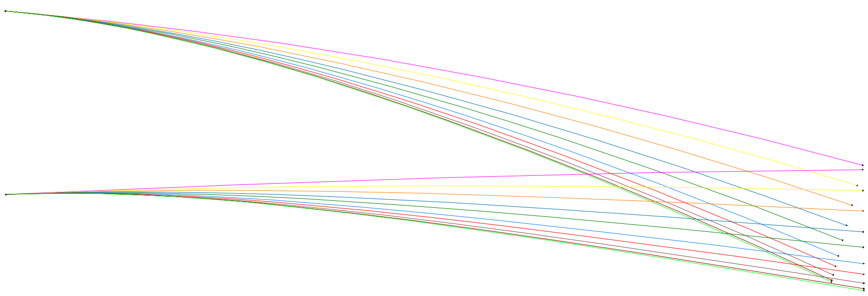

**Figure 3-10 Ten status during beam rotation**

Every colour in Figure 3-9 stands for upper and lower skins in one position, for example, two yellow lines stand for upper and lower skins at 10° TE rotation angle. When creating the skins, make sure that the curve length is not changed, because the 'parallel' tool with law will increase or decrease the length according to the curvature of the curve. Cutting or extending of the skins when needed.

## 3.6 Creating Discs

The concept of a twisted disc fixed on the beam and rotated to actuate the skins was described in previous chapter (Refer to 2.4). This section presents the way to determine the radii and angle of the disc.

The software used to build the model presented in this thesis was CATIA V5. Base on the eccentric beam and skins created before, it is possible to create a twisted disc when the position of the disc is determined. The position of disc is not determined at this stage, it will be discussed later in Chapter 4. It is assumed that the disc was created at 50% of the beam in order to illustrate the design. Its 'radii' are determined to be in contact with the flap surface, given a NACA4412 profile, with 1200mm chord length, 500mm span width and 2mm skin thickness.

Once the position is determined, the next step consists of creating the radius between the skins and the beam. A plane is created through the middle point of the axis, and normal to the axis. The point on the skin is created by using the intersection, and then measure the length between the point and the front point along the skin. Other points on different status can be created. This is done by ‘point’, in the point definition box, select point type 'on curve', and enter the distance measured before. These points are number from $P_{0u}$ to $P_{9u}$.

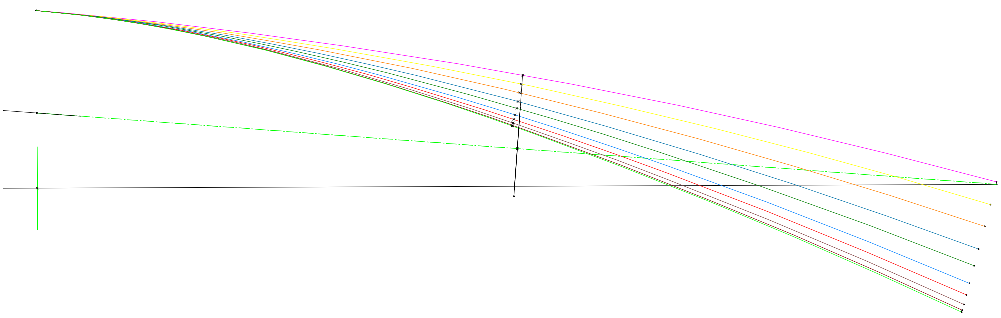

**Figure 3-11 Deflection of the upper skin (90° down)**

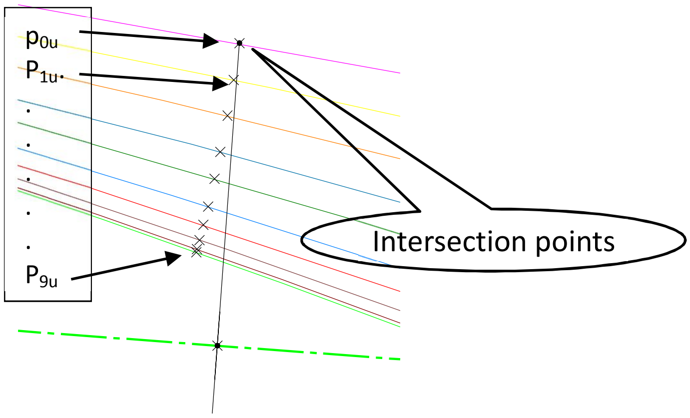


**Figure 3-12  Points on upper skin during rotation**

Since the contact point on the skin is 3-D, so lines which go through the points created in Figure 3-11 are created and number from $L_{0u}$ to $L_{9u}$.  Refer to Figure 3-13

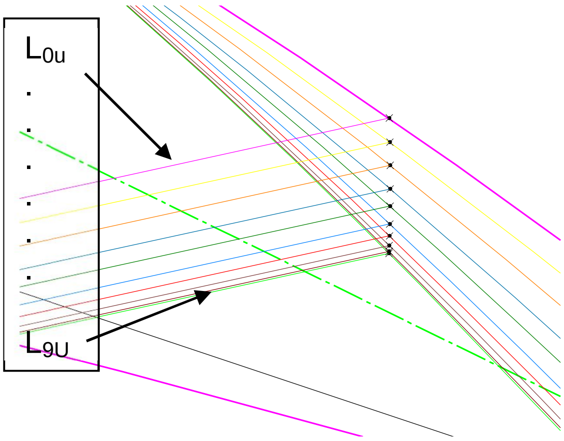


**Figure 3-13  Lines created through points on the skin**

Points on the eccentric beam are created by  base on Figure 3-7.

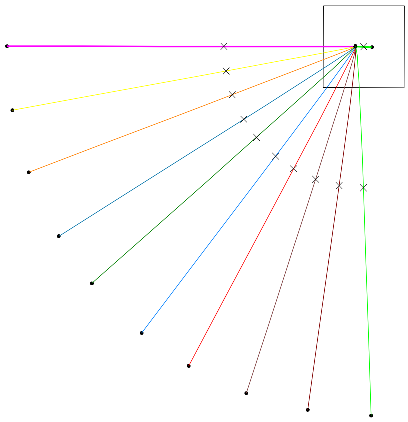

**Figure 3-14  Points on the curve**

After all the steps above are done, next step is connecting the skins and the beams to create the disc radius at different rotation status.

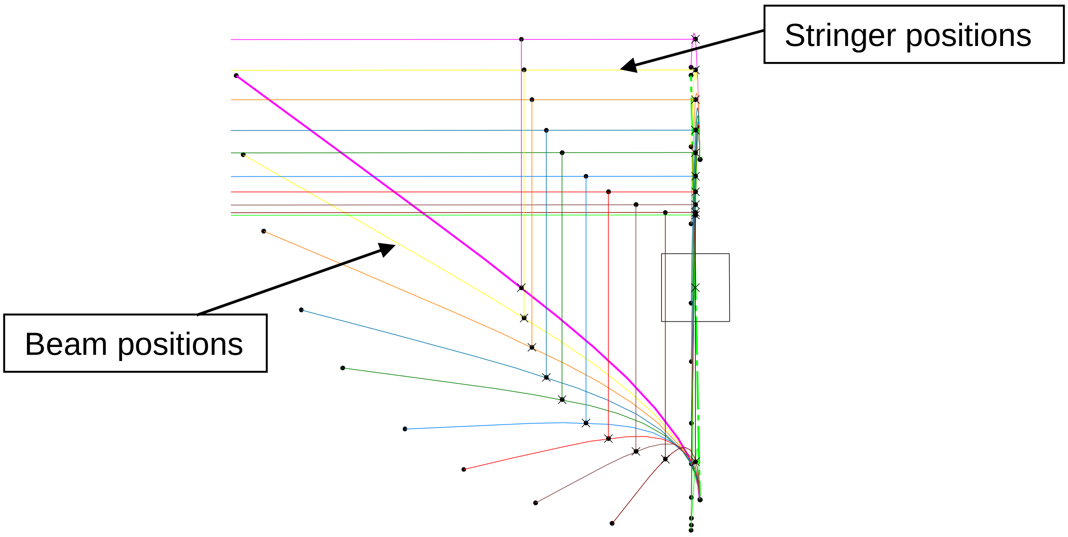


**Figure 3-15 Connection between upper skin and beam in yz plane**

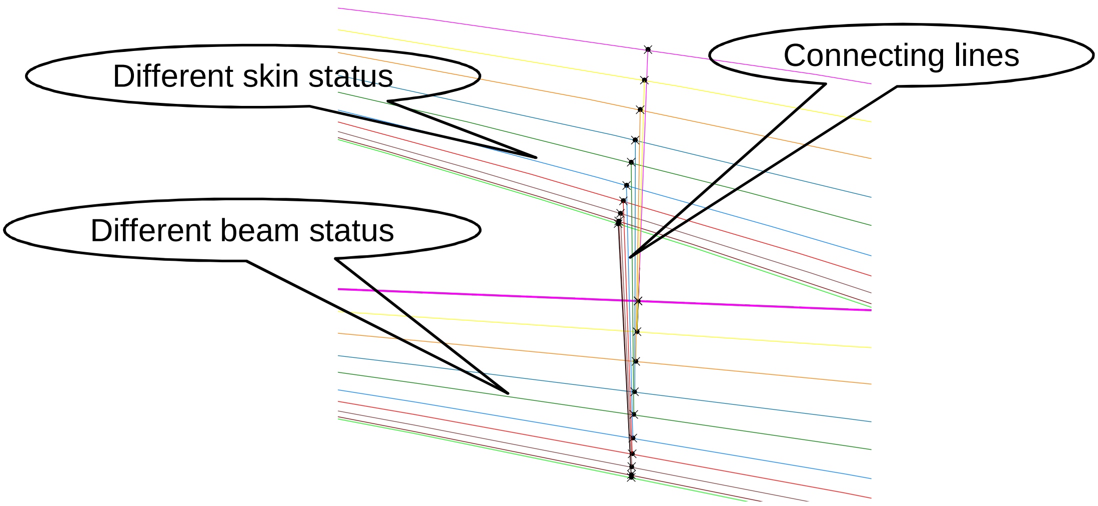


**Figure 3-16 Connection between upper skin and beam in xz plane**

Ten lines in the figure 3-16 indicate the different status of the connection between the skin and the beam, and the angle between the skin and disc is changing. The points on the beam move follow an arc track in yz plane, which means the points on the beam move in a line in xz plane. While the points on the skin move follow an arc track in xz plane, which causes the twist of the disc.

The same procedure can be processed on the lower surface. After all the connection between the skin and beam is created, the next step is to rotate them back to the original position to create a disc. As it can be known, the line of 10° TE rotation angle should be rotated around the axis -10° to the original position. The tool 'spline' is used to create the one quarter ‘circle’ of the upper disc and lower disc. Then tool 'connect curve'  is used to connect the two one quarter circles together. Then by combining the 4 curves together, the disc at the middle points is created, this is done by the tool ‘fill’. Refer to figure 3-19.

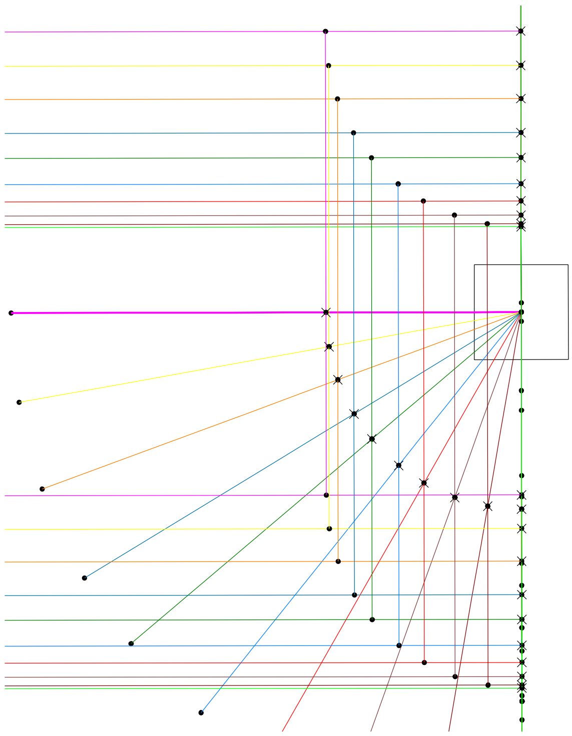

**Figure 3-17 Connections between skin and beam from x direction**

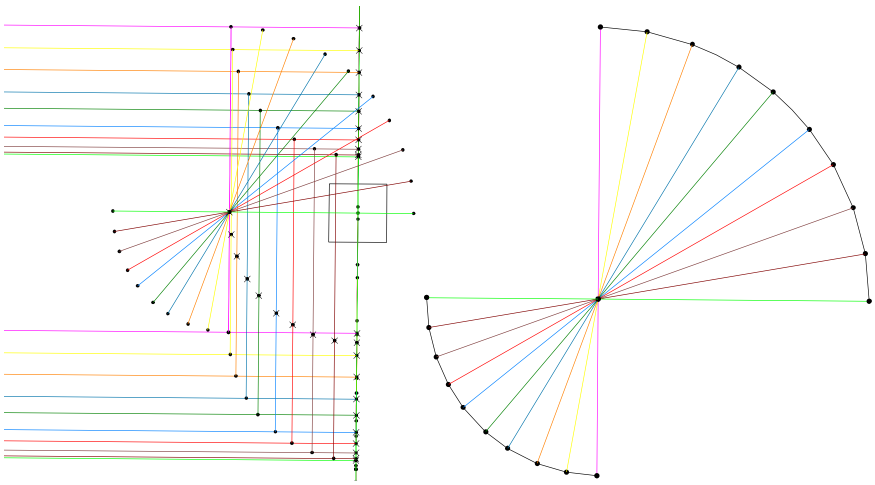

**Figure 3-18 Creating the disc**

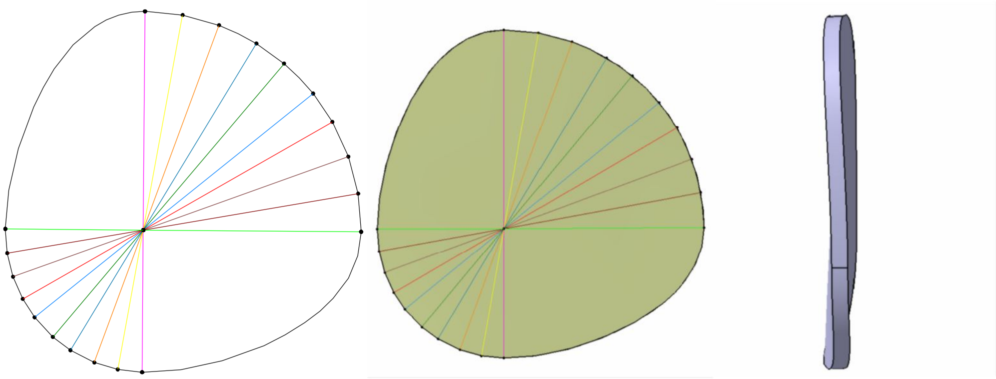

**Figure 3-19 Model of the disc**

The Figure 3-19 shows the CAD model of the disc on the beam.

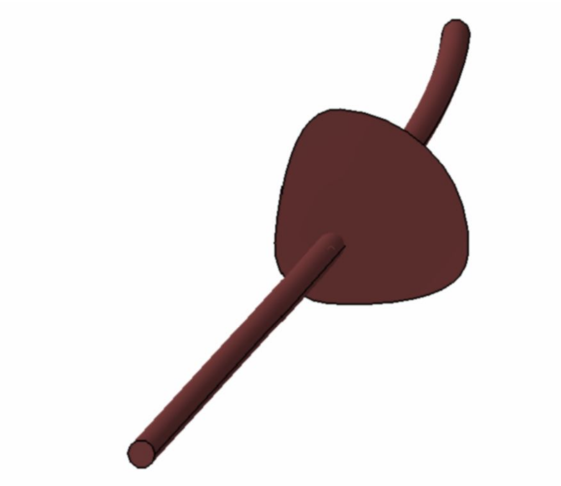

**Figure 3-20 CAD model of beam and one disc**

At this stage, the eccentric beam and the disc are created. Considering that a 2mm skin is quite flexible, stringers are needed not only to increase the stiffness of the skin but also provide the track for the disc. Every disc is connected to two stringers, so five stringers on the upper skin and five on the lower skin are created. The number of discs is decided by the optimization procedure, which will be illustrated in Chapter 4.

The approach described above assumed that the stringer have a constant height of the web. Actually, it's changeable, and the disc diameter is also changed accordingly.

## 3.7 Creating Stringers

Stringers are used to enhance the stiffness of the skin and connected to the disc so that the disc can slide on it. I cross section is chosen for the stringers considering the motion and connection between the discs and stringers. Initial dimension of I section are listed in table 2-3:

**Table 3-2 I cross section parameters (unit: mm)**

| Sequence number | H | w1 | w2 | t1 | t2 | t |
|---|---|---|---|---|---|---|
| 1 | 16 | 20 | 20 | 2 | 2 | 2 |
| 2 | 14 | 20 | 20 | 2 | 2 | 2 |
| 3 | 12 | 20 | 20 | 2 | 2 | 2 |
| 4 | 8 | 20 | 20 | 2 | 2 | 2 |
| 5 | 5 | 20 | 20 | 2 | 2 | 2 |

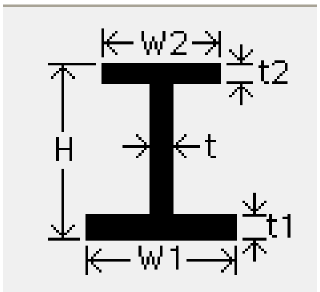


**Figure 3-21 I cross section**

Since the disc is not directly connected to skin, the height of the stringer is considered when creating the disc. Instead of creating lines from the points ($L_{0u}$ to $L_{9u}$) on the skin, lines which are normal to skin and through the points ($L_{0u}$ to $L_{9u}$) created before, with a constant length of H (Refer to table 3.2) are built. Other steps of creating the disc follow the same procedure described previously.

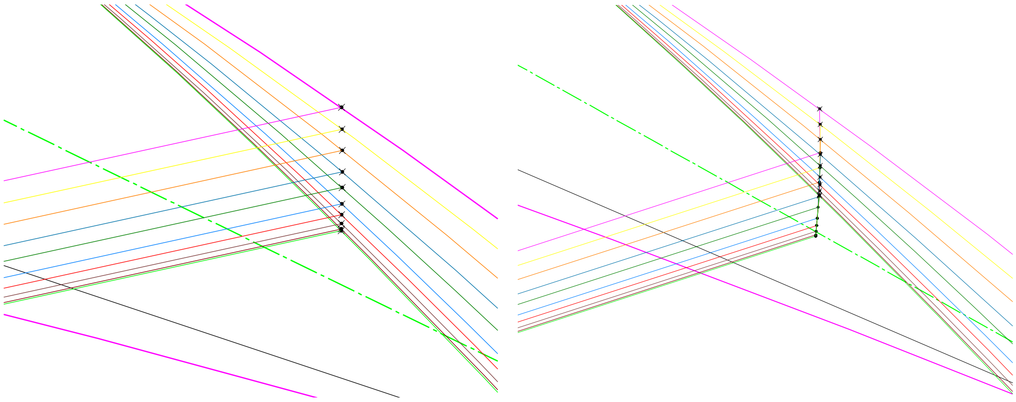

**Figure 3-22 Change the way to create $L_{0u}$ to $L_{9u}$**

To be noted that, from the span wise direction, the angle between the skin and disc is changing continuously, which means the motion of the disc is not a straight line sliding, which will increase the difficulty of designing the mechanism. One solution is to have a twisted stringer, which change cross section continuously, which can make sure that the disc and stringer flange stay perpendicular.

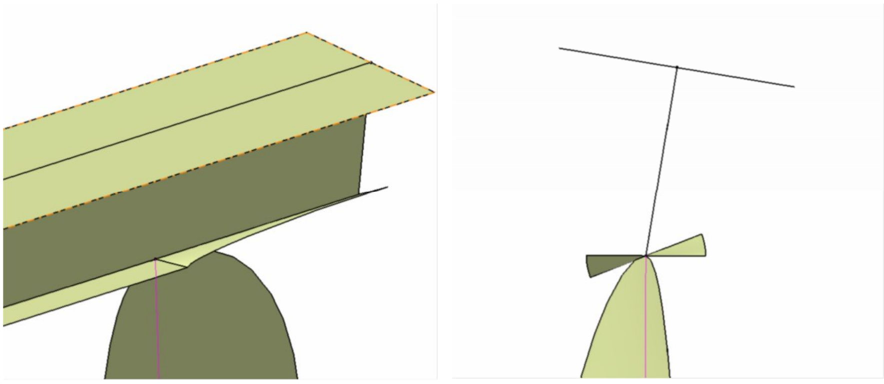

**Figure 3-23 Twisted stringer**

As described before, the disc slide along the y direction during rotation of the beam, the stringer cross section at different rotate angle can be known.

Considering that the stringer web is always normal to the skin, where the flange is normal to the disc radius, so at every beam rotate angle, the angle between web and disc is measured from the CATIA, and this is later used to create the stringer. The project points of the eccentric beam during rotation on the $L_{0u}$ correspond to the flange of the upper stringer.

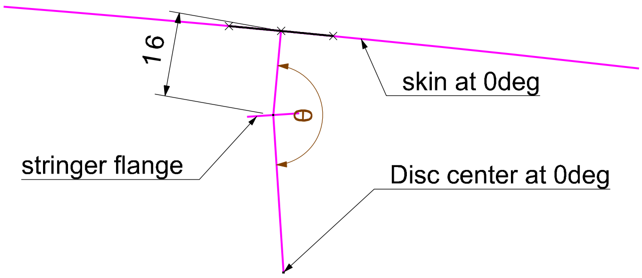


**Figure 3-24  Angle between the disc and the stringer**

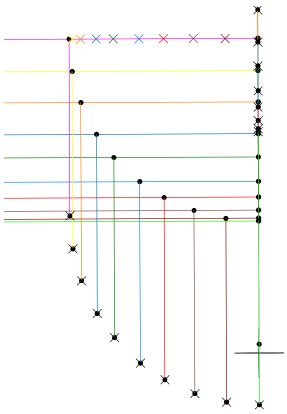

**Figure 3-25  Upper stringer lower flange correspond to $L_{0u}$**

The Table 3.3-3.7 gives the angle of disc, stringer and radius of the disc at five different positions along the chord wise direction.

**Table 3-3  First disc position at x=0.0995m**

| Upper stringer | | | Lower stringer | | |
|---|---|---|---|---|---|
| **Rotate angle** | **Radius** | **Angle** | **Rotate angle** | **Radius** | **Angle** |
| 0 | 44.7mm | 176.6° | 0 | 36.3mm | 170.4° |
| 10 | 44.6mm | 175.4° | 10 | 36.2mm | 171.8° |
| 20 | 44.6mm | 174.1° | 20 | 36.1mm | 173.1° |
| 30 | 44.6mm | 172.9° | 30 | 36.0mm | 174.4° |
| 40 | 44.6mm | 171.9° | 40 | 35.9mm | 175.4° |
| 50 | 44.6mm | 170.9° | 50 | 35.9mm | 176.5° |
| 60 | 44.6mm | 170.2° | 60 | 35.8mm | 177.2° |
| 70 | 44.6mm | 169.7° | 70 | 35.8mm | 177.7° |
| 80 | 44.6mm | 169.3° | 80 | 35.8mm | 178.1° |
| 90 | 44.6mm | 169.2° | 90 | 35.8mm | 178.2° |

**Table 3-4  Second disc position at x=0.1996m**

| Upper stringer | | | Lower stringer | | |
|---|---|---|---|---|---|
| **Rotate angle** | **Radius** | **Angle** | **Rotate angle** | **Radius** | **Angle** |
| 0 | 38.8mm | 174.0° | 0 | 24.9mm | 169.5° |
| 10 | 38.8mm | 171.8° | 10 | 24.7mm | 172.5° |

| | | | | | |
|---|---|---|---|---|---|
| 20 | 38.9mm | 169.6° | 20 | 24.6mm | 175.2° |
| 30 | 38.9mm | 167.3° | 30 | 24.4mm | 177.9° |
| 40 | 39.0mm | 165.5° | 40 | 24.4mm | 179.9° |
| 50 | 39.1mm | 163.6° | 50 | 24.3mm | 178.2° |
| 60 | 39.1mm | 162.4° | 60 | 24.3mm | 176.9° |
| 70 | 39.2mm | 161.3° | 70 | 24.2mm | 175.9° |
| 80 | 39.3mm | 160.7° | 80 | 24.2mm | 175.2° |
| 90 | 39.3mm | 160.5° | 90 | 24.2mm | 175.0° |

**Table 3-5 Third disc position at x=0.3013m**

| Rotate angle | Radius | Angle | Rotate angle | Radius | Angle |
|---|---|---|---|---|---|
| 0 | 29.8mm | 170.9° | 0 | 13.9mm | 167.2° |
| 10 | 29.9mm | 167.6° | 10 | 13.7mm | 172.9° |
| 20 | 30.1mm | 164.2° | 20 | 13.5mm | 178.1° |
| 30 | 30.3mm | 160.5° | 30 | 13.5mm | 177.1° |
| 40 | 30.6mm | 157.7° | 40 | 13.4mm | 173.8° |
| 50 | 30.9mm | 154.6° | 50 | 13.4mm | 170.7° |
| 60 | 31.2mm | 152.6° | 60 | 13.4mm | 168.7° |
| 70 | 31.4mm | 150.9° | 70 | 13.3mm | 167.3° |
| 80 | 31.6mm | 149.8° | 80 | 13.3mm | 166.4° |
| 90 | 31.6mm | 149.5° | 90 | 13.3mm | 166.1° |

**Table 3-6 Fourth disc position at x=0.3967m**

| Rotate angle | Radius | Angle | Rotate angle | Radius | Angle |
|---|---|---|---|---|---|
| 0 | 22.7mm | 168.6° | 0 | 8.2mm | 166.3° |
| 10 | 22.8mm | 164.0° | 10 | 8.0mm | 176.1° |
| 20 | 23.1mm | 159.1° | 20 | 8.0mm | 175.6° |
| 30 | 23.6mm | 153.8° | 30 | 8.0mm | 168.6° |
| 40 | 24.1mm | 149.7° | 40 | 8.0mm | 164.2° |
| 50 | 24.7mm | 145.3° | 50 | 8.0mm | 160.5° |
| 60 | 25.2mm | 142.4° | 60 | 8.0mm | 158.4° |
| 70 | 25.7mm | 140.0° | 70 | 7.9mm | 157.0° |
| 80 | 26.0mm | 138.6° | 80 | 7.9mm | 156.2° |
| 90 | 26.1mm | 138.1° | 90 | 7.9mm | 156.0° |

**Table 3-7 Fifth disc position at x=0.5097m**

| Rotate angle | Radius | Angle | Rotate angle | Radius | Angle |
|---|---|---|---|---|---|
| 0 | 12.9mm | 167.1° | 0 | 4.6mm | 169.3° |
| 10 | 13.2mm | 158.9° | 10 | 4.5mm | 173.7° |
| 20 | 13.7mm | 150.1° | 20 | 4.7mm | 161.2° |
| 30 | 14.6mm | 140.7° | 30 | 4.9mm | 152.5° |
| 40 | 15.6mm | 134.0° | 40 | 4.9mm | 148.2° |
| 50 | 16.9mm | 127.3° | 50 | 4.9mm | 145.3° |
| 60 | 17.9mm | 123.2° | 60 | 4.8mm | 144.1° |
| 70 | 18.9mm | 120.0° | 70 | 4.6mm | 143.6° |
| 80 | 19.5mm | 118.1° | 80 | 4.5mm | 143.6° |
| 90 | 19.7mm | 117.5° | 90 | 4.5mm | 143.6° |

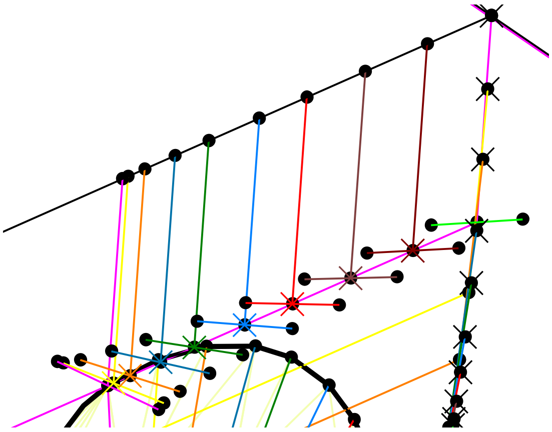

**Figure 3-26  Ten cross section of the upper stringer during rotation**

After creating ten cross sections with the same height of stringer web, the next consist of combining them together to get the stringer flange. The tool 'multi-sections surface'  in the 'Generative Shape Design' module is used to combine them one by one.

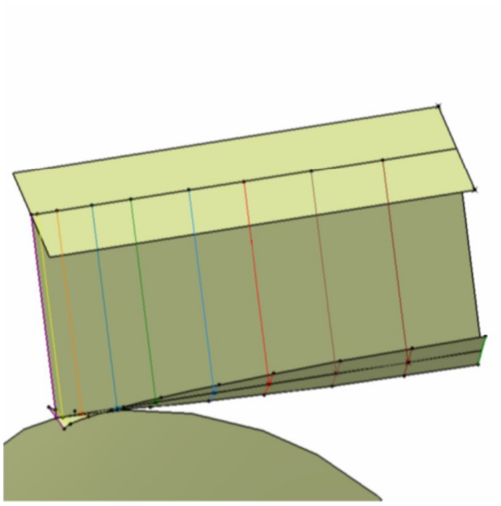

**Figure 3-27  Twisted stringer**

As can be seen from Figure 3-26, a dramatic twisted angle cause a sharp surface of the stringer. From the Table 3-5, the cross sections of 0° and 10° have a 0.488mm distance while the angle of them change 3.314°. Compared to the other neighbour cross section, this is a huge change. And when creating the flange with 2mm thickness, an error occurs and prompts: ’Current offset value leads to a local degeneration on a surface: body cannot be built’. Since this angle is created follow strictly normal to the disc radius criteria, to avoid a sharp surface, the 0° cross section angle is set to be the same as the 10° one. This different, however, could not be too erroneous since only a small angle is altered.

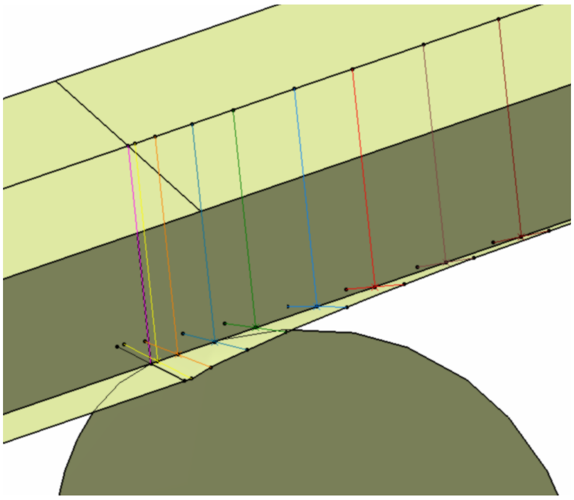

**Figure 3-28 smooth twisted stringer**

## 3.8 Eccentric Beam Mechanism

By now, two flexible skins with twisted stringers, eccentric beam and twisted discs are created and showed by curves or surfaces. To start with the mechanism design, 3-D parts are created in 'part design module'.

The disc is given a thickness of 2mm, and edge fillet of 1mm, so that it can slide on the stringer smoothly. The twisted stringer is also created, the dimensions of cross section are listed in Table 3-5.

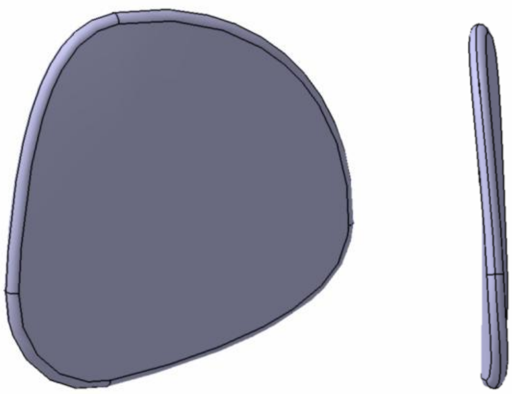

**Figure 3-29 3-D model of the twisted disc**

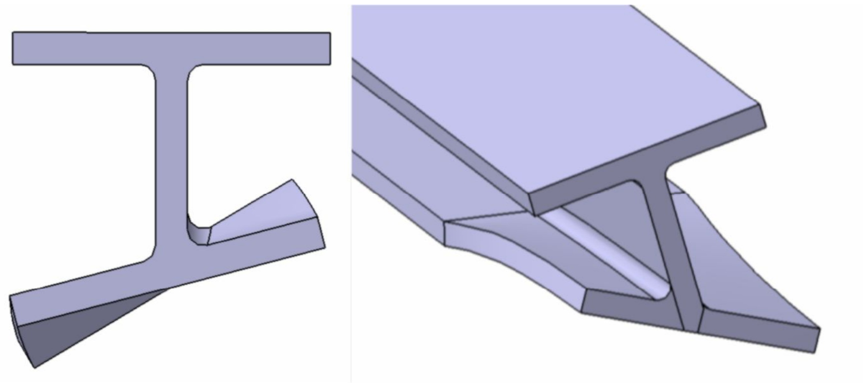

**Figure 3-30  3-D model of twisted stringer**

To connect the stringer and disc together, a mechanism is needed to allow their relatively sliding and rotation.  The schematic diagram is shown in Figure 3-30.  Two C-section connectors are created with two rollers on each of them.  A flange of the disc is also built so that the connector can work properly.  Due to the rotation between the stringer and disc, a minimum distance between disc flange and stringer flange should be considered.  For the stringer have a W2 of 20mm, and rotate angle 21.446° (=170.901-149.455) during 90° eccentric beam rotation, the minimum distance is:

$$d = \frac{W_2}{2} \times \sin(21.466\deg) = 3.66mm \qquad \textbf{(3-18)}$$

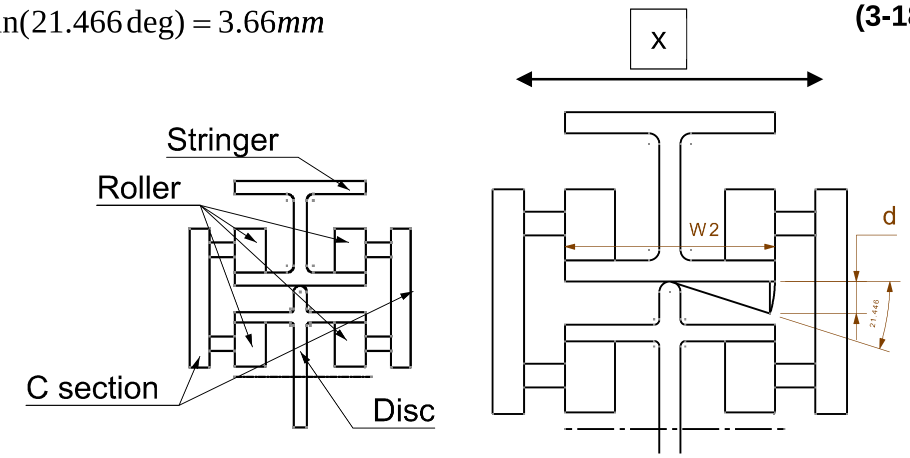


**Figure 3-31  Schematic diagram for the connection of stringer and disc**

The C-connector described above solve the problem in two-Dimension, However, in 3-Dimension situation, the issue becomes more complicated.  The Figure 3-32 shows the model of C-connectors and the connection with the stringer and disc.  As C-connector connects the twisted disc and stringer, so it is also twisted. However, the C-connector itself does not fix, because it cannot withstand the x direction indicated in figure 3-31. To solve this issue, the C-connectors are extended so that they have the space to connect to the other one, meanwhile without creating any hole on the stringer or disc. The Figure 3-33 illustrates the C-connector and its extending configuration. Then two C-connectors are connected with bolts. Another consideration when the C-connector sliding along the stringer is that the clearance between the C-connectors and the stringer should be kept at a minimum (less than 1mm) so that it can work properly without clash with the stringer flange and without sliding out of the stringer and disc, as shown in figure 3-34. The purpose and advantage of the twisted stringer design is to keep the c-connector works and minimize the gap between disc and stringer contact surface.

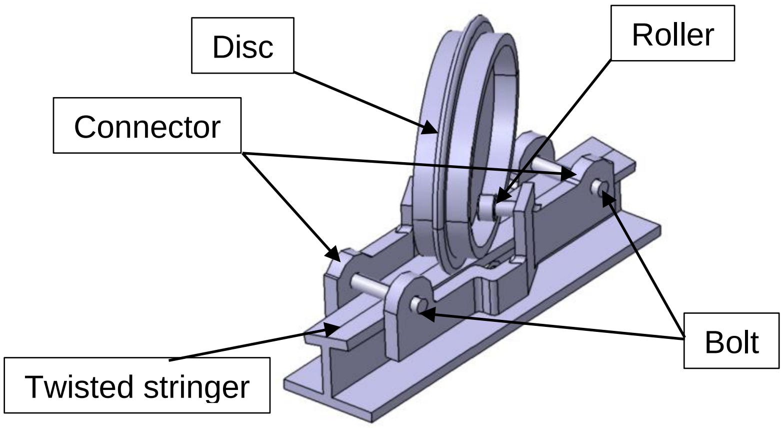


**Figure 3-32 C-connector mechanism**

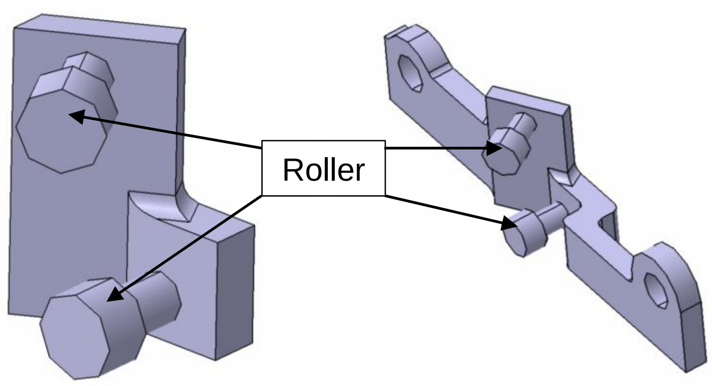


**Figure 3-33 C-connector before and after extending**

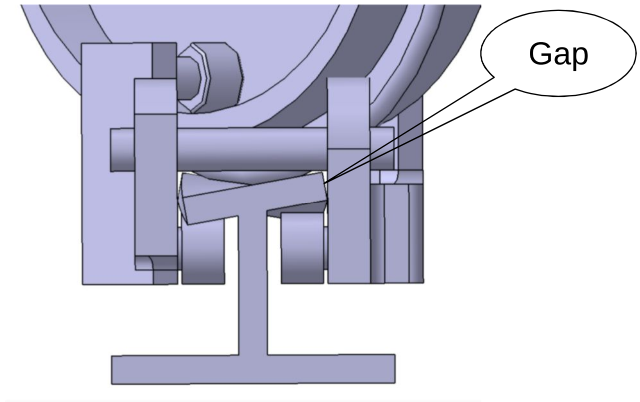


**Figure 3-34 Gap between C-connector and stringer**

## 3.9 Sliding Connection at Open Trailing Edge

As can be seen from Figure 3-9, there is relatively motion along x direction between the trailing edge upper skin and lower skin. This means that the connection of the upper and lower skin should be flexible to allow their relatively sliding while still connected with each other. Figure 3-35 demonstrate a possible solution to implement the sliding connection at the flap trailing edge. The upper and lower skins end with a triangle solid part. At the lower skin there is a cylinder flange, while at the upper skin there is a slot, so that when the upper and lower skin slide along the other, the track and cylinder flange can still connect with each other, avoid vertical motion.

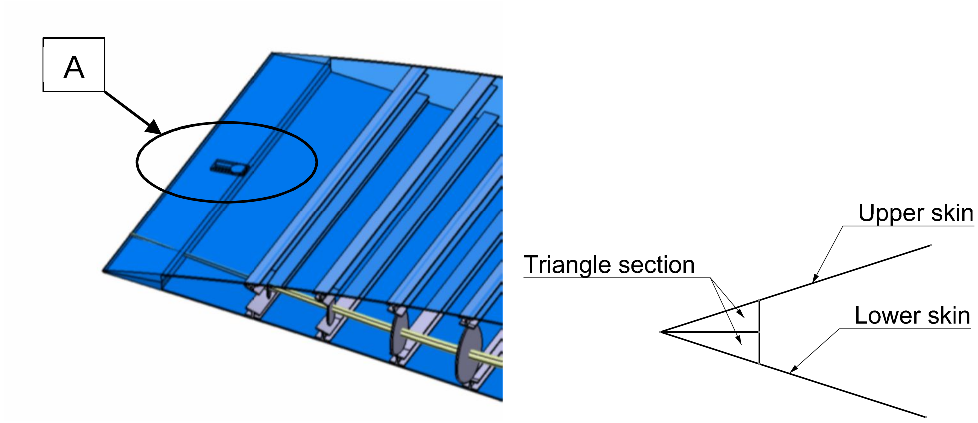


**Figure 3-35 Connection between upper and lower skins at the trailing edge**

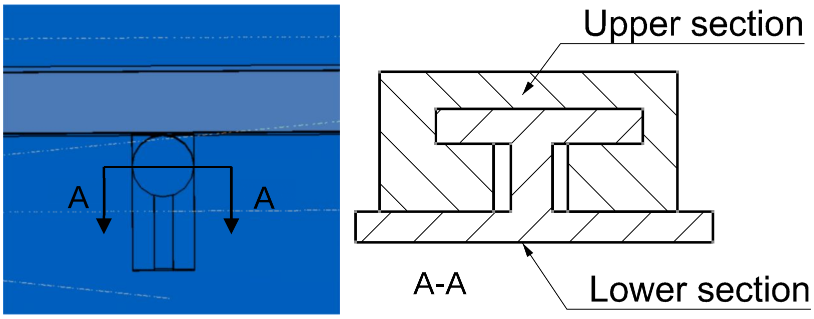


**Figure 3-36 Detail structures of upper and lower skins**

## 3.10 Discussion

In this chapter, the way of how to create the EBAM is presented. The medium status of the morphing can be designed according to different requirements. The discs created closer to the flap rear spar are relatively flat, with a small setting angle, without too much twist. The radii of the disc are bigger than that of closer to the trailing edge. And motion of which are small, due to small morphing magnitude. While when it comes near the trailing edge, the disc radii decrease ascribed to the reducing space at the trailing edge, and the twisted disc surface is obvious.

The closer the connected point on the skin to the rear part, the greater the setting angle will be. This is mainly because at the rear part of the skin the morphing angle becomes bigger compare to the front part, and it leads to the distance increases from the skin to the rotate plane.

# 4 Optimization of the Morphing Flap Structure

Structural optimization methods traditionally had the main objective to minimize the structural weight meanwhile keep the load carrying capability of the structure. The optimization of a morphing flap structure, however, requires a different approach to the issue. As mentioned by Moorhouse, Sander et al. in [21], it is expected that a morphing structure is heavier than a conventional structure due to additional hinges, actuators and mechanism. So the main objective of the optimization is not to minimize the mechanism weight but to achieve the target deflection. Other parameters such as material strength requirements and the actuation torque needed to morph the flap are also taken into account.

This chapter presents two ways for the design optimization of a morphing structure and its application to the flap with morphing trailing edge. In order to obtain the desired morphing shape and calculate the torque of the actuating system, optimization of the support positions of the eccentric beam discs are carried out. The objective function is the standard deviation of the differences between the target shape and achieved morphing shape.

## 4.1 The Morphing Flap Target Shape

The target deflected shape of a flap structure with morphing ability is normally based on aerodynamic considerations, in order to achieve high aerodynamic performance of the flap. This thesis is focus on the structure issues, thus specific aerofoil shape is ignored, and a methodology developed in this thesis can be applied to any other situation.

Author takes the parameters directly from geometrical design as a case study, and the target curvature for this study is as follow:

$$y(x) = -0.2693x^5 + 0.808x^4 - 0.9696x^3 + 0.5818x^2 \qquad \textbf{(4-1)}$$

Since the morphing of the flap is actuated by an eccentric beam with discs fixed on it, which means the loads applied on the skin is not only tapered distributed pressure, but also the loads from the discs, thus generate some differences between the target shape and morphing shape achieved by eccentric beam actuation system. The objective of the optimization study conducted in this part is to minimize such shape differences by acting on the characteristics of the actuation mechanism. The analysis presented in this section is to improve the morphing shape achieved by acting on the number and axial position of the actuating loads.

## 4.2 Beam Model of Morphing Skin

To simplify the results, the morphing skin was represented as a cantilever beam deflected by several transverse loads applied at various locations along the chord. The error introduced by assuming the skin as a beam will be compared with the FEA results in chapter 5.

The general equation of the deflection curve of the beam is:

$$EI\frac{d^2y}{dx^2}=-M \quad \textbf{(4-2)}$$

Where M is the bending moment applied to the morphing skins, which is a function of x only when transverse concentrated loads are applied.

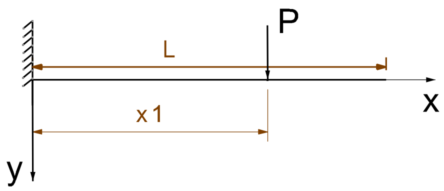


**Figure 4-1 Cantilever beam under transverse concentrated load**

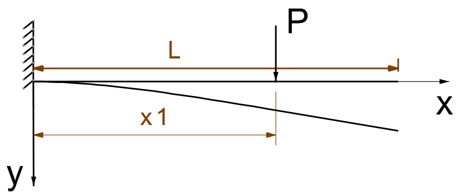


**Figure 4-2 Deflection of a cantilever beam under transverse load**

The deflection of a cantilever beam under a transverse load P applied is:

$$EI\frac{d^2y}{dx^2}=P(x_1-x) \quad 0 \leq x \leq x_1 \tag{4-3}$$

$X_1$ is where the P is applied.

By integration, the equation becomes:

$$EI\frac{dy}{dx}=Px(x_1-\frac{x}{2})+C_1 \tag{4-4}$$

$$EIy=Px^2(\frac{x_1}{2}-\frac{x}{6})+C_1x+C_2 \tag{4-5}$$

The constants C1 and C2 can be calculated by applying the boundary condition of beam clamped at its left hand. The deflection and the slope at x=0 are 0, therefore, $C_1=C_2=0$.

Hence,

$$y=\frac{Px_1}{2EI}x^2-\frac{P}{6EI}x^3 \tag{4-6}$$

Considering a cantilever beam, having a length of L, with a load P applied in $x_1$, its deflection will follow Equation 4.6 for $0 \leqslant x \leqslant x_1$ and it will become linear for $x_1 \leqslant x \leqslant L$:

$$y=\frac{Px_1}{2EI}x^2-\frac{P}{6EI}x^3 \quad 0 \leq x \leq x_1 \tag{4-7}$$

$$y=\frac{P}{3EI}x_1^3+\frac{P}{2EI}x_1^2(x-x_1) \quad x_1 \leq x \leq L \tag{4-8}$$

For the situation of more than one transverse load is applied, the deflection in each point of the beam can be calculated by applying the superposition principle and superimposing the deflections produced by each of the single load at that point.

The application of the beam theory is straight forward once the concentrated transverse loads applied on the structure are known. In the case of a morphing flap that needs to conform to a given shape, however, the problem to be analysed is slightly different. The loads applied on the structure to get the desired shape are unknown since they depend on the position where they are applied. However, they can be determined based on the values assumed by each couple of points (x, y), where x is the chord wise coordinate and y is the corresponding desired vertical coordinate at that point.

In this research, an inverse method is adopted to determine the loads required in specific locations along the beam in order to achieve the desired deflection. The steps followed in the calculation of the transverse loads and beam deformed shape were:

- For a cantilever beam with N transverse loads applied to it, the generic expression of the deflection was obtained from the basic beam equation by using the superposition principle;
- N tentative positions $x_i$ along the beam were selected for the loads and the vertical deflection $y_i$ in these points was set equal to the target shape at $x_i$ in order to get the minimum difference;
- Substituting the $N(x_i, y_i)$ values in the expression of the deformed shape, a set of N equations in the N unknown loads $P_i$ was obtained and its solution allowed to evaluate the magnitude of the loads in the specified positions $x_i$;
- Once the transverse loads were known, they were applied back to the deformed beam equation in order to evaluate the deflection in all the coordinate locations.

A total number of loading points was specified along the beam and the procedure was repeated for all the possible combinations of loading positions. For each load combination, the deflection curve of the beam was determined and its distance from the desired deflection was evaluated over the interval. The configuration with least difference from the target shape was selected as the optimal one.

### 4.2.1 Beam with Three Loads

The beam was subjected to three vertical loads $P_1$, $P_2$ and $P_3$ applied in three generic locations $x_1$, $x_2$ and $x_3$ along the beam, as shown in Figure 4-3, the deflection curve of the beam can be described piecewise as:

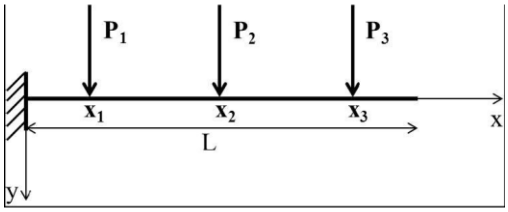


**Figure 4-3 Cantilever beam with three concentrated loads**

$$y = \frac{(P_1x_1 + P_2x_2 + P_3x_3)}{2EI}x^2 - \frac{(P_1 + P_2 + P_3)}{6EI}x^3 \quad 0 \le x \le x_1 \tag{4-9}$$

$$\begin{aligned} y &= \frac{P_1}{3EI}x_1^3 + \frac{P_1}{2EI}x_1^2(x - x_1) \\ &+ \frac{(P_2x_2 + P_3x_3)}{2EI}x^2 - \frac{(P_2 + P_3)}{6EI}x^3 \end{aligned} \quad x_1 \le x \le x_2 \tag{4-10}$$

$$\begin{aligned} y &= \frac{P_1}{3EI}x_1^3 + \frac{P_1}{2EI}x_1^2(x - x_1) \\ &+ \frac{P_2}{3EI}x_2^3 + \frac{P_2}{2EI}x_2^2(x - x_2) \quad x_2 \le x \le x_3 \\ &+ \frac{P_3x_3}{2EI}x^2 - \frac{P_3}{6EI}x^3 \end{aligned} \tag{4-11}$$

$$\begin{aligned} y &= \frac{P_1}{3EI}x_1^3 + \frac{P_1}{2EI}x_1^2(x - x_1) \\ &+ \frac{P_2}{3EI}x_2^3 + \frac{P_2}{2EI}x_2^2(x - x_2) \quad x_3 \le x \le L \\ &+ \frac{P_3}{3EI}x_3^3 + \frac{P_3}{2EI}x_3^2(x - x_3) \end{aligned} \tag{4-12}$$

The three transverse loads $P_1$, $P_2$ and $P_3$ in the above equations are unknown. Their value can be determined by expressing them as a function of the desired deflections $y_1$, $y_2$ and $y_3$ and of the loading points $x_1$, $x_2$ and $x_3$. The following matrix of three equations in the three unknowns $P_1$, $P_2$ and $P_3$ was obtained:

A*p=b **(4-13)**

Where p is a vector containing the three unknown applied loads $P_1$, $P_2$ and $P_3$, A and b are two matrices 3x3 and 3x1 whose terms are known and equal to:

$$A=\begin{pmatrix} 2x_1^3 & 3x_1^2x_2-x_1^3 & 3x_1^2x_3-x_1^3 \\ 3x_1^2x_2-x_1^3 & 2x_2^3 & 3x_2^2x_3-x_2^3 \\ 3x_1^2x_3-x_1^3 & 3x_2^2x_3-x_2^3 & 2x_3^3 \end{pmatrix},\ p=\begin{pmatrix} \frac{P_1}{6EI} \\ \frac{P_2}{6EI} \\ \frac{P_3}{6EI} \end{pmatrix},\ b=\begin{pmatrix} y_1 \\ y_2 \\ y_3 \end{pmatrix}$$

It is possible to solve the matrix 4.13 for each combination of $N_1(x_1,y_1)$, $N_2(x_2,y_2)$, $N_3(x_3,y_3)$ to obtain three loads $P_1$, $P_2$ and $P_3$ to apply.

### 4.2.2 Beam with Four Loads

The same procedure was repeated for a cantilever beam subjected to four concentrate transverse loads, as shown in Figure 4-4.

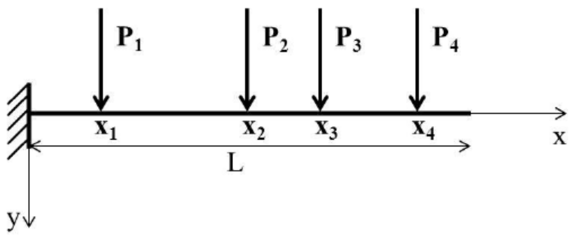


**Figure 4-4 Cantilever beam with four concentrated loads**

Follow a similar approach, the beam curve can be described piecewise as:

$$y=\frac{(P_1x_1+P_2x_2+P_3x_3+P_4x_4)}{2EI}x^2-\frac{(P_1+P_2+P_3+P_4)}{6EI}x^3 \quad 0\le \mathrm{x}\le \mathrm{x}_1 \tag{4-14}$$

$$\begin{aligned} \mathrm{y}&=\frac{P_1}{3EI}x_1^3+\frac{P_1}{2EI}x_1^2(x-x_1) \\ &+\frac{(P_2x_2+P_3x_3+P_4x_4)}{2EI}x^2-\frac{(P_2+P_3+P_4)}{6EI}x^3 \end{aligned} \quad \mathrm{x}_1\le \mathrm{x}\le \mathrm{x}_2 \tag{4-15}$$

$$\begin{aligned} y = &\frac{P_1}{3EI}x_1^3 + \frac{P_1}{2EI}x_1^2(x-x_1) \\ &+\frac{P_2}{3EI}x_2^3 + \frac{P_2}{2EI}x_2^2(x-x_2) \qquad x_2 \le x \le x_3 \\ &+\frac{(P_3x_3+P_4x_4)}{2EI}x^2 - \frac{(P_3+P_4)}{6EI}x^3 \end{aligned} \tag{4-16}$$

$$\begin{aligned} y = &\frac{P_1}{3EI}x_1^3 + \frac{P_1}{2EI}x_1^2(x-x_1) \\ &+\frac{P_2}{3EI}x_2^3 + \frac{P_2}{2EI}x_2^2(x-x_2) \qquad x_3 \le x \le x_4 \\ &+\frac{P_3}{3EI}x_3^3 + \frac{P_3}{2EI}x_3^2(x-x_3) \\ &+\frac{P_4x_4}{2EI}x^2 - \frac{P_4}{6EI}x^3 \end{aligned} \tag{4-17}$$

$$\begin{aligned} y = &\frac{P_1}{3EI}x_1^3 + \frac{P_1}{2EI}x_1^2(x-x_1) \\ &+\frac{P_2}{3EI}x_2^3 + \frac{P_2}{2EI}x_2^2(x-x_2) \qquad x_4 \le x \le L \\ &+\frac{P_3}{3EI}x_3^3 + \frac{P_3}{2EI}x_3^2(x-x_3) \\ &+\frac{P_4}{3EI}x_4^3 + \frac{P_4}{2EI}x_4^2(x-x_4) \end{aligned} \tag{4-18}$$

The four transverse loads $P_1$, $P_2$, P3 and $P_4$ in the above equations are unknown. Their value also can be determined by expressing them as a function of the desired deflections $y_1$, $y_2$, $y_3$ and $y_4$ and of the loading points $x_1$, $x_2$, $x_3$ and $x_4$. The following matrix of four equations in the four unknowns $P_1$, $P_2$, $P_3$ and $P_4$ was obtained:

A*P=b **(4-19)**

Where p is a vector containing the four unknown applied loads $P_1$, $P_2$, $P_3$ and $P_4$, A and b are two matrices 4 x 4 and 4 x 1 whose terms are known and equal to:

$$A=\begin{pmatrix} 2x_1^3 & 3x_1^2x_2-x_1^3 & 3x_1^2x_3-x_1^3 & 3x_1^2x_4-x_1^3 \\ 3x_1^2x_2-x_1^3 & 2x_2^3 & 3x_2^2x_3-x_2^3 & 3x_4x_2^2-x_2^3 \\ 3x_1^2x_3-x_1^3 & 3x_2^2x_3-x_2^3 & 2x_3^3 & 3x_3^2x_4-x_3^3 \\ 3x_1^2x_4-x_1^3 & 3x_4x_2^2-x_2^3 & 3x_3^2x_4-x_3^3 & 2x_4^3 \end{pmatrix},\ p=\begin{pmatrix} \dfrac{P_1}{6EI} \\ \dfrac{P_2}{6EI} \\ \dfrac{P_3}{6EI} \\ \dfrac{P_4}{6EI} \end{pmatrix},\ b=\begin{pmatrix} y1 \\ y2 \\ y3 \\ y4 \end{pmatrix}$$

### 4.2.3 Beam with Five Loads

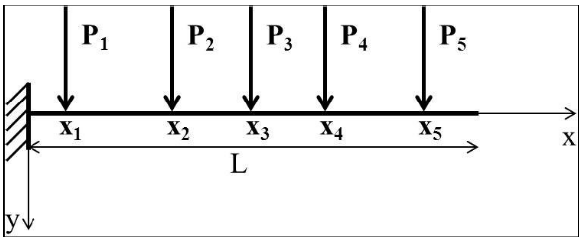


**Figure 4-5 Cantilever beam with five concentrated transverse loads**

The case of a cantilever beam subject to five transverse loads was also considered. The deflection curve can be described piecewise as:

$$y=\frac{(\mathrm{P_1x_1+P_2x_2+P_3x_3+P_4x_4+P_5x_5})}{\mathrm{2EI}}\mathrm{x}^2-\frac{(\mathrm{P_1+P_2+P_3+P_4+P_5})}{\mathrm{6EI}}\mathrm{x}^3 \quad 0\le \mathrm{x}\le \mathrm{x_1} \tag{4-20}$$

$$\begin{aligned}\mathrm{y}=&\frac{P_1}{3EI}x_1^3+\frac{P_1}{2EI}x_1^2(x-x_1)\\&+\frac{(P_2x_2+P_3x_3+P_4x_4+\mathrm{P}_5x_5)}{2EI}x^2-\frac{(P_2+P_3+P_4+\mathrm{P}_5)}{6EI}x^3\end{aligned} \quad \mathrm{x_1}\le \mathrm{x}\le \mathrm{x_2} \tag{4-21}$$

$$\begin{aligned}\mathrm{y}=&\frac{P_1}{3EI}x_1^3+\frac{P_1}{2EI}x_1^2(x-x_1)\\&+\frac{P_2}{3EI}x_2^3+\frac{P_2}{2EI}x_2^2(x-x_2)\\&+\frac{(P_3x_3+P_4x_4+\mathrm{P}_5x_5)}{2EI}x^2-\frac{(P_3+P_4+\mathrm{P}_5)}{6EI}x^3\end{aligned} \quad \mathrm{x_2}\le \mathrm{x}\le \mathrm{x_3} \tag{4-22}$$

$$
\begin{aligned}
\mathrm{y} = {} & \frac{P_1}{3EI}x_1^3 + \frac{P_1}{2EI}x_1^2(x-x_1) \\
& + \frac{P_2}{3EI}x_2^3 + \frac{P_2}{2EI}x_2^2(x-x_2) \\
& + \frac{P_3}{3EI}x_3^3 + \frac{P_3}{2EI}x_3^2(x-x_3) \\
& + \frac{(P_4x_4 + \mathrm{P}_5x_5)}{2EI}x^2 - \frac{(P_4+P_5)}{6EI}x^3
\end{aligned}
\qquad \mathrm{x}_3 \le \mathrm{x} \le \mathrm{x}_4 \tag{4-23}
$$

$$
\begin{aligned}
\mathrm{y} = {} & \frac{P_1}{3EI}x_1^3 + \frac{P_1}{2EI}x_1^2(x-x_1) \\
& + \frac{P_2}{3EI}x_2^3 + \frac{P_2}{2EI}x_2^2(x-x_2) \\
& + \frac{P_3}{3EI}x_3^3 + \frac{P_3}{2EI}x_3^2(x-x_3) \quad \mathrm{x}_4 \le \mathrm{x} \le \mathrm{x}_5 \\
& + \frac{P_4}{3EI}x_4^3 + \frac{P_4}{2EI}x_4^2(x-x_4) \\
& + \frac{\mathrm{P}_5x_5}{2EI}x^2 - \frac{P_5}{6EI}x^3
\end{aligned}
\tag{4-24}
$$

$$
\begin{aligned}
\mathrm{y} = {} & \frac{P_1}{3EI}x_1^3 + \frac{P_1}{2EI}x_1^2(x-x_1) \\
& + \frac{P_2}{3EI}x_2^3 + \frac{P_2}{2EI}x_2^2(x-x_2) \\
& + \frac{P_3}{3EI}x_3^3 + \frac{P_3}{2EI}x_3^2(x-x_3) \qquad \mathrm{x}_5 \le \mathrm{x} \le \mathrm{L} \\
& + \frac{P_4}{3EI}x_4^3 + \frac{P_4}{2EI}x_4^2(x-x_4) \\
& + \frac{P_5}{3EI}x_5^3 + \frac{P_5}{2EI}x_5^2(x-x_5)
\end{aligned}
\tag{4-25}
$$

$$
A = \begin{pmatrix}
2x_1^3 & 3x_1^2x_2 - x_1^3 & 3x_1^2x_3 - x_1^3 & 3x_1^2x_4 - x_1^3 & 3x_1^2x_5 - x_1^3 \\
3x_1^2x_2 - x_1^3 & 2x_2^3 & 3x_2^2x_3 - x_2^3 & 3x_4x_2^2 - x_2^3 & 3x_5x_2^2 - x_2^3 \\
3x_1^2x_3 - x_1^3 & 3x_2^2x_3 - x_2^3 & 2x_3^3 & 3x_3^2x_4 - x_3^3 & 3x_3^2x_5 - x_3^3 \\
3x_1^2x_4 - x_1^3 & 3x_4x_2^2 - x_2^3 & 3x_3^2x_4 - x_3^3 & 2x_4^3 & 3x_4^2x_5 - x_4^3 \\
3x_1^2x_5 - x_1^3 & 3x_5x_2^2 - x_2^3 & 3x_3^2x_5 - x_3^3 & 3x_5x_4^2 - x_4^3 & 2x_5^3
\end{pmatrix},
\quad p = \begin{pmatrix} \frac{P_1}{6EI} \\ \frac{P_2}{6EI} \\ \frac{P_3}{6EI} \\ \frac{P_4}{6EI} \\ \frac{P_5}{6EI} \end{pmatrix},
\quad b = \begin{pmatrix} y1 \\ y2 \\ y3 \\ y4 \\ y5 \end{pmatrix}
$$

The beam approximation adopted in this paragraph provided a simple but effective way to represent the trailing edge deflection under transverse loads and to select the most suitable actuation load distribution for the flap morphing skin. The application of the beam equation automatically allowed achieving a realistic deflection of the structure.

### 4.2.4 Beam under Tapered Distributed Aerodynamic Load

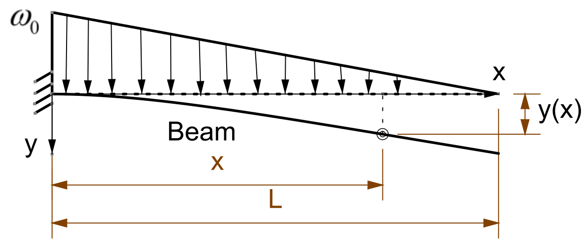


**Figure 4-6 Beam under tapered distributed load**

The morphing skin is not only actuated by the concentrate transverse loads but also withstands the aerodynamic load. The aerodynamic load in this thesis was obtained from xfoil [22] calculation, considering a flap with span of 500mm and chord of 1200mm, under the Mach number of 0.2, Reynolds number of $6\times10^6$, and with the angle of attack of 13°. The pressure coefficient $c_p$ versus x was exported from the xfoil program and read by MATLAB. As showed in Figure 4-7, the aerodynamic load of the trailing edge part can be approximated as tapered distributed load because the load exported from the xfoil program have little differences compared to the tapered distributed load.

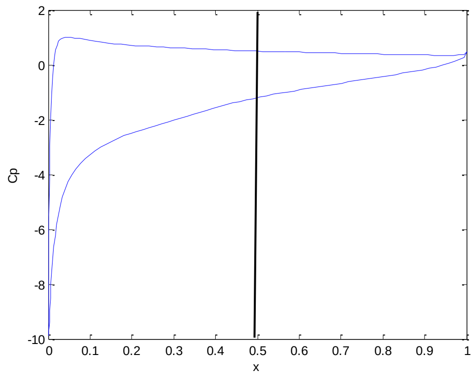


**Figure 4-7 Pressure coefficient $c_p$ versus x**

The load was calculated from $C_{PU}$ and $C_{PL}$ and multiplied by a dynamic pressure, which is 1/2*ρ*$\upsilon_\infty^2$. $C_{PU}$ is the pressure coefficient of upper surface; $C_{PL}$ is the pressure coefficient of lower surface. $P_U$ is the pressure on the upper surface, $P_L$ is the pressure on the lower surface, $P_\infty$ is the pressure of the same altitude at infinite place, ρ is the density of the air, $\upsilon_\infty$ is the velocity of the freestream. The equation for the $C_{PU}$ and $C_{PL}$ can be described as follows:

$$C_{PU} = \frac{P_U - P_\infty}{\frac{1}{2}\rho\upsilon_\infty^2} \tag{4-26}$$

$$C_{PL} = \frac{P_L - P_\infty}{\frac{1}{2}\rho\upsilon_\infty^2} \tag{4-27}$$

$$\begin{aligned} P_U - P_L &= (C_{PU} - C_{PL}) \times \frac{1}{2}\rho\upsilon_\infty^2 \\ &= (-1.18 - 0.4981) \times 0.5 \times 1.27 \times (0.2 \times 340)^2 \\ &= -4.9273e + 03N / m^2 \end{aligned} \tag{4-28}$$

$$\omega_0 = (P_U - P_L) \times S \tag{4-29}$$

Where S is the span of the morphing skin, and S=0.5m,

Hence:

$$\omega_0 = (P_U - P_L) \times s = 2463.65N / m \tag{4-30}$$

As discussed in equation 3-1, the cantilever beam under tapered distributed load, the deflection equation is as follow:

$$\mathrm{y1}(x) = \frac{2463.65}{\mathrm{EI}} \frac{1}{\mathrm{L}} [\frac{L^3x^2}{12} - \frac{x^5}{120} - \frac{L^2x^3}{12} + \frac{Lx^4}{24}] \quad 0 \le x \le 0.6 \tag{4-31}$$

## 4.3 The Achieved Morphing Shape

This section consists of superimposing of three loads, four loads and five loads situation with the aerodynamic load. The loads applied to each position can be calculated, and the achieved deflected shape can be obtained. By comparing with the target deflected shape, the objective function of the optimization can be obtained.

### 4.3.1 Beam under Three Loads and Aerodynamic Load

Once the aerodynamic load and three positions of the support disc are known, by superimposing the function, the following results are obtained:

| | |
|---|---|
| $\mathrm{y1}(x_1)=\frac{2463.65}{\mathrm{EI}}\frac{1}{\mathrm{L}}[\frac{L^3x_1^2}{12}-\frac{x_1^5}{120}-\frac{L^2x_1^3}{12}+\frac{Lx_1^4}{24}]$ | **(4-32)** |
| $\mathrm{y1}(x_2)=\frac{2463.65}{\mathrm{EI}}\frac{1}{\mathrm{L}}[\frac{L^3x_2^2}{12}-\frac{x_2^5}{120}-\frac{L^2x_2^3}{12}+\frac{Lx_2^4}{24}]$ | **(4-33)** |
| $\mathrm{y1}(x_3)=\frac{2463.65}{\mathrm{EI}}\frac{1}{\mathrm{L}}[\frac{L^3x_3^2}{12}-\frac{x_3^5}{120}-\frac{L^2x_3^3}{12}+\frac{Lx_3^4}{24}]$ | **(4-34)** |

Function y1 is the deflection caused by the aerodynamic load, y3 is the deflection caused by the three disc support.

The matrix system for three transverse loads is A*p=b, hence p=A\b:

$$A=\begin{pmatrix} 2x_1^3 & 3x_1^2x_2-x_1^3 & 3x_1^2x_3-x_1^3 \\ 3x_1^2x_2-x_1^3 & 2x_2^3 & 3x_2^2x_3-x_2^3 \\ 3x_1^2x_3-x_1^3 & 3x_2^2x_3-x_2^3 & 2x_3^3 \end{pmatrix}\quad p=\begin{pmatrix} \frac{P_1}{6EI} \\ \frac{P_2}{6EI} \\ \frac{P_3}{6EI} \end{pmatrix}\quad b=\begin{pmatrix} y3(x_1) \\ y3(x_2) \\ y3(x_3) \end{pmatrix} \qquad \textbf{(4-35)}$$

And the target deflected shape is:

$$\mathrm{y}(x)=\text{-}0.2693\mathrm{x}^5+0.808\mathrm{x}^4-0.9696\mathrm{x}^3+0.5818\mathrm{x}^2 \qquad \textbf{(4-36)}$$

Hence, it becomes:

$$\begin{cases} y1(x_1)+y3(x_1)=y(x_1) \\ y1(x_2)+y3(x_2)=y(x_2) \\ y1(x_3)+y3(x_3)=y(x_3) \end{cases} \Rightarrow \begin{cases} y3(x_1)=y(x_1)-y1(x_1) \\ y3(x_2)=y(x_2)-y1(x_2) \\ y3(x_3)=y(x_3)-y1(x_3) \end{cases} \qquad \textbf{(4-37)}$$

Substitute equation 4-37 into 4-35, the value of p can be determined.

$$b = \begin{pmatrix} y(x_1) - y1(x_1) \\ y(x_2) - y1(x_2) \\ y(x_3) - y1(x_3) \end{pmatrix} \tag{4-38}$$

$$p = A \backslash b = \begin{pmatrix} 2x_1^3 & 3x_1^2 x_2 - x_1^3 & 3x_1^2 x_3 - x_1^3 \\ 3x_1^2 x_2 - x_1^3 & 2x_2^3 & 3x_2^2 x_3 - x_2^3 \\ 3x_1^2 x_3 - x_1^3 & 3x_2^2 x_3 - x_2^3 & 2x_3^3 \end{pmatrix} \backslash \begin{pmatrix} y(x_1) - y1(x_1) \\ y(x_2) - y1(x_2) \\ y(x_3) - y1(x_3) \end{pmatrix} \tag{4-39}$$

At this stage, the loads $P_1$, $P_2$ and $P_3$ are obtained. They were then applied back to the equation 4-9, 4-10, 4-11 and 4-12 and superimpose with y1(x) to get the achieved deflected shape. How to choose the three positions of the support discs refer to section 4.5. Four and five positions of the support discs are similar.

### 4.3.2 Beam under Four Loads and Aerodynamic Load

Once again, by using the same procedure, the aerodynamic load with four positions of the support disc is considered, by superimposing the function, the results are as follows:

$$\mathrm{y1}(x_1) = \frac{2463.65}{\mathrm{EI}} \frac{1}{\mathrm{L}} [\frac{L^3 x_1^2}{12} - \frac{x_1^5}{120} - \frac{L^2 x_1^3}{12} + \frac{L x_1^4}{24}] \tag{4-40}$$

$$\mathrm{y1}(x_2) = \frac{2463.65}{\mathrm{EI}} \frac{1}{\mathrm{L}} [\frac{L^3 x_2^2}{12} - \frac{x_2^5}{120} - \frac{L^2 x_2^3}{12} + \frac{L x_2^4}{24}] \tag{4-41}$$

$$\mathrm{y1}(x_3) = \frac{2463.65}{\mathrm{EI}} \frac{1}{\mathrm{L}} [\frac{L^3 x_3^2}{12} - \frac{x_3^5}{120} - \frac{L^2 x_3^3}{12} + \frac{L x_3^4}{24}] \tag{4-42}$$

$$\mathrm{y1}(x_4) = \frac{2463.65}{\mathrm{EI}} \frac{1}{\mathrm{L}} [\frac{L^3 x_4^2}{12} - \frac{x_4^5}{120} - \frac{L^2 x_4^3}{12} + \frac{L x_4^4}{24}] \tag{4-43}$$

The matrix system for four transverse loads is A*p=b:

$$A=\begin{pmatrix} 2x_1^3 & 3x_1^2x_2-x_1^3 & 3x_1^2x_3-x_1^3 & 3x_1^2x_4-x_1^3 \\ 3x_1^2x_2-x_1^3 & 2x_2^3 & 3x_2^2x_3-x_2^3 & 3x_4x_2^2-x_2^3 \\ 3x_1^2x_3-x_1^3 & 3x_2^2x_3-x_2^3 & 2x_3^3 & 3x_3^2x_4-x_3^3 \\ 3x_1^2x_4-x_1^3 & 3x_4x_2^2-x_2^3 & 3x_3^2x_4-x_3^3 & 2x_4^3 \end{pmatrix} \quad p=\begin{pmatrix} \frac{P_1}{6EI} \\ \frac{P_2}{6EI} \\ \frac{P_3}{6EI} \\ \frac{P_4}{6EI} \end{pmatrix} \quad b=\begin{pmatrix} y4(x_1) \\ y4(x_2) \\ y4(x_3) \\ y4(x_4) \end{pmatrix} \qquad \textbf{(4-44)}$$

And the target deflected shape is:

$$\mathrm{y}(x)=-0.2693\mathrm{x}^5+0.808\mathrm{x}^4-0.9696\mathrm{x}^3+\ 0.5818\mathrm{x}^2 \qquad \textbf{(4-45)}$$

Hence, it becomes:

$$\begin{cases} y1(x_1)+y4(x_1)=y(x_1) \\ y1(x_2)+y4(x_2)=y(x_2) \\ y1(x_3)+y4(x_3)=y(x_3) \\ y1(x_4)+y4(x_4)=y(x_4) \end{cases} \Rightarrow \begin{cases} y4(x_1)=y(x_1)-y1(x_1) \\ y4(x_2)=y(x_2)-y1(x_2) \\ y4(x_3)=y(x_3)-y1(x_3) \\ y4(x_4)=y(x_4)-y1(x_4) \end{cases} \qquad \textbf{(4-46)}$$

Substitute equation 4.46 into 4.44, the value of p can be determined.

$$b=\begin{pmatrix} y(x_1)-y1(x_1) \\ y(x_2)-y1(x_2) \\ y(x_3)-y1(x_3) \\ y(x_4)-y1(x_4) \end{pmatrix} \qquad \textbf{(4-47)}$$

$$p=A\backslash b=\begin{pmatrix} 2x_1^3 & 3x_1^2x_2-x_1^3 & 3x_1^2x_3-x_1^3 & 3x_1^2x_4-x_1^3 \\ 3x_1^2x_2-x_1^3 & 2x_2^3 & 3x_2^2x_3-x_2^3 & 3x_4x_2^2-x_2^3 \\ 3x_1^2x_3-x_1^3 & 3x_2^2x_3-x_2^3 & 2x_3^3 & 3x_3^2x_4-x_3^3 \\ 3x_1^2x_4-x_1^3 & 3x_4x_2^2-x_2^3 & 3x_3^2x_4-x_3^3 & 2x_4^3 \end{pmatrix} \backslash \begin{pmatrix} y(x_1)-y1(x_1) \\ y(x_2)-y1(x_2) \\ y(x_3)-y1(x_3) \\ y(x_4)-y1(x_4) \end{pmatrix} \qquad \textbf{(4-48)}$$

At this stage, the loads $P_1$, $P_2$, $P_3$ and $P_4$ are obtained. They were then applied back to the equation 4.14 - 4.18 and superimpose with y1(x) to get the achieved deflected shape.

### 4.3.3 Beam under Five Loads and Aerodynamic Load

Once again, by using the same procedure, the aerodynamic load with five positions of the support disc is considered, by superimposing the function, the following results are obtained:

$$\mathrm{y1}(x_1)=\frac{2463.65}{\mathrm{EI}}\frac{1}{\mathrm{L}}[\frac{L^3x_1^2}{12}-\frac{x_1^5}{120}-\frac{L^2x_1^3}{12}+\frac{Lx_1^4}{24}] \quad \textbf{(4-49)}$$

$$\mathrm{y1}(x_2)=\frac{2463.65}{\mathrm{EI}}\frac{1}{\mathrm{L}}[\frac{L^3x_2^2}{12}-\frac{x_2^5}{120}-\frac{L^2x_2^3}{12}+\frac{Lx_2^4}{24}] \quad \textbf{(4-50)}$$

$$\mathrm{y1}(x_3)=\frac{2463.65}{\mathrm{EI}}\frac{1}{\mathrm{L}}[\frac{L^3x_3^2}{12}-\frac{x_3^5}{120}-\frac{L^2x_3^3}{12}+\frac{Lx_3^4}{24}] \quad \textbf{(4-51)}$$

$$\mathrm{y1}(x_4)=\frac{2463.65}{\mathrm{EI}}\frac{1}{\mathrm{L}}[\frac{L^3x_4^2}{12}-\frac{x_4^5}{120}-\frac{L^2x_4^3}{12}+\frac{Lx_4^4}{24}] \quad \textbf{(4-52)}$$

$$\mathrm{y1}(x_5)=\frac{2463.65}{\mathrm{EI}}\frac{1}{\mathrm{L}}[\frac{L^3x_5^2}{12}-\frac{x_5^5}{120}-\frac{L^2x_5^3}{12}+\frac{Lx_5^4}{24}] \quad \textbf{(4-53)}$$

The matrix system for five transverse loads is A*p=b:

$$A=\begin{pmatrix} 2x_1^3 & 3x_1^2x_2-x_1^3 & 3x_1^2x_3-x_1^3 & 3x_1^2x_4-x_1^3 & 3x_1^2x_5-x_1^3 \\ 3x_1^2x_2-x_1^3 & 2x_2^3 & 3x_2^2x_3-x_2^3 & 3x_4x_2^2-x_2^3 & 3x_5x_2^2-x_2^3 \\ 3x_1^2x_3-x_1^3 & 3x_2^2x_3-x_2^3 & 2x_3^3 & 3x_3^2x_4-x_3^3 & 3x_3^2x_5-x_3^3 \\ 3x_1^2x_4-x_1^3 & 3x_4x_2^2-x_2^3 & 3x_3^2x_4-x_3^3 & 2x_4^3 & 3x_4^2x_5-x_4^3 \\ 3x_1^2x_5-x_1^3 & 3x_5x_2^2-x_2^3 & 3x_3^2x_5-x_3^3 & 3x_5x_4^2-x_4^3 & 2x_5^3 \end{pmatrix} p=\begin{pmatrix} \frac{P_1}{6EI} \\ \frac{P_2}{6EI} \\ \frac{P_3}{6EI} \\ \frac{P_4}{6EI} \\ \frac{P_5}{6EI} \end{pmatrix} b=\begin{pmatrix} y5(x_1) \\ y5(x_2) \\ y5(x_3) \\ y5(x_4) \\ y5(x_5) \end{pmatrix} \quad \textbf{(4-54)}$$

And the target deflected shape is:

$$\mathrm{y}(x)=-0.2693\mathrm{x}^5+0.808\mathrm{x}^4-0.9696\mathrm{x}^3+\ 0.5818\mathrm{x}^2 \quad \textbf{(4-55)}$$

Hence, it becomes:

$$\begin{cases} y1(x_1)+y5(x_1)=y(x_1) \\ y1(x_2)+y5(x_2)=y(x_2) \\ y1(x_3)+y5(x_3)=y(x_3) \\ y1(x_4)+y5(x_4)=y(x_4) \\ y1(x_5)+y5(x_5)=y(x_5) \end{cases} \Rightarrow \begin{cases} y5(x_1)=y(x_1)-y1(x_1) \\ y5(x_2)=y(x_2)-y1(x_2) \\ y5(x_3)=y(x_3)-y1(x_3) \\ y5(x_4)=y(x_4)-y1(x_4) \\ y5(x_5)=y(x_5)-y1(x_5) \end{cases} \tag{4-56}$$

Substitute equation 4.56 to 4.54, the value of p can be determined.

$$b=\begin{pmatrix} y(x_1)-y1(x_1) \\ y(x_2)-y1(x_2) \\ y(x_3)-y1(x_3) \\ y(x_4)-y1(x_4) \\ y(x_5)-y1(x_5) \end{pmatrix} \tag{4-57}$$

$$p=A\backslash b=\begin{pmatrix} 2x_1^3 & 3x_1^2x_2-x_1^3 & 3x_1^2x_3-x_1^3 & 3x_1^2x_4-x_1^3 & 3x_1^2x_5-x_1^3 \\ 3x_1^2x_2-x_1^3 & 2x_2^3 & 3x_2^2x_3-x_2^3 & 3x_4x_2^2-x_2^3 & 3x_5x_2^2-x_2^3 \\ 3x_1^2x_3-x_1^3 & 3x_2^2x_3-x_2^3 & 2x_3^3 & 3x_3^2x_4-x_3^3 & 3x_3^2x_5-x_3^3 \\ 3x_1^2x_4-x_1^3 & 3x_4x_2^2-x_2^3 & 3x_3^2x_4-x_3^3 & 2x_4^3 & 3x_4^2x_5-x_4^3 \\ 3x_1^2x_5-x_1^3 & 3x_5x_2^2-x_2^3 & 3x_3^2x_5-x_3^3 & 3x_5x_4^2-x_4^3 & 2x_5^3 \end{pmatrix}\backslash\begin{pmatrix} y(x_1)-y1(x_1) \\ y(x_2)-y1(x_2) \\ y(x_3)-y1(x_3) \\ y(x_4)-y1(x_4) \\ y(x_5)-y1(x_5) \end{pmatrix} \tag{4-58}$$

At this stage, the loads $P_1$, $P_2$, $P_3$, $P_4$ and $P_5$ are obtained. They were then applied back to the equation 4.20-4.25 and superimpose with y1(x) to get the achieved deflected shape.

## 4.4 Actuation Torque Evaluation

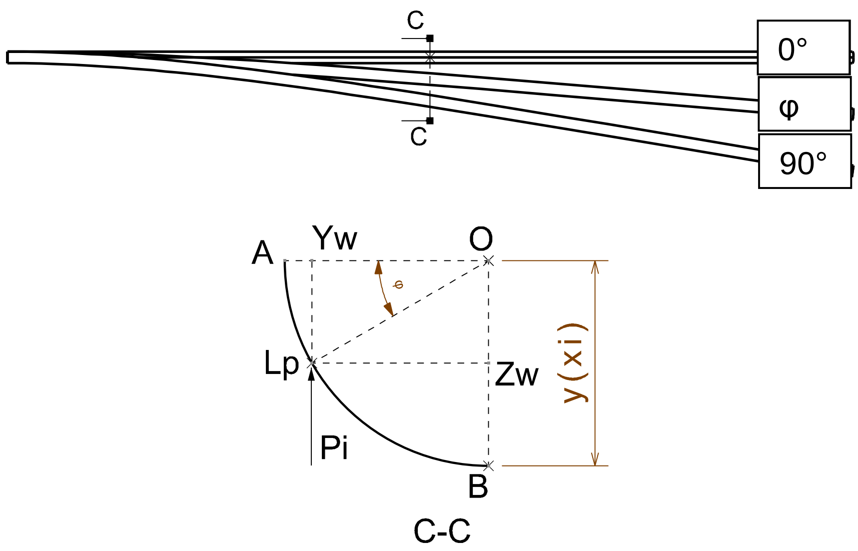


**Figure 4-8 Torque calculation at position $x_i$**

As shown in Figure 4-8, the eccentric beam actuates the skins to the desired shape, O is the rotate centre, A is the initial position of the beam at $x_i$, B is the position of A after morphing, $L_p$ stands for the medium position during the rotation angle φ. $P_i$ is load comes from morphing and aerodynamic load. As the connections between the skins and beam are discs, the load generated from morphing and aerodynamic load can be confirmed as along Z direction, hence the torque becomes:

$$\mathrm{T_i} = \mathrm{P_i} \times \mathrm{Y_w} \tag{4-59}$$

While:

$$\mathrm{Y_w} = \mathrm{y}(x_i) \times \cos(\varphi) \tag{4-60}$$

$$\mathrm{Z_w} = \mathrm{y}(\mathrm{x}_i) \times \sin(\varphi) \tag{4-61}$$

Due to lack of aerodynamic load data at every rotating angle φ, one simplified method is to assume that the morphing load together with aerodynamic load at 90° rotation applies to the 0° rotation status. Because maximum aerodynamic load and maximum morphing load both appears at 90° rotation, while the biggest moment arm appears at 0° rotation. This will increase the magnitude of torque, but due to the morphing load only accounted for a small part (about 10%, refer to table 4-2, table 4-3) of the total load, it is still possible to compare with different number of support positions.

Here it comes:

$$\mathrm{T_i} = \mathrm{P_i} \times \mathrm{Y_w} = \mathrm{P_i} \times y(x_i) \tag{4-62}$$

For a cantilever beam with three transverse loads at eccentric position, the torque diagram refers to Figure 4-9.

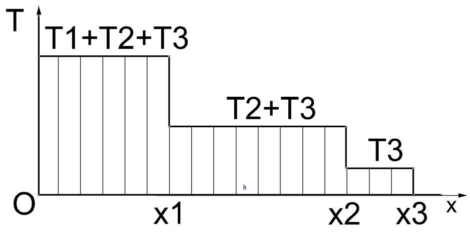


**Figure 4-9 Torque diagram along x direction**

$$T=\sum_{i=1}^{n} T_i \text{ (n=3, 4 and 5)} \quad \textbf{(4-63)}$$

Then 3, 4 and 5 support positions of the torque at the root of the beam will be calculated, and the one with least torque should be chosen. Based on the above equation, the torque needed for the actuator can be calculated.

## 4.5 Objective Function of the Optimization

In this thesis, the objective of optimization is to minimize the differences between the target shape and achieved deflected shape. For the optimization using ‘optimization tool box’, an initial value $x_0$= [L/i, L*2/i, ... , L*i/i] (i=3,4,5) is given to finish the optimization. For the optimization using MATLAB code, the position is generated by the permutation and combination. For example, x=linspace (0, 0.6, 6)=[0 0.12 0.24 0.36 0.48 0.6] divide the length 0.6 into 5(=6-1) same parts. N=combntns (2:6, 3) will calculate all the possible combination to choose 3 from 2 to 6 and store the vector in N matrix. N= $[2\ 3\ 4;2\ 3\ 5;2\ 3\ 6;2\ 4\ 5;2\ 4\ 6;\ 2\ 5\ 6;3\ 4\ 5;3\ 4\ 6;3\ 5\ 6;4\ 5\ 6]$ , and x(N(1,;)) means [x(2),x(3),x(4)]=[0.12, 0.24, 0.36]. The equation for the target shape and achieved deflected shape has been described before. The difference is represented as:

$$\Delta y = y1(x) - yi(x) \quad (i = 3,4,5) \ \ 0 \leqslant x \leqslant 0.6 \quad \textbf{(4-64)}$$

The standard deviation of ⍰y is the objective function of the optimization. N includes all the possible combination of position and it can be used to calculate the deflected shape and compared with target shape.

## 4.6 Optimization using 'MATLAB Optimization Toolbox' [24]

MATLAB is a powerful numerical computing environment and programming language. It allows matrix manipulations, plotting of functions and data, implementation of algorithms, creation of user interfaces, and interfacing with programs written in other languages, including C, C++, Java, and FORTRAN. Also, Optimization Toolbox provides widely used algorithms for standard and large-scale optimization. These algorithms solve constrained and unconstrained continuous and discrete problems. The toolbox's optimization software includes functions for linear programming, quadratic programming, binary integer programming, nonlinear optimization, nonlinear least squares, systems of nonlinear equations, and multi-objective optimization. They can be used to find optimal solutions, perform trade-off analyses, balance multiple design alternatives, and incorporate optimization methods into algorithms and models.

In this optimization, the optimization tool 'fmincon' is used to find minimum of constrained nonlinear multi-variable function. It is used to find the minimum of a problem specified by:

$$\min_x f(x) \text{such that} \begin{cases} c(x) \le 0 \\ ceq(x) = 0 \\ A \cdot x \le b \\ Aeq \cdot x = beq \\ lb \le x \le ub \end{cases}$$

Where x, b, beq, lb and ub are vectors, A and Aeq are matrices, c(x) and ceq(x) are functions that return vectors, and f(x) is the objective function that returns a scalar. f(x), c(x), and ceq(x) can be nonlinear functions.

Syntax:

[x, fval, exitflag, output, lambda, grad, hessian]

=fmincon (fun, x0,A,b,Aeq,beq,lb,ub,options)

Description: fmincon attempts to find a constrained minimum of a scalar function of several variables starting at an initial estimate $x_0$. Which is subjected to the linear inequalities A*x ≤ b, and to the linear equalities Aeq*x = beq. Lb and ub defines a set of lower and upper bounds on the design variables in x, so that the solution is always in the range lb ≤ x ≤ ub. If no equalities exist, set Aeq = [] and beq = [] ([] means empty matrix). If linear equalities exist, and $\begin{cases} a_{11}x_1 + a_{12}x_2 + ... + a_{1n}x_n = b_1; \\ a_{21}x_1 + a_{22}x_2 + ... + a_{2n}x_n = b_2; \\ ... \\ a_{n1}x_1 + a_{n2}x_2 + ... + a_{nn}x_n = b_{n.} \end{cases}$, then Aeq=$\begin{bmatrix} a_{11}, a_{12}, ..., a_{1n} \\ a_{21}, a_{22}, ..., a_{2n} \\ ... \\ a_{n1}, a_{n2}, ..., a_{nn} \end{bmatrix}$, b=$\begin{bmatrix} \mathrm{b}_1 \\ b_2 \\ ... \\ b_n \end{bmatrix}$, If no inequalities exist, set A = [] and b = []. Fval returns the function value at x.

### 4.6.1 Study Case 1: One Disc Support Position of the Skin

#### 4.6.1.1 Creation of Objective Function m file

The MATLAB objective function code for this section can be found in Appendix F.1. The objective function is based on the section 4.5 and section 4.2, a support position p is needed as an input, and its deflection is set the same as the target shape, and deflection under aerodynamic load at that point is also calculated. Then by applying superimpose principle the load at point p is obtained. The next step consists of applying the load back to the equation 4-7 and 4-8, and superimpose with the deflection under aerodynamic load, and the curvature of the achieved deflection supported at that point p is obtained and stored in function f1. And the differences between the f1 and target shape y can be obtained by using f=std(f1-y,1,2). f calculates the standard deviation of the f1-y, and return to function myopt1() as an output.

#### 4.6.1.2 Optimization

After the objective function is created, the optimization is done by following steps by typing in MATLAB command window:

x0=0.3; % Set an initial value of position x0

lb=0; % lb stands for the lower boundary condition of x

ub=0.6; % ub stands for the upper boundary condition of x

A=[ ]; b=[ ];  %  No inequalities exist in this section, set A=[ ] and b=[ ] ([ ] means empty matrix)

options=optimset('Tolfun',1e-15,'Tolcon',1e-6,'Display','iter','TolX',1e-10, 'algorithm', 'active-set', 'GradObj','on');

The options set the tolerance for the function, constrains, etc.

[x,fval,exitflag,output,lambda,grad,hessian]=fmincon(@myopt1,x0,A,b,[],[],lb,ub)

The results are as follows:

x=0.3409; fval =0.0021; Maximum difference=0.0059m.

Target shape and achieved shape can be found in Figure 4-9, the differences between them view Figure 4-10.

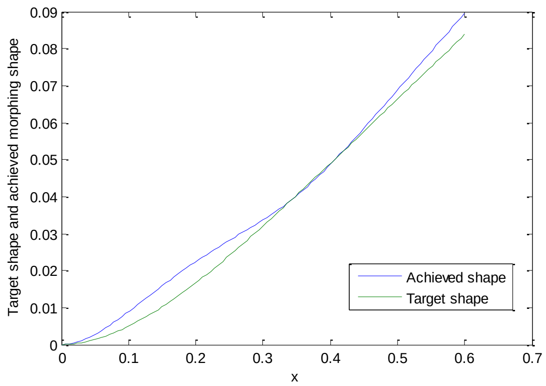


**Figure 4-10  Target shape and Achieved shape**

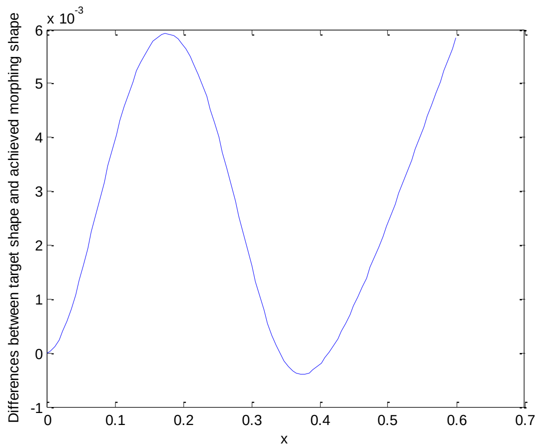


**Figure 4-11  Differences between target shape and achieved morphing shape**

#### 4.6.1.3 Comparison

By typing myopt1(0.3), an achieved shape before optimization can be obtained, and the results are as follows:

$x_0$=0.3, Maximum Difference=0.0356m. Target shape and achieved shape as shown in Figure 4-11, the differences between them as shown in Figure 4-12

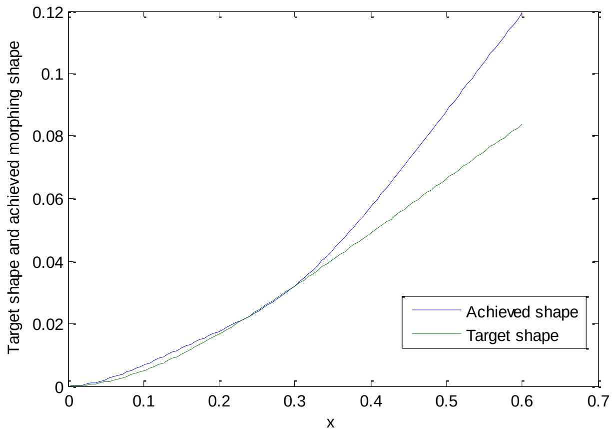


**Figure 4-12 Achieved shape and target shape**

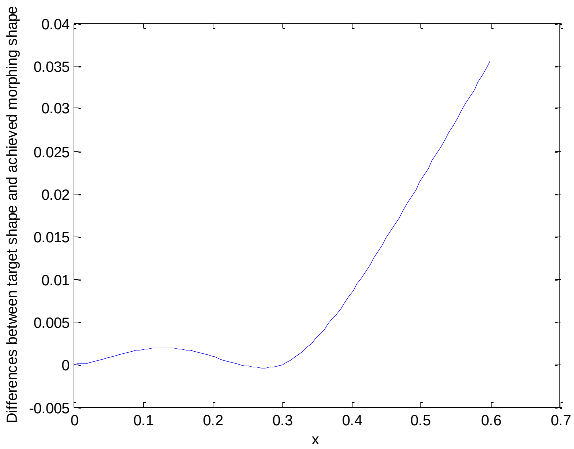


**Figure 4-13 Differences between target shape and achieved morphing shape**

From the pictures and datum above, the maximum difference of the skin deflection from the target shape 0.0356m was observed before optimization, while only 0.0059m was observed after optimization.

### 4.6.2 Study Case 2: Three Disc Support Positions of the Skin

#### 4.6.2.1 Creation of Objective Function m File

The MATLAB objective function code for this section can be found in Appendix F.2. The objective function is based on the section 4.5 and section 4.3, a serial of support positions of p (1 by 3 vector) is needed as an input, and its deflection is set the same as the target shape, and deflection under aerodynamic load at those points are also calculated. Then by applying superimpose principle the loads at vector p is obtained. The next step consists of applying the loads back to the equation 4-9, 4-10, 4-11 and 4-12 and superimpose with deflection under aerodynamic loads to get the achieved deflected shape f1. And the differences between the f1 and target shape y can be obtained by using f=std(f1-y,1,2), f calculates the standard deviation of the f1-y, and return to function myopt3() as an output.

#### 4.6.2.2 Optimization

After the objective function is created, the optimization is done by following steps typing in MATLAB command window:

x0=[0.2, 0.4, 0.6]; % x0 is a vector contains 3 positions

lb=zeros(3,1); % lb stands for the lower boundary condition of x

ub=0.6*ones(3,1); % ub stands for the lower boundary condition of x

A=[1 -1 0;0 1 -1]; b=[0;0];

% Matrix A and vector b comes from the linear inequalities constrains:

$$\begin{cases} x_1 \le x_2 \\ x_2 \le x_3 \end{cases} \Rightarrow \begin{cases} x_1 - x_2 + 0 * x_3 \le 0 \\ 0 * x_1 + x_2 - x_3 \le 0 \end{cases}$$

options=optimset('Tolfun',1e-15,'Tolcon',1e-6,'Display','iter','TolX',1e-10, 'algorithm', 'active-set', 'GradObj','on');

[x]=fmincon(@myopt3,x0,A,b,[],[],lb,ub)

x=[0.1449 0.3001 0.4716]; Maximum Difference is 2.0e-04m

Target shape and achieved shape can be found in Figure 4-13, the differences between them can be found in Figure 4-14. Fmincon will use the active-set algorithm to optimize the objective function and give new x0 as an output.

#### 4.6.2.3 Comparison

By typing myopt3([0.2, 0.4, 0.5]), an achieved shape before optimization can be obtained, and the results are as follows:

$x_0$=[0.2, 0.4, 0.5], Maximum Difference=7.4e-04m. Target shape and achieved shape can be found in Figure 4-15, the differences between them can be found in Figure 4-16.

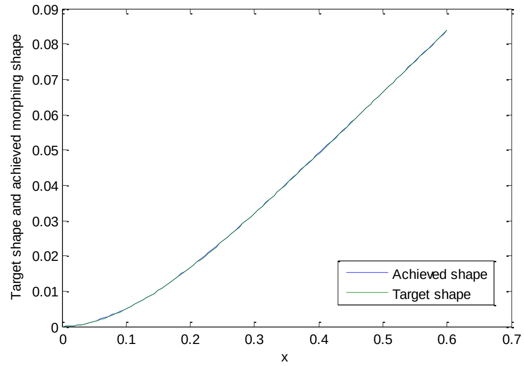


**Figure 4-14 Target shape and Achieved shape**

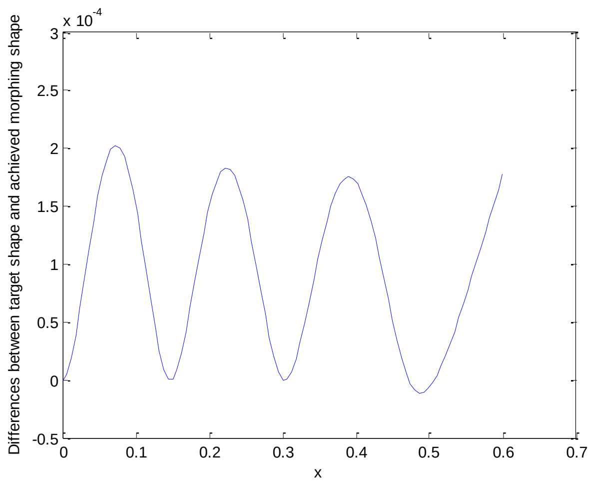


**Figure 4-15 Differences between target shape and achieved shape**

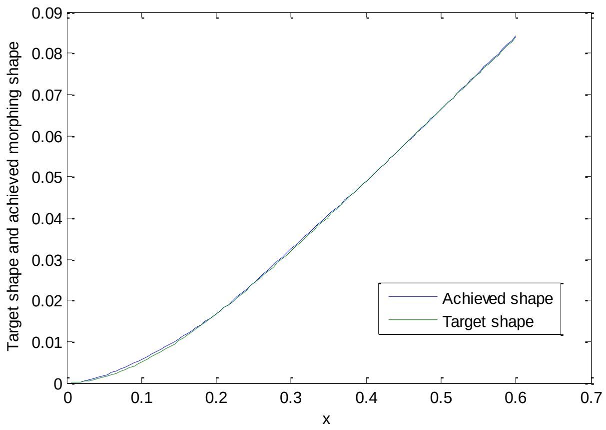


**Figure 4-16 Target shape and Achieved shape**

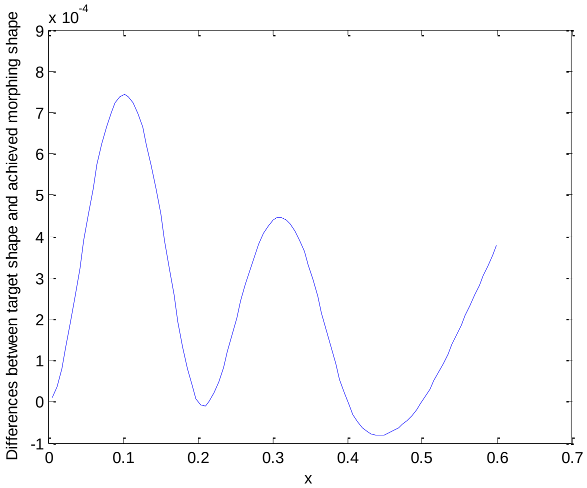


**Figure 4-17 Differences between target shape and achieved shape**

From the pictures and datum above, the maximum difference of the skin deflection from the target shape 7.4e-04m was obtained before optimization, while only 2.0e-04m was obtained after optimization.

## 4.6.3 Study Case 3: Four Disc Support Positions of the Skin

### 4.6.3.1 Creation of Objective Function

The same procedure was repeated for four positions optimization, the objective function for this section can be found in Appendix F.3.

#### 4.6.3.2 Optimization

After the objective function is created, the optimization is done by following steps by typing in MATLAB command window as follows:

x0=0.6*[0.25,0.5,0.75,1]; lb=zeros(4,1); ub=0.6*ones(4,1); A=[1 -1 0 0;0 1 -1 0;0 0 1 -1]; b=[0;0;0];

[x,fval,exitflag,output,lambda]=fmincon(@myopt4,x0,A,b,[],[],lb,ub)

The results are as follows:

x=[0.1296 0.2682 0.4243 0.5999]; Maximum Difference =1.3922e-04m

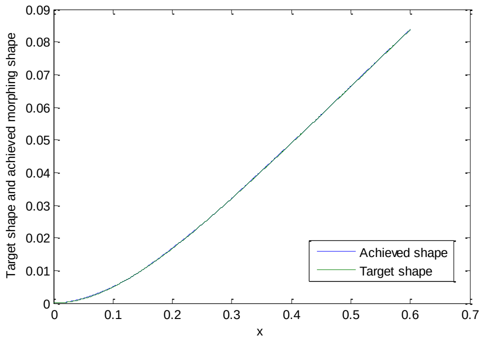


**Figure 4-18 Target shape and achieved shape**

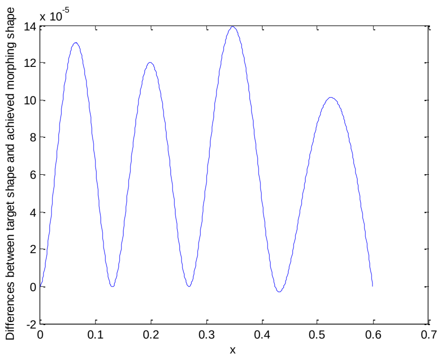


**Figure 4-19 Differences between target shape and achieved morphing shape**

#### 4.6.3.3 Comparison

By typing myopt4 (0.6*[0.25,0.5,0.75,1]), an achieved shape before optimization can be obtained, and the results are as follows:

$x_0$=0.6*[0.25,0.5,0.75,1], Maximum Difference=2.4e-04m. Target shape and achieved shape are shown in Figure 4-19, the differences between them are shown in Figure 4-20.

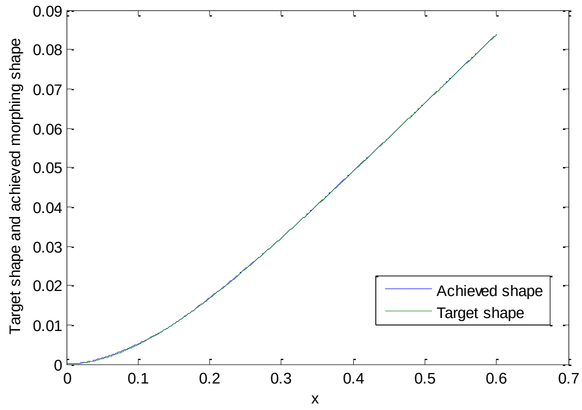


**Figure 4-20 Target shape and achieved shape**

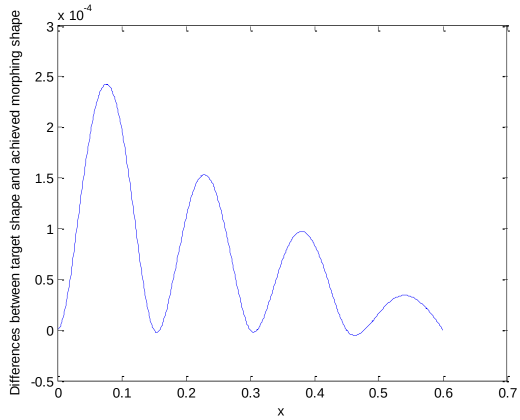


**Figure 4-21 Differences between target shape and achieved morphing shape**

From the pictures and datum above, the maximum difference of the skin deflection from the target shape 2.4-04m was obtained before optimization, while only 1.4e-04m was obtained after optimization.

## 4.6.4 Study Case 4: Five Disc Support Positions of the Skin

### 4.6.4.1 Creation of Objective Function

The same procedure was repeated for five positions optimization, the objective function for this section can be found in Appendix F.4.

#### 4.6.4.2 Optimization

After the objective function is created, the optimization is done by following steps by typing in MATLAB command window as follows:

$x_0$=[0.1 0.2 0.3 0.4 0.500]; lb=zeros(5,1); ub=0.6*ones(5,1);

A=[1 -1 0 0 0;0 1 -1 0 0;0 0 1 -1 0;0 0 0 1 -1]; b=[0;0;0;0];

option=optimset('LargeScale','off','Tolfun',1e-15,'Tolcon',1e-10,'Display','iter', 'TolX', 1e-15,'algorithm', 'trust-region-reflective', 'GradObj','on')

[x,fval,exitflag,output,lambda,grad,hessian]=fmincon(@myopt5,x0,A,b,[],[],lb,ub)

The results are as follows:

x =[0.0995 0.1996 0.3013 0.3967 0.5097], Maximum Difference=4.8e-05m

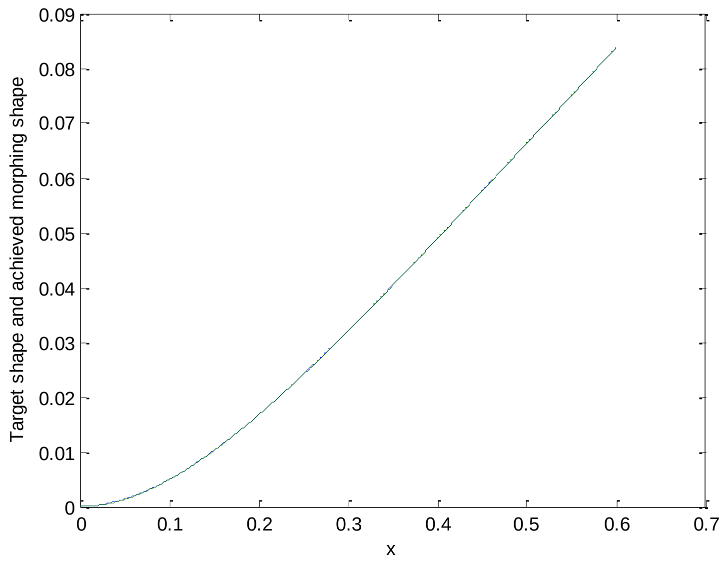


**Figure 4-22 Target shape and achieved shape**

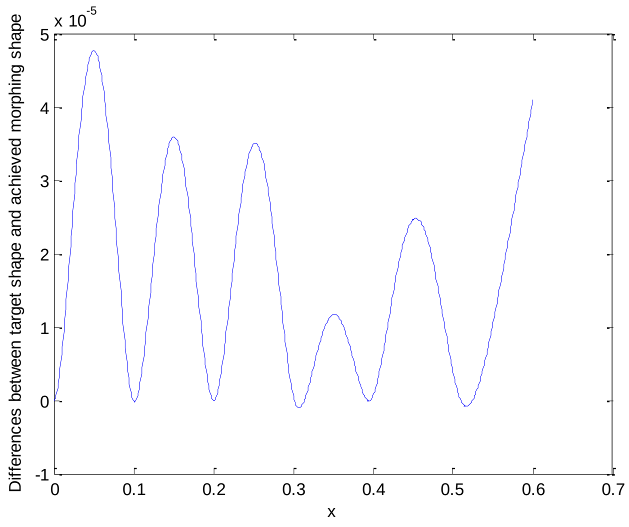


**Figure 4-23  Differences between target shape and achieved morphing shape**

### 4.6.4.3 Comparison

By typing myopt5 ([0.1 0.2 0.3 0.4 0.500]), an achieved shape before optimization can be obtained, and the results are as follows:

X0=[0.1 0.2 0.3 0.4 0.500], Maximum Difference=1.6e-04m.  Target shape and achieved shape is shown in Figure 4-23, the differences between them are shown in Figure 4-24.

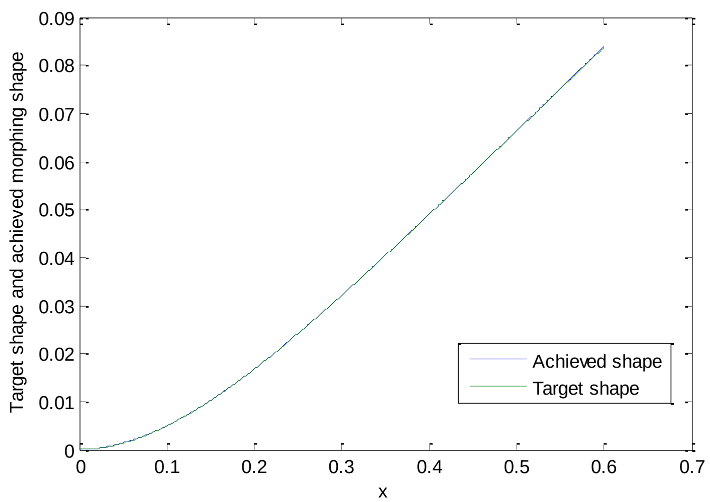


**Figure 4-24  Target shape and achieved shape**

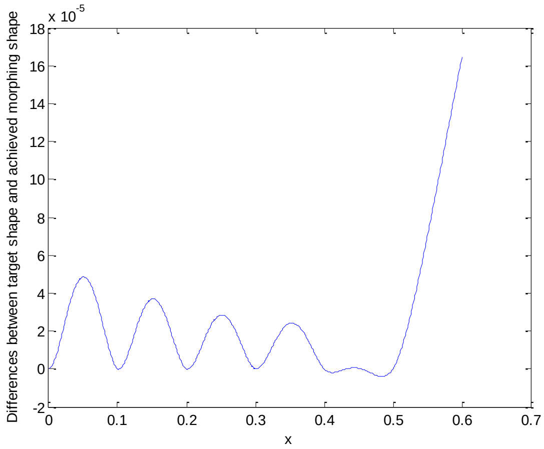


**Figure 4-25 Differences between target shape and achieved morphing shape**

From the pictures and datum above, the maximum difference of the skin deflection from the target shape 1.6e-04m was obtained before optimization, while only 4.8e-05 was obtained after optimization.

## 4.7 Optimization with Direct Search Method

At first, the deflection of a cantilever beam under a concentrate transverse load was carried out and the load needed to actuate the skin to the optimal position is gained. MATLAB function m file is used for optimization. The code for calculating the load and the achieved optimal curve is as follows:

### 4.7.1 Beam with One Load

It searches all the possible support positions along the beam, and calculates all achieved shape, then by comparing the differences between them, the one which have the least standard deviation will be chosen as optimal one. The MATLAB code for this section can be found in Appendix D.1.

The results are as follows:

The optimal position x=0.341m; the load at x position is F=68.65N;

The maximum difference between achieved deflected shape and target shape is 0.00004m at 0.374m;

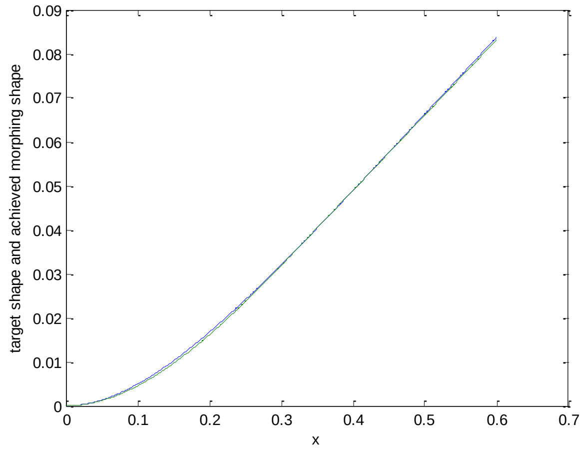


**Figure 4-26 Target shape and achieved deflected shape**

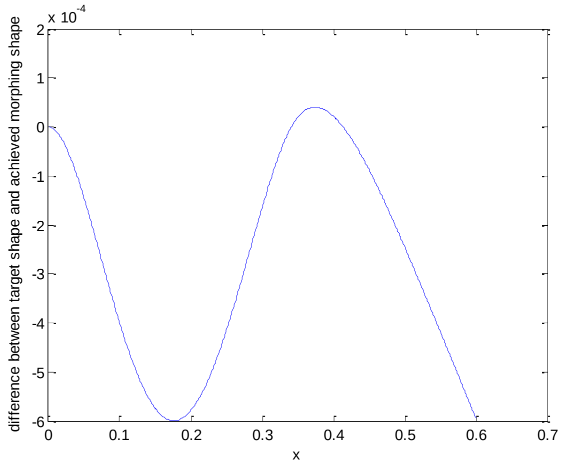


**Figure 4-27 Differences between target shape and achieved morphing shape**

The result shows that the skin under one concentrate transverse load can achieve the target shape with only a small difference 0.00004m, and the load needed to morph the skin is 68.65N at x=0.341m.

Then the aerodynamic load is considered with one support situation, and the load needed to support the skin will be carried out. The codes for the optimization can be found in Appendix D.2.

The results are as follows:

The optimal position is 0.341m; the load on the position is -678.9N;

The torque at the root of the beam -26.4N*m;

The bending moment at the root of the beam is -231.5N*m;

Maximum Difference is 0.005933m at x=0.176m;

The results show that the load at the optimal position is 678.866N, compared to 68.653N when no aerodynamic load was applied.  However, in this load case, a large difference of 0.005933m was observed.

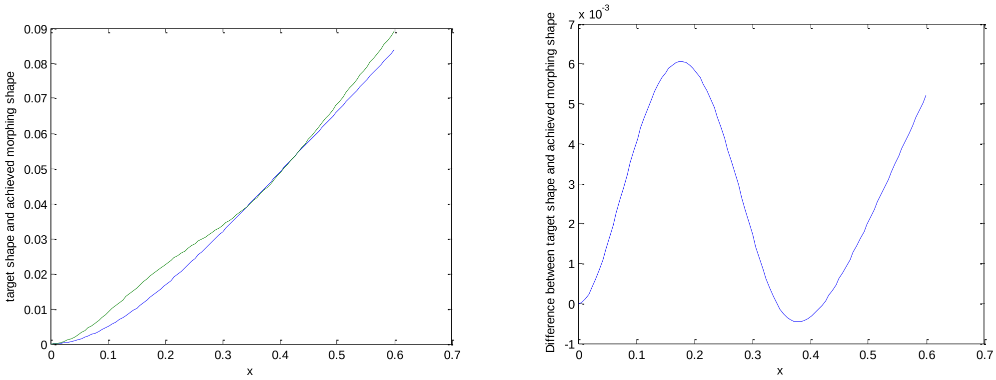


**Figure 4-28  Target shape and achieved morphing shape**

### 4.7.2 Beam with Three Loads

The same procedure was conducted on the three loads case, the MATLAB code can be found in Appendix E.1.

The results show that the optimal position, p=[0.1388  0.2945  0.4682], and the maximum difference position at x=0.6m, with maximum difference of 2.4e-04m.

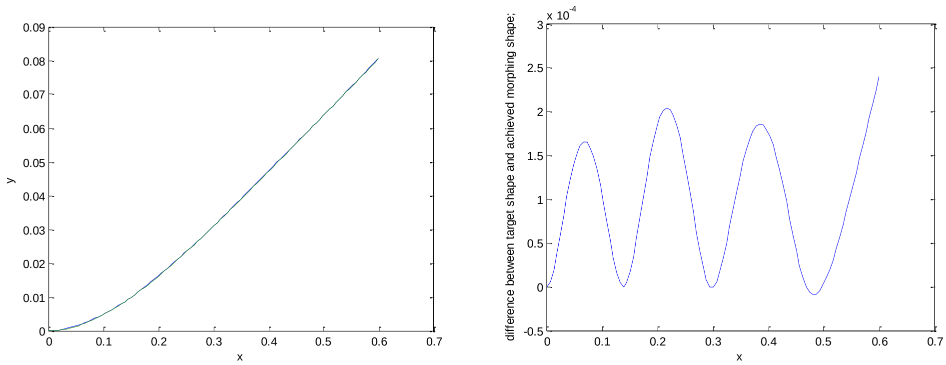


**Figure 4-29  Target shape and achieved shape**

### 4.7.3 Beam with Four Loads

The same procedure was repeated on the four loads case, the MATLAB code can be found in Appendix E.2.

The results show that the optimal position, p=[0.1206 0.2313 0.3566 0.4967], and the maximum difference position at x= 0.069m, with maximum difference of 7.9e-05m.

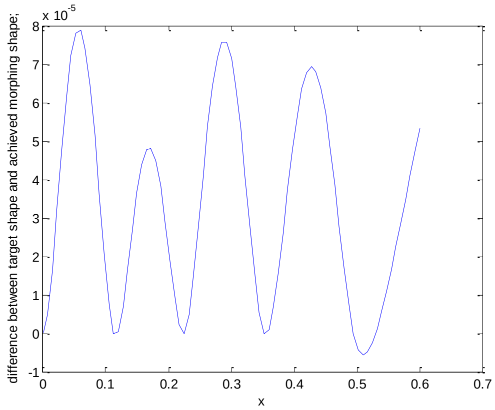


**Figure 4-30 Differences between target shape and achieved morphing shape**

### 4.7.4 Beam with Five Loads

The same procedure was repeated on the five loads case, the MATLAB code can be found in Appendix E.3. The results show that the optimal position, p=[0.1044 0.2106 0.3286 0.4584 0.6000], and the maximum difference position at x=0.2696m, with maximum difference of 5.9e-05m.

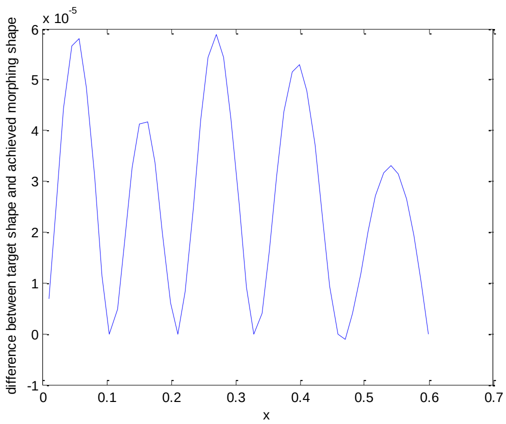


**Figure 4-31 Differences between target shape and achieved morphing shape**

## 4.8 Discussion and Conclusions

At the root of the eccentric beam, the torque and bending moment can be seen in Table4-1:

**Table 4-1  Bending moment, Actuation torque and Maximum Difference**

| | 3 loads | 4 loads | 5 loads |
|---|---|---|---|
| Bending moment | -262.073Nm | -263.927Nm | -264.580 Nm |
| Actuation Torque | -26.767Nm | -26.775Nm | -26.776Nm |
| Max Difference | 2.4e-04m | 7.9e-05m | 5.9e-05m |

As can be seen from Table 4-1, there is only slightly differences between the above three situations about the actuation torque and bending moment.  Hence, actually the number of support positions does not change the bending moment and torque at the root of the eccentric beam.  The reason for almost the same total actuation torque in different disc number and locations is the same work done under the same external loading and mechanical and elastic deflection. However, as the number of the discs increases, the maximum difference of the skin does decrease.

And in the Appendix G, when the function in y1, which is the deflection cause by the aerodynamic loads, is set to 0, then the loads needed to morphing the skin to the desired shape can be obtained, as shown in Table 4-2:

**Table 4-2  the loads needed to actuate the skin without aerodynamic load**

| | X1 | X2 | X3 | X4 | X5 | Torque | Bending Moment |
|---|---|---|---|---|---|---|---|
| 3 loads | 50.3N | 36.8N | 17. 9N | | | 2.7Nm | 26.4Nm |
| 4 loads | 42.7N | 33.6N | 24.4N | 12.1N | | 2.7Nm | 26.8Nm |
| 5 loads | 36.8N | 33.0N | 23.7N | 16.9N | 8.1N | 2.7Nm | 26.9Nm |

Also the loads needed to actuate the skin considering aerodynamic load can be obtained, as shown in Table 4-3:

**Table 4-3 the loads needed to actuate the skin considering aerodynamic load**

| | X1 | X2 | X3 | X4 | X5 | Torque | Bending Moment |
|---|---|---|---|---|---|---|---|
| 3 loads | -504.7N | -374.5N | -174.3N | | | -26.8Nm | -262.0Nm |
| 4 loads | -414.2N | -313.1N | -243.7N | -108.4N | | -26.8Nm | -263.1Nm |
| 5 loads | -387.6N | -321.5N | -251.7N | -143.3N | -13.4N | -26.8Nm | -264.6Nm |

From the Table 4-2 and Table 4-3, it can be seen that the loads needed to actuate the skin without considering the aerodynamic load is only about 10% of the loads needed to actuate the skin considering the aerodynamic load, so the skin is flexible enough for the actuation mechanism. On the other hand, the achieved shape is quite closer to the target shape, the differences between them are all less than 1mm, and so the skin panel is stiff enough to withstand the aerodynamic load without too much deformation. And the optimization results either from ‘optimization tool’ or by MATLAB code was almost the same considering the coding was less accurate when the number of support positions increases.

# 5 Finite Element Analysis of the Morphing Flap Structure

## 5.1 Objective of the Chapter

This chapter presents the results of the finite element analysis conducted on the morphing flap. The feasibility of EBAM as an internal actuation mechanism has been proved in chapter 3 and the optimization of the disc distribution has been conducted to minimize the shape discrepancy to the target deflected shape. However, the analyses of the morphing flap are more of 2-Dimensional consideration. In fact, because the beam is eccentric, the loads applied to the skin and the beams are both 3-Dimensional. Also, the deformations of skins between the neighbouring eccentric beams have not yet considered.

The objective of this chapter is to obtain the deformation of the aerodynamic load apply to the skin, which will be used to compare with results obtained from the theoretical calculation in optimization. In this chapter, the FE model was built and analysis results are obtained by Msc.Patran-Nastran.

In order to compare with the results obtained by theoretical calculation, the author chooses the same load applied on the skin model in the FE analysis.

In the first stage of the analysis, the trailing edge flap was analysed under the effect of the air pressure load to prove that the proposed design of a flap with integrated eccentric beam mechanism was able to withstand the external loads. The aerodynamic load presented in Section 4.2.4 was applied to both upper and lower skin surfaces. The flap trailing edge was considered clamped at the rear spar and supported by the disc at its morphing position. Table 5-1 summarizes the material selection of the trailing edge.

**Table 5-1 Material selection**

| Name | skin | stringer | disc | Eccentric beam |
|---|---|---|---|---|
| material | aluminium | aluminium | Steel | Steel |
| elastic modulus | 7E+10 | 7E+10 | 2E+011 | 2E+011 |

| Name | skin | stringer | disc | Eccentric beam |
|---|---|---|---|---|
| Shear modulus | | | 7.58E+010 | 7.58E+010 |
| Poisson ratio | 0.3 | 0.3 | 0.32 | 0.32 |
| density | 2700Kg/m$^3$ | 2700 Kg/m$^3$ | 7800 Kg/m$^3$ | 7800 Kg/m$^3$ |

Aluminium was selected as the skin and stringer's material, while steel was selected as the beam and disc material, considering that the beam and disc should be stiffer and skins should be more flexible.

The eccentric beams and the discs which are considered as stiff enough in the optimization procedure are now considered as beam elements with corresponding property. The beams are given a tube cross section with different diameter along the x direction and are clamped at their root area. The material for the beams and discs are alloy steel AISI 4340l.

## 5.2 Eccentric Beam Cross Section Calculation:

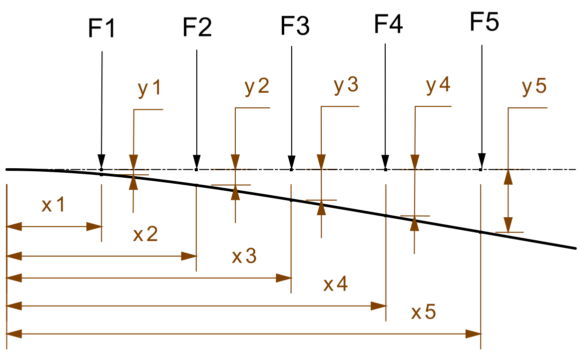


**Figure 5-1 Eccentric beam cross section calculation**

For a five discs support, at the root of the beam, the bending moment:

$$M_0 = F_1 \times x_1 + F_2 \times x_2 + F_3 \times x_3 + F_4 \times x_4 + F_5 \times x_5 \qquad (5\text{-}1)$$

The torque:

$$T_0 = F_1 \times y_1 + F_2 \times y_2 + F_3 \times y_3 + F_4 \times y_4 + F_5 \times y_5 \qquad (5\text{-}2)$$

And the stress:

$$\sigma_{\max} = \frac{My}{I} = \frac{M}{W_z} \tag{5-3}$$

$$\alpha = d / D \tag{5-4}$$

Section modulus in bending:

$$W_z = \frac{\pi D^3}{32}(1-\alpha^4) \tag{5-5}$$

Section modulus in torsion:

$$W_t = \frac{\pi D^3}{16}(1-\alpha^4) \tag{5-6}$$

$$\tau_{\max} = \frac{T}{W_t} \tag{5-7}$$

Assume α=0.8;

$$\sigma_{\max} = \frac{My}{I} = \frac{M}{W_z} = \frac{M}{\frac{\pi D^3}{32}(1-\alpha^4)} = \frac{32 \times M}{\pi D^3 (1-\alpha^4)} \le F_{ty} \tag{5-8}$$

$$\Rightarrow D \ge \sqrt[3]{\frac{32 \times M}{\pi (1-\alpha^4) F_{ty}}} \tag{5-9}$$

Where, M=264.58Nm, $F_{ty}$=1496MPa

Hence, D⩾ (264.58*32/pi/(1-0.8$^4$)/1496/10$^6$)^(1/3)=0.0145m

$$\tau_{\max} = \frac{T}{W_t} = \frac{T}{\frac{\pi D^3}{16}(1-\alpha^4)} = \frac{T \times 16}{\pi D^3 (1-\alpha^4)} \le F_{su} \tag{5-10}$$

Where T=26.8Nm, $F_{su}$=1075MPa

$$D \ge \sqrt[3]{\frac{T \times 16}{\pi (1-\alpha^4) F_{su}}} \tag{5-11}$$

$$\Rightarrow D \geq \sqrt[3]{\frac{26.8\times 16}{\pi(1-0.8^4)\times 1075\times 10^6}} = 0.0056m \qquad \textbf{(5-12)}$$

From the calculation above, it can be seen that the bending moment is the main consideration when designing the cross section. Other beam cross section can also be obtained using the same way.

## 5.3 Meshing

The model has been created by importing the CATIA surface and lines to the software Msc Patran/Nastran. The skins have been meshed with QUAD4 shell elements and given a thickness of 2mm. The stringers are meshed with 1D beam element, and the cross section of it can be obtained from Table 3-2. The discs are not interested at the moment and they are considered as a rod with a 5mm diameter.

Considering that the connections between the stringers and discs are C-connector, which allows the y direction sliding and rotation. So the contact points between the stringer and disc are connected by MPC Rjoints. Also, in order to simulate the open trailing edge, MPC connection sliding surface is used to connect the trailing edge upper and lower skins.

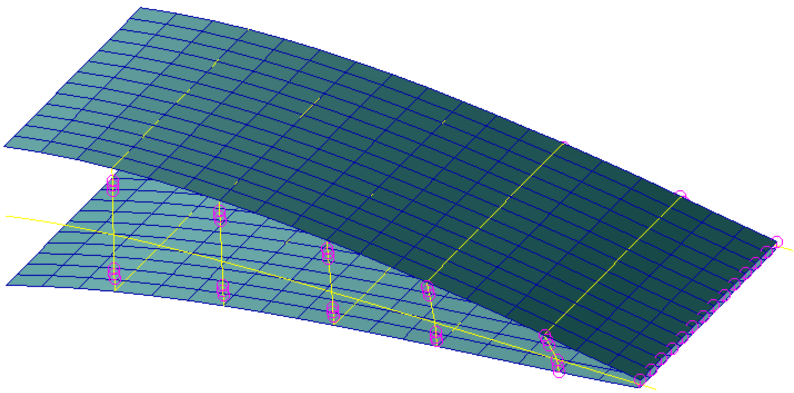

**Figure 5-2 MPC connections**

## 5.4 Loads and Boundary Conditions

The loads are created with field in Patran, with a parameter of x only, the function 2463.65-2463.65/0.6*('x-0.6) (0<x≤0.6), which represent tapered distributed loads. Then the loads are applied to the surface of the skins. The beams as well as upper and lower skins are considered as clamped at the rear spar. In this FEA, the morphing of the skins is not by applying loads from disc to skins to get the desired shape. The model for this analysis comes from the morphing shape and beam and discs at corresponding position, and the aerodynamic loads are applied to skins to calculate the displacement.

## 5.5 FEA Results

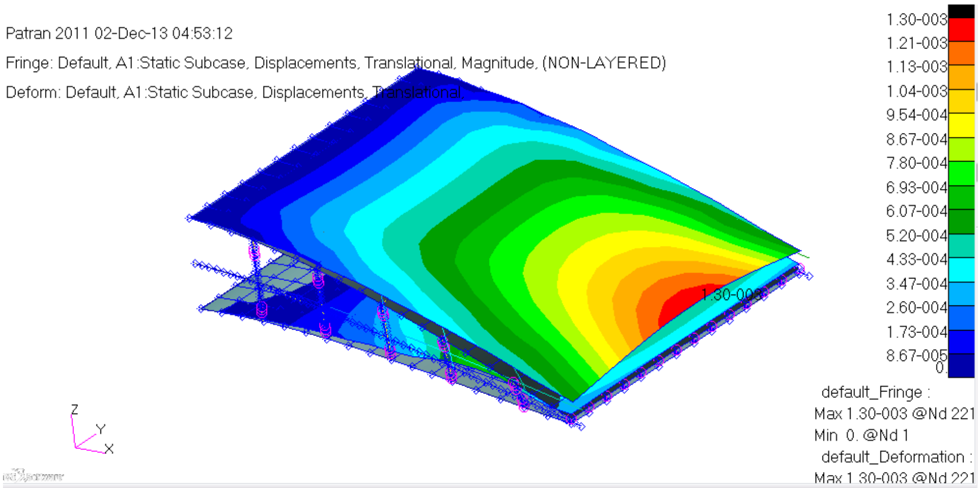


**Figure 5-3 Displacement deformation**

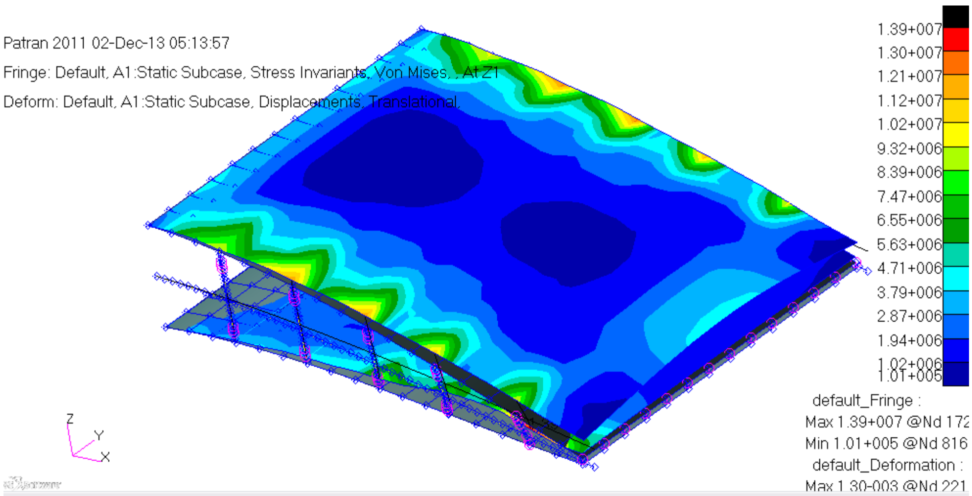


**Figure 5-4 Von Mises stress**

The result shown in Figure 5-3 is the displacement deformation, the maximum displacement of 1.3e-3m lies at the trailing edge in the middle of the upper skin. Where at the disc support area, only a small deformation 4.33e-4m was observed.

Figure 5-4 illustrates the Von Mises stress distribution on the trailing edge. It can be seen that the connections between stringers and discs have high level of Von Mises stress, which is 1.39e+7Pa.

This chapter shows that the deformation of the skin at the morphing position is quite small and is acceptable. This result can make sure the morphing flap achieve aerodynamic benefit.

# 6 3D Flap Morphing and Simulation

## 6.1 Objective of the Chapter

In the previous chapter, the morphing concept has been illustrated and structure design is introduced. Then the optimization of the disc positions and finite element analysis has been carried out to prove its feasibility. As an innovative design, the eccentric beam actuation mechanism, developed by Dr Guo and other PhD students need an easy way to demonstrate to understand it easily and quickly. A video seems to be a good solution to illustrate the system after all the structure models are built. This chapter presents how to create the video to illustrate how the EBAM works.

## 6.2 Creating a Video

Creating a video for a mechanism can be done with CATIA. In the ‘Digital Mock-up’ module, ‘DMU kinematics’ is widely used in industry to simulate the mechanism to reduce time and money to build a physical model. It can handle a rigid mechanism quite well. However, it cannot deal with a flexible material. So, the only solution to simulate a morphing flap actuated by the BEAM is to make several pictures during its rotation.

For the beam and the discs, its deflection status can be easily obtained by rotating around its axis for a certain angle. However, for the skin, the only way to change its deflection status is to create a new one each time during its rotation. For the stringers, although it is twisted, it can be assembled in the CATIA ‘Assembly Design’ module. The author decided to create 10 TE rotation statuses from 0° to 90° with increment of 10° to illustrate the process. Totally, for the simulation, 10 products are built for each rotating angle and each product contains 19 parts, including an upper skin, a lower skin, 10 stringers, five discs, a beam and a reference part for assembly.

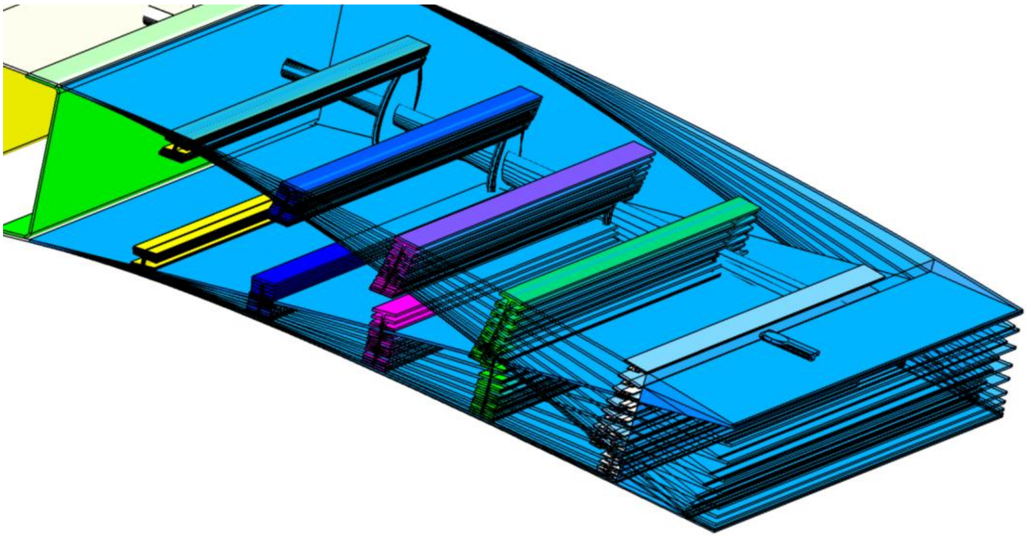

**Figure 6-1  10 deflection status of morphing simulation**

To start with, a morphing flap with 10 deflection status is created. At each deflection position, the discs and the beam are created by rotating around the axis at a corresponding angle to form a new one. A reference part is created with the axial line of the stringers, and also the plane parallel to the stringer web. Then in the 'Assembly Design', the stringers are imported, and assembled to the reference part by using 'Coincidence Constraint'  and 'Offset Constraint' .

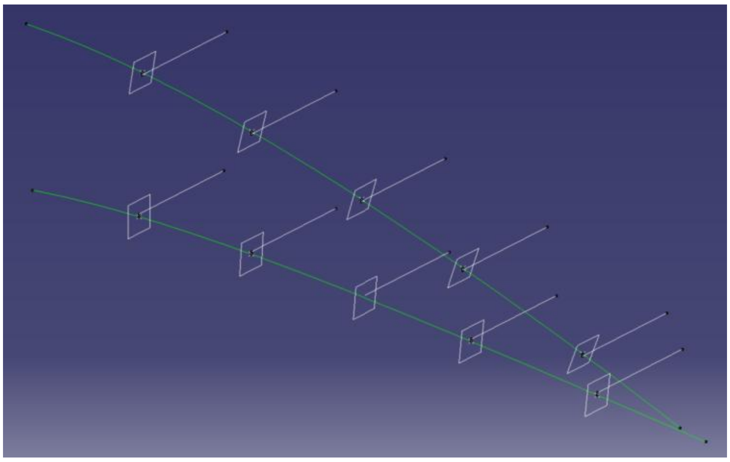

**Figure 6-2  Reference part**

After completing the creation of the model, it is ready to create the video. The tool 'capture' is used to take photos of the deflection of different status. In the

CATIA tree select the one that needs to be taken a picture while hiding the others.

‘Picasa 3’ [23] was adopted to create the video.

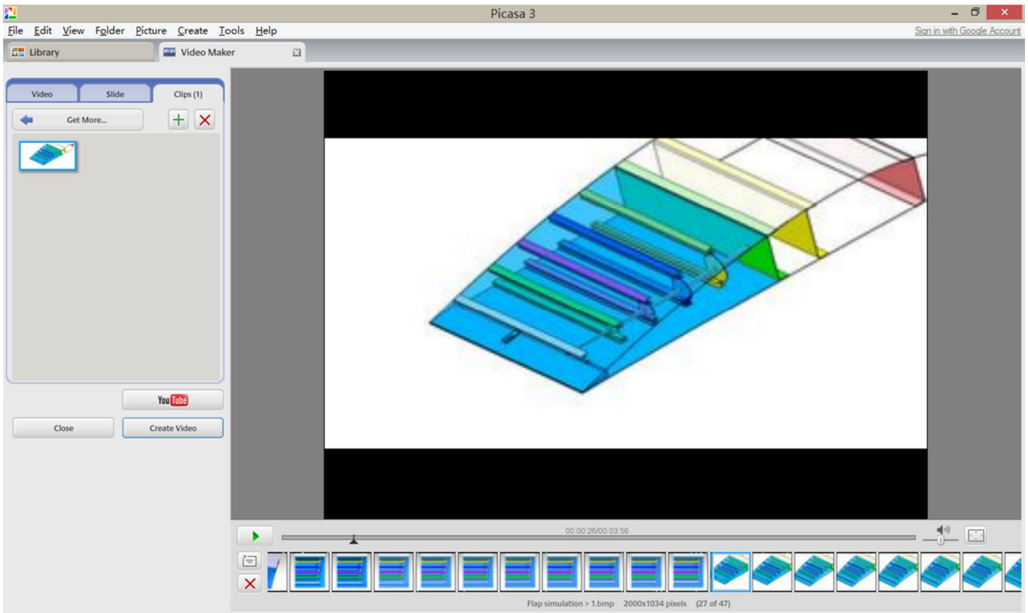


**Figure 6-3  Picasa 3**

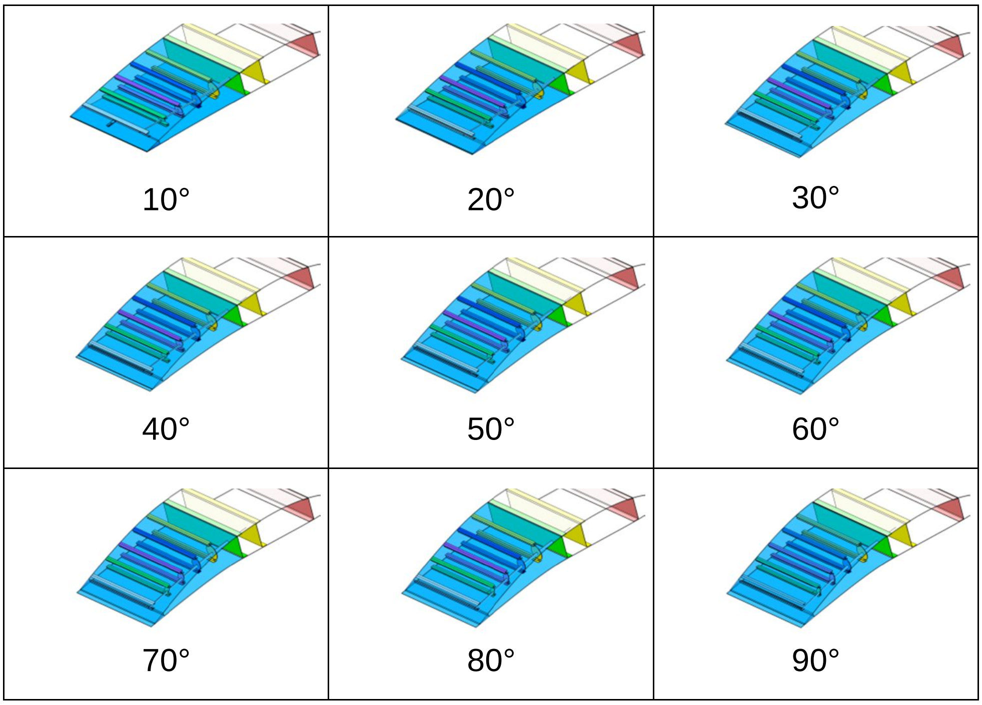


**Figure 6-4  Isometric view of rotation of a morphing flap**

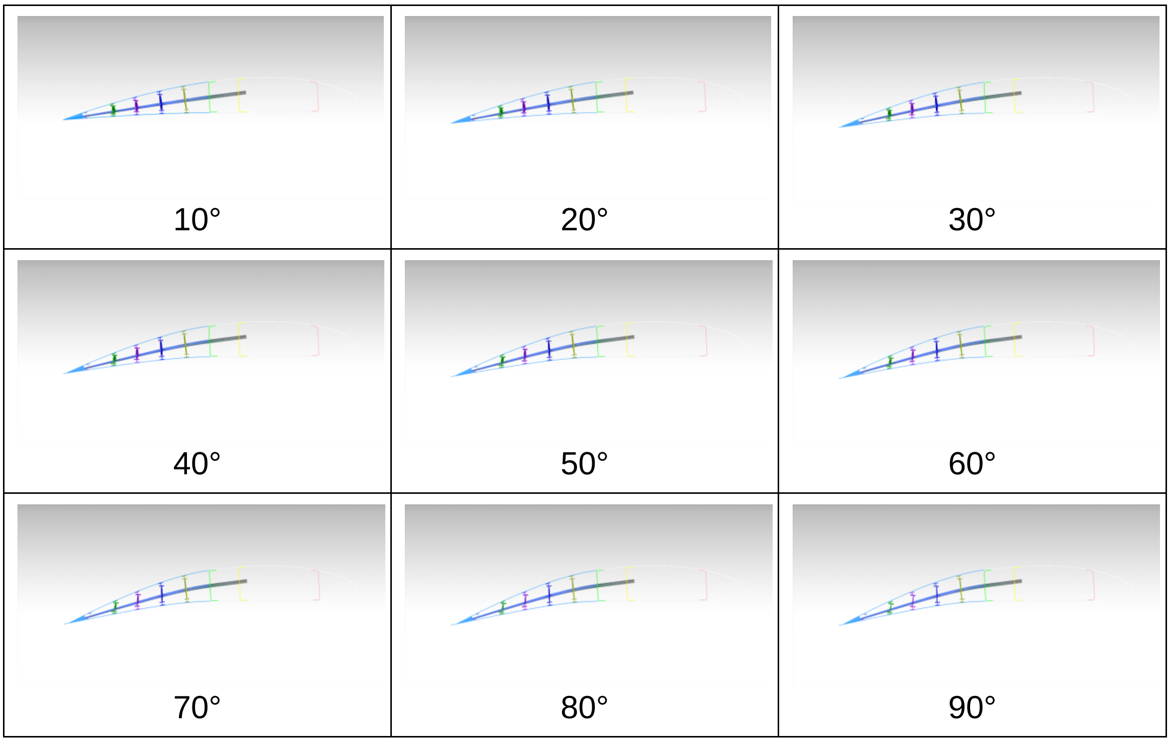


**Figure 6-5  Right view of rotation of a morphing flap**

The video has been created in 5 parts. The first part of video is based on the neutral position to show the main features of the EBAM, including skins, discs, stringers and beam. Attention is paid to show clearly what an EBAM looks like.

The second part, the author illustrates the morphing deflection by using 10 pictures from a isometric view of the morphing flap integrated with EBAM, as shown in Figure 6-4(0° status is not showed). Then 10 pictures from right view of the EBAM are also showed to understand the x and z direction motion during deflection, as shown in Figure 6-5(0° status is not showed). Also, top view of the mechanism is demonstrated in order to show the y direction motion of the eccentric beam.

In order to have a clear view of the rotation during morphing, the third part is focused on the discs, beam and stringers. This part helps readers to understand the motion of the discs and stringers, as shown in Figure 6-6(0° status is not showed).

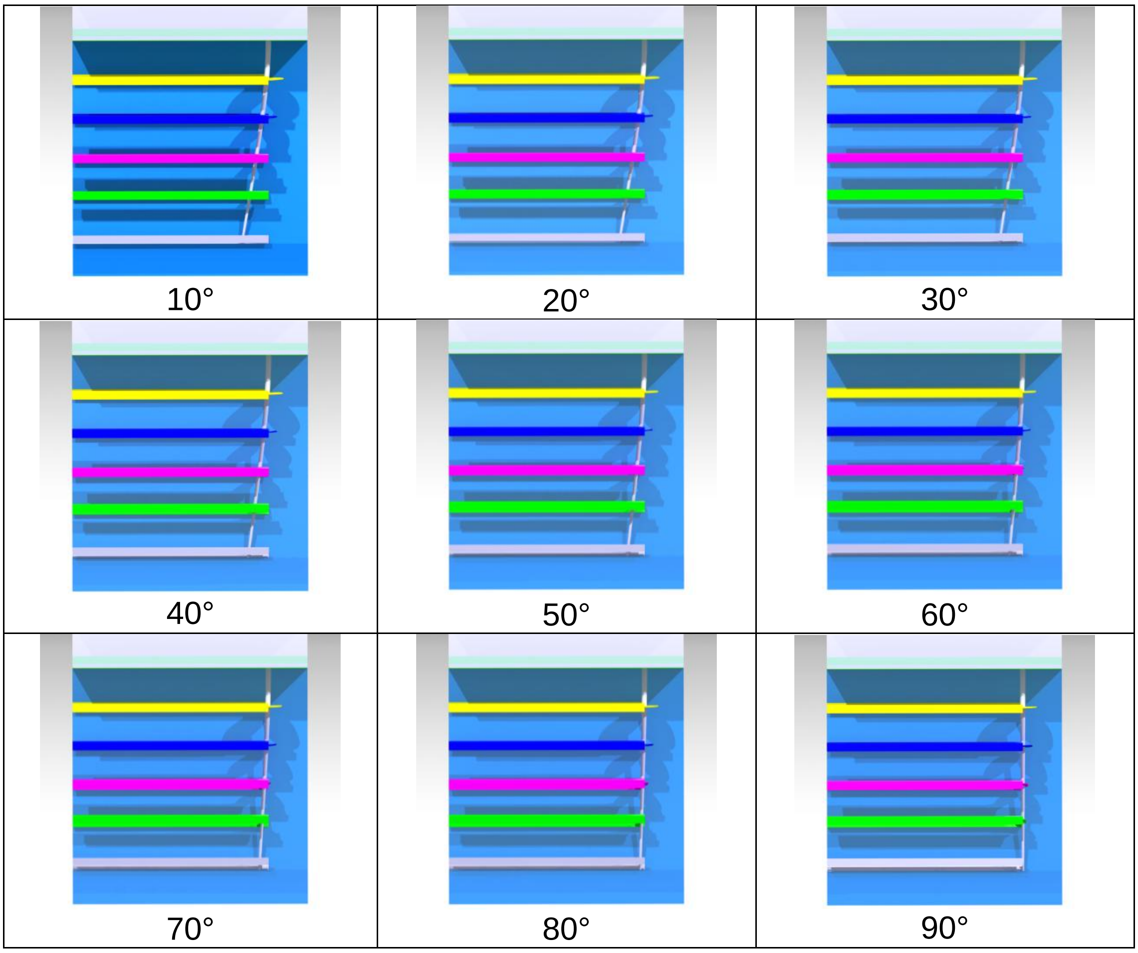


**Figure 6-6 Top view of deflection of a morphing flap**

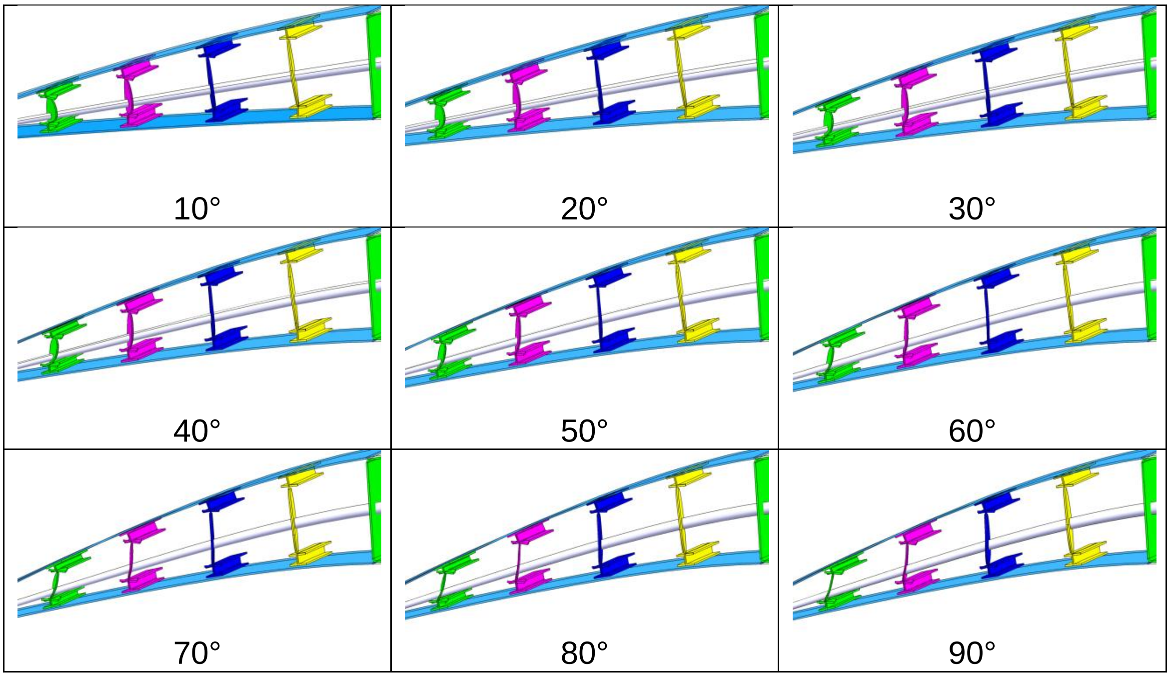


**Figure 6-7 Detailed view of discs and stringers**

## 6.3 Summary

This chapter illustrates what an EBAM looks like as a whole, and how it actuates the skin. Especially, an open sliding trailing edge can be observed during the beam rotation. However, it is too complicated to create the C-connector at every rotational angle, and is ignored at this chapter.

# 7 Conclusions and Future Work

## 7.1 Conclusions

This study is based on an eccentric beam actuation mechanism (EBAM) and morphing flap design in previous research. However the previous work is lack of detailed design of the disc-skin linkage and a detailed study of the mechanism optimization in relation to the actuation torque is required. In the current study, contribution has been made to the detailed design of the EBAM especially the shape and distribution of the discs to meet the specified shape requirement of the morphing flap.

Detailed design of every part of the EBAM including the eccentric beam and twisted disc has been carried out. It was noted that the beam curvature, the disc mounting angle, twisted shape and locations are the key design parameters. The desired morphing shape can be achieved by optimizing those parameters of the mechanism.

In the design optimization process, the skin is considered as an elastic plate analysed in beam bending theory under distributed aerodynamic load. The optimization method in MATLAB code is adopted to conduct the work. The actuation torque calculation has been included in the analysis. The result of the optimization show that for the optimal location of a three, four and five disc EBAM, the bending moment and torque at the root of the beam remain almost the same although more discs result in better shape. This indicates that the number and location of discs has little effect on actuation torque which is dominated by the external load and skin stiffness.

To ensure the connection between the EBAM and the skin-stringer, a C-linkage and a twisted stringer flange was designed.

The finite element analysis is conducted to validate the design of the beam, the discs, the stringers and the skins.

Finally, the kinematic simulation is carried out to demonstrate the feasibility of the above design. Although it cannot be simulated by the CATIA kinematic module, it is still worth the effort because the video illustrates most characteristics of the system.

## 7.2 Future Work

Despite the entire EBAM models are all created and kinematic simulation has been carried out to demonstrate the feasibility of the mechanism. However, the connection between the stringers and discs remain quite complex. Hopefully, a physical model should be built, and test of mechanism as well as its deflection should be carried out.

# REFERENCES


[1] Perera, M. and Guo, S. (2009), "Optimal design of a seamless aeroelastic wing structure", *Collection of Technical Papers - AIAA/ASME/ASCE/AHS/ASC Structures, Structural Dynamics and Materials Conference,* .

[2] Trapani, M. and Guo, S. (2009), "Design and analysis of a rudderless aeroelastic fin", *Proceedings of the Institution of Mechanical Engineers, Part G: Journal of Aerospace Engineering,* vol. 223, no. 6, pp. 701-710.

[3] Di Matteo, N., Guo, S. and Li, D. (2011), "Morphing trailing edge flap for high lift wing", *Collection of Technical Papers - AIAA/ASME/ASCE/AHS/ASC Structures, Structural Dynamics and Materials Conference,* .

[4] Lemoine, P. and Guo, S. (2008), *Design of an actuation mechanism for a seamless aeroelastic wing / P. Lemoine,* .

[5] Di Matteo, N. and Guo, S. J. (2012), *Optimal design and numerical analysis of a morphing flap structure [electronic resource] / Natalia Di Matteo,* .

[6] Arguelles, P., Bischoff, M., Busquin, P., Drost, B. A. C., Evans, R., Kroll, W., Lagardere, J., Lina, A., Lumsden, J., Ranque, D., Rasmussen, P., Reutinger, P., Robins, R., Terho, H. and Wittlov, A. (JANUARY 2001), *EUROPEAN AERONAUTICS: A VISION FOR 2020-Meeting society's needs and winning global leadership,* .

[7] Babikian, R., Lukachko, S. P. and Waitz, I. A. (2002), "The historical fuel efficiency characteristics of regional aircraft from technological, operational, and cost perspectives", *Journal of Air Transport Management,* vol. 8, no. 6, pp. 389-400.

[8] Rudolph, P. K. C. (1996), *High lift systems on commercial subsonic air liners / Peter K. C. Rudolph,* Washington, D.C. : NASA, 1996.

[9] Patel, S., Majji, M., Koh, B., Junkins, J. and Rediniotisx, O. (2005), *Morphing wing: A demonstration of aero servo elastic distributed sensing and control,* .

[10] Cesnik, C. E., Last, H. R. and Martin, C. A. (2004), "A FRAMEWORK FOR MORPHING CAPABILITY ASSESSMENT", .

[11] Johnston, C., Neal, D., Wiggins, L., Robertshaw, H., Mason, W. and Inman, D. (2003), "A Model to Compare the Flight Control Energy Requirements of Morphing and Conventionally Actuated Wings", .

[12] Monner, H. P., Kintscher, M., Lorkowski, T. and Storm, S. (2009), "Design of a smart droop nose as leading edge high lift system for transportation aircrafts", *Collection of Technical Papers - AIAA/ASME/ASCE/AHS/ASC Structures, Structural Dynamics and Materials Conference,* .

[13] Monner, H. P. (2001), "Realization of an optimized wing camber by using formvariable flap structures", *Aerospace Science and Technology,* vol. 5, no. 7, pp. 445-455.

[14] Monner, H., Sachau, D. and Breitbach, E. (2000), "Design Aspects of the Elastic Trailing Edge for an Adaptive Wing", *Structural Aspects of Flexible Aircraft Control,* .

[15] Carlsson, M. and Cronander, C. (2005), "Efficient roll control using distributed control surfaces and aeroelastic effects", *Aerospace Science and Technology,* vol. 9, no. 2, pp. 143-150.

[16] Perera, M. and Guo, S., ( 2009), *Optimal design of an aeroelastic wing structure with seamless control surfaces*.

[17] Ricci, S., Scotti, A. and Terraneo, M. (2006), "Design, manufacturing and preliminary test results of an adaptive wing camber model", *Collection of Technical Papers - AIAA/ASME/ASCE/AHS/ASC Structures, Structural Dynamics and Materials Conference,* Vol. 8, pp. 5439.

[18] Thill, C., Etches, J., Bond, I., Potter, K. and Weaver, P. (2008), "Morphing skins", *The Aeronautical Journal,* vol. 112, no. 1129, pp. 117-139.

[19] Bartley-Cho, J. D., Wang, D. P., Martin, C. A., Kudva, J. N. and West, M. N. (2004), "Development of high-rate, adaptive trailing edge control surface for the smart wing phase 2 wind tunnel model", *Journal of Intelligent Material Systems and Structures,* vol. 15, no. 4, pp. 279-291.

[20] Gandhi, F. and Anusonti-Inthra, P. (2008), "Skin design studies for variable camber morphing airfoils", *Smart Materials and Structures,* vol. 17, no. 1.

[21] Moorhouse, D., Sanders, B., Von Spakovsky, M. and Butt, J. (2006), "Benefits and design challenges of adaptive structures for morphing aircraft", *Aeronautical Journal,* vol. 110, no. 1105, pp. 157-162.

[22] Xfoil http://web.mit.edu/drela/Public/web/xfoil/ access on 15th November

[23] ‘Picasa 3’ http://picasa.google.com/ access on 15th November.

[24] ‘MATLAB help

# APPENDICES

## Appendix A : Equation of the Beam Curve

In order to determine the vertical displacement y(x) for each point x of a cantilever beam under tapered distributed pressure, it is necessary to calculate the bending moment applied on each of these points. The curvilinear abscissa s has to be used and the equation for the distributed force must be known.

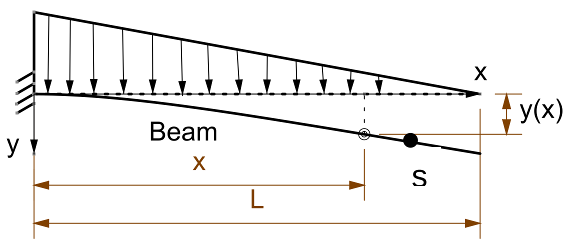


**Figure A-1 Cantilever beam under tapered distributed load**

Using: y''(x)=-M(x)/EI

And: $$M(x) = -\int_x^L \omega(s)(s-x)ds$$

Where: $\omega(s) = \omega_o(1 - s/L)$

The following equation can be found:

$$y(x) = \frac{\omega_0}{EI}\frac{1}{L}\left[\frac{L^3x^2}{12} - \frac{x^5}{120} - \frac{L^2x^3}{12} + \frac{Lx^4}{24}\right]$$

We also have the TE rotation angle:

$$\theta(x) = y'(x) = \frac{\omega_0}{EI}\frac{1}{L}\left[\frac{L^3x}{6} - \frac{x^4}{24} - \frac{L^2x^2}{4} + \frac{Lx^3}{6}\right]$$

Then finally the maximum vertical displacement at the beam extremity is given by:

$$y_{max} = y(L) = \frac{\omega_0}{EI}\frac{L^4}{30}$$

# Appendix B : NACA 4412 Airfoil Coordinates

| | NACA 4412 | | | | | | | |
|---|---|---|---|---|---|---|---|---|
| | x | y | | x | y | | x | y |
| 1 | 1 | 0.00126 | 59 | 0.112692 | 0.0682 | 117 | 0.292278 | -0.02291 |
| 2 | 0.99392 | 0.002917 | 60 | 0.099926 | 0.064304 | 118 | 0.309339 | -0.02205 |
| 3 | 0.98332 | 0.00577 | 61 | 0.087758 | 0.060251 | 119 | 0.326355 | -0.02122 |
| 4 | 0.970969 | 0.009039 | 62 | 0.076338 | 0.056103 | 120 | 0.343323 | -0.02042 |
| 5 | 0.957164 | 0.012623 | 63 | 0.06582 | 0.051941 | 121 | 0.36025 | -0.01965 |
| 6 | 0.942357 | 0.016387 | 64 | 0.056328 | 0.047854 | 122 | 0.37715 | -0.01893 |
| 7 | 0.926955 | 0.020214 | 65 | 0.047924 | 0.043919 | 123 | 0.394052 | -0.01826 |
| 8 | 0.911228 | 0.024031 | 66 | 0.040593 | 0.040192 | 124 | 0.411006 | -0.01762 |
| 9 | 0.895329 | 0.027796 | 67 | 0.034259 | 0.0367 | 125 | 0.428032 | -0.01696 |
| 10 | 0.879335 | 0.031491 | 68 | 0.028809 | 0.033442 | 126 | 0.445114 | -0.01628 |
| 11 | 0.863285 | 0.035105 | 69 | 0.024123 | 0.030403 | 127 | 0.462237 | -0.01559 |
| 12 | 0.847197 | 0.038634 | 70 | 0.020083 | 0.027559 | 128 | 0.47939 | -0.01489 |
| 13 | 0.831082 | 0.042076 | 71 | 0.016592 | 0.024884 | 129 | 0.496562 | -0.01419 |
| 14 | 0.814945 | 0.04543 | 72 | 0.013566 | 0.022352 | 130 | 0.513737 | -0.01349 |
| 15 | 0.798788 | 0.048695 | 73 | 0.010941 | 0.01994 | 131 | 0.5309 | -0.01279 |
| 16 | 0.782615 | 0.051871 | 74 | 0.008665 | 0.017626 | 132 | 0.548047 | -0.0121 |
| 17 | 0.766426 | 0.054956 | 75 | 0.006699 | 0.015393 | 133 | 0.565177 | -0.01142 |
| 18 | 0.750223 | 0.057951 | 76 | 0.005014 | 0.013226 | 134 | 0.582289 | -0.01075 |
| 19 | 0.734008 | 0.060855 | 77 | 0.003588 | 0.011112 | 135 | 0.599386 | -0.0101 |
| 20 | 0.717782 | 0.063667 | 78 | 0.00241 | 0.009042 | 136 | 0.616469 | -0.00947 |
| 21 | 0.701547 | 0.066385 | 79 | 0.00147 | 0.007012 | 137 | 0.633539 | -0.00885 |
| 22 | 0.685303 | 0.069009 | 80 | 0.000765 | 0.005022 | 138 | 0.650597 | -0.00825 |
| 23 | 0.669054 | 0.071539 | 81 | 0.000291 | 0.003074 | 139 | 0.667646 | -0.00767 |
| 24 | 0.652799 | 0.073972 | 82 | 0.000044 | 0.001182 | 140 | 0.684687 | -0.00712 |
| 25 | 0.636541 | 0.076307 | 83 | 0.000013 | -0.00065 | 141 | 0.701721 | -0.00659 |
| 26 | 0.62028 | 0.078542 | 84 | 0.000205 | -0.0025 | 142 | 0.71875 | -0.00608 |
| 27 | 0.60402 | 0.080677 | 85 | 0.000652 | -0.00437 | 143 | 0.735774 | -0.0056 |
| 28 | 0.587761 | 0.082709 | 86 | 0.001378 | -0.00623 | 144 | 0.752795 | -0.00514 |
| 29 | 0.571505 | 0.084637 | 87 | 0.002392 | -0.00805 | 145 | 0.769815 | -0.00471 |
| 30 | 0.555255 | 0.086458 | 88 | 0.003694 | -0.00981 | 146 | 0.786833 | -0.00431 |
| 31 | 0.539011 | 0.088171 | 89 | 0.005276 | -0.01149 | 147 | 0.803852 | -0.00393 |
| 32 | 0.522777 | 0.089772 | 90 | 0.007132 | -0.01308 | 148 | 0.820872 | -0.00357 |
| 33 | 0.506554 | 0.09126 | 91 | 0.009264 | -0.0146 | 149 | 0.837891 | -0.00324 |
| 34 | 0.490346 | 0.092632 | 92 | 0.011681 | -0.01604 | 150 | 0.854907 | -0.00294 |
| 35 | 0.474157 | 0.093885 | 93 | 0.014403 | -0.01742 | 151 | 0.871914 | -0.00266 |
| 36 | 0.457992 | 0.095016 | 94 | 0.017464 | -0.01874 | 152 | 0.888893 | -0.00241 |
| 37 | 0.441863 | 0.096021 | 95 | 0.020909 | -0.02002 | 153 | 0.905806 | -0.00218 |
| 38 | 0.425787 | 0.096897 | 96 | 0.0248 | -0.02125 | 154 | 0.922569 | -0.00197 |
| 39 | 0.409798 | 0.09764 | 97 | 0.029219 | -0.02244 | 155 | 0.939012 | -0.00179 |
| 40 | 0.393975 | 0.098239 | 98 | 0.034269 | -0.02359 | 156 | 0.95482 | -0.00163 |
| 41 | 0.378331 | 0.098646 | 99 | 0.040077 | -0.02469 | 157 | 0.969517 | -0.0015 |
| 42 | 0.362789 | 0.098849 | 100 | 0.046799 | -0.02574 | 158 | 0.982576 | -0.00139 |
| 43 | 0.347319 | 0.098846 | 101 | 0.054604 | -0.02672 | 159 | 0.99368 | -0.00131 |
| 44 | 0.331908 | 0.098636 | 102 | 0.06364 | -0.0276 | 160 | 1 | -0.00126 |
| 45 | 0.316554 | 0.098215 | 103 | 0.074007 | -0.02835 | | | |
| 46 | 0.301259 | 0.097579 | 104 | 0.085705 | -0.02892 | | | |
| 47 | 0.286027 | 0.096726 | 105 | 0.098623 | -0.0293 | | | |
| 48 | 0.270866 | 0.095651 | 106 | 0.112564 | -0.02947 | | | |
| 49 | 0.255782 | 0.094349 | 107 | 0.127303 | -0.02944 | | | |
| 50 | 0.240785 | 0.092818 | 108 | 0.142642 | -0.02923 | | | |
| 51 | 0.225887 | 0.091053 | 109 | 0.158427 | -0.02886 | | | |
| 52 | 0.2111 | 0.08905 | 110 | 0.174546 | -0.02836 | | | |
| 53 | 0.19644 | 0.086806 | 111 | 0.190924 | -0.02775 | | | |
| 54 | 0.181926 | 0.084317 | 112 | 0.207506 | -0.02705 | | | |
| 55 | 0.167581 | 0.081581 | 113 | 0.224253 | -0.02629 | | | |
| 56 | 0.153438 | 0.078597 | 114 | 0.241137 | -0.02548 | | | |
| 57 | 0.139535 | 0.075367 | 115 | 0.258127 | -0.02463 | | | |
| 58 | 0.125928 | 0.071896 | 116 | 0.275191 | -0.02377 | | | |

# Appendix C : NACA 4412 Airfoil Pressure Coefficient Versus X

| | NACA 4412 | | | | | | | |
|---|---|---|---|---|---|---|---|---|
| | x | Cp | | x | Cp | | x | Cp |
| 1 | 1 | 0.47021 | 59 | 0.11269 | -3.12546 | 117 | 0.29228 | 0.62551 |
| 2 | 0.99392 | 0.27555 | 60 | 0.09993 | -3.26688 | 118 | 0.30934 | 0.61347 |
| 3 | 0.98332 | 0.18324 | 61 | 0.08776 | -3.42496 | 119 | 0.32635 | 0.60215 |
| 4 | 0.97097 | 0.10581 | 62 | 0.07634 | -3.60435 | 120 | 0.34332 | 0.59103 |
| 5 | 0.95716 | 0.03861 | 63 | 0.06582 | -3.80496 | 121 | 0.36025 | 0.58054 |
| 6 | 0.94236 | -0.02124 | 64 | 0.05633 | -4.02904 | 122 | 0.37715 | 0.56965 |
| 7 | 0.92695 | -0.07757 | 65 | 0.04792 | -4.27664 | 123 | 0.39405 | 0.55793 |
| 8 | 0.91123 | -0.12919 | 66 | 0.04059 | -4.54681 | 124 | 0.41101 | 0.54423 |
| 9 | 0.89533 | -0.17792 | 67 | 0.03426 | -4.83958 | 125 | 0.42803 | 0.53361 |
| 10 | 0.87933 | -0.22445 | 68 | 0.02881 | -5.15416 | 126 | 0.44511 | 0.52375 |
| 11 | 0.86328 | -0.26911 | 69 | 0.02412 | -5.49247 | 127 | 0.46224 | 0.51476 |
| 12 | 0.8472 | -0.31187 | 70 | 0.02008 | -5.8542 | 128 | 0.47939 | 0.50634 |
| 13 | 0.83108 | -0.35368 | 71 | 0.01659 | -6.24045 | 129 | 0.49656 | 0.49814 |
| 14 | 0.81494 | -0.39459 | 72 | 0.01357 | -6.65201 | 130 | 0.51374 | 0.49067 |
| 15 | 0.79879 | -0.4349 | 73 | 0.01094 | -7.09192 | 131 | 0.5309 | 0.48338 |
| 16 | 0.78261 | -0.47371 | 74 | 0.00867 | -7.5511 | 132 | 0.54805 | 0.47625 |
| 17 | 0.76643 | -0.51387 | 75 | 0.0067 | -8.02989 | 133 | 0.56518 | 0.46957 |
| 18 | 0.75022 | -0.55217 | 76 | 0.00501 | -8.51278 | 134 | 0.58229 | 0.4629 |
| 19 | 0.73401 | -0.59161 | 77 | 0.00359 | -8.9813 | 135 | 0.59939 | 0.45666 |
| 20 | 0.71778 | -0.63025 | 78 | 0.00241 | -9.393 | 136 | 0.61647 | 0.45041 |
| 21 | 0.70155 | -0.66878 | 79 | 0.00147 | -9.71364 | 137 | 0.63354 | 0.44379 |
| 22 | 0.6853 | -0.70869 | 80 | 0.00077 | -9.86022 | 138 | 0.6506 | 0.43836 |
| 23 | 0.66905 | -0.74763 | 81 | 0.00029 | -9.78257 | 139 | 0.66765 | 0.43198 |
| 24 | 0.6528 | -0.78711 | 82 | 4.00E-05 | -9.43467 | 140 | 0.68469 | 0.42625 |
| 25 | 0.63654 | -0.82812 | 83 | 1.00E-05 | -8.84493 | 141 | 0.70172 | 0.4203 |
| 26 | 0.62028 | -0.86856 | 84 | 0.00021 | -8.02513 | 142 | 0.71875 | 0.41453 |
| 27 | 0.60402 | -0.91021 | 85 | 0.00065 | -6.89497 | 143 | 0.73577 | 0.40824 |
| 28 | 0.58776 | -0.95222 | 86 | 0.00138 | -5.57228 | 144 | 0.7528 | 0.40251 |
| 29 | 0.57151 | -0.99574 | 87 | 0.00239 | -4.20831 | 145 | 0.76981 | 0.3969 |
| 30 | 0.55525 | -1.03959 | 88 | 0.00369 | -2.96696 | 146 | 0.78683 | 0.39073 |
| 31 | 0.53901 | -1.0851 | 89 | 0.00528 | -1.92606 | 147 | 0.80385 | 0.38522 |
| 32 | 0.52278 | -1.13161 | 90 | 0.00713 | -1.10633 | 148 | 0.82087 | 0.37913 |
| 33 | 0.50655 | -1.1799 | 91 | 0.00926 | -0.48436 | 149 | 0.83789 | 0.37312 |
| 34 | 0.49035 | -1.2295 | 92 | 0.01168 | -0.02146 | 150 | 0.85491 | 0.36782 |
| 35 | 0.47416 | -1.28134 | 93 | 0.0144 | 0.31558 | 151 | 0.87191 | 0.36164 |
| 36 | 0.45799 | -1.33546 | 94 | 0.01746 | 0.55958 | 152 | 0.88889 | 0.35648 |
| 37 | 0.44186 | -1.39286 | 95 | 0.02091 | 0.73266 | 153 | 0.90581 | 0.35192 |
| 38 | 0.42579 | -1.45384 | 96 | 0.0248 | 0.85229 | 154 | 0.92257 | 0.34694 |
| 39 | 0.4098 | -1.52011 | 97 | 0.02922 | 0.93165 | 155 | 0.93901 | 0.34419 |
| 40 | 0.39397 | -1.60269 | 98 | 0.03427 | 0.97999 | 156 | 0.95482 | 0.34265 |
| 41 | 0.37833 | -1.67606 | 99 | 0.04008 | 1.00433 | 157 | 0.96952 | 0.34527 |
| 42 | 0.36279 | -1.74353 | 100 | 0.0468 | 1.01004 | 158 | 0.98258 | 0.35338 |
| 43 | 0.34732 | -1.80966 | 101 | 0.0546 | 1.00122 | 159 | 0.99368 | 0.37664 |
| 44 | 0.33191 | -1.87558 | 102 | 0.06364 | 0.98145 | 160 | 1 | 0.47021 |
| 45 | 0.31655 | -1.94143 | 103 | 0.07401 | 0.954 | | | |
| 46 | 0.30126 | -2.00744 | 104 | 0.0857 | 0.92199 | | | |
| 47 | 0.28603 | -2.07467 | 105 | 0.09862 | 0.88818 | | | |
| 48 | 0.27087 | -2.14227 | 106 | 0.11256 | 0.8547 | | | |
| 49 | 0.25578 | -2.21154 | 107 | 0.1273 | 0.82286 | | | |
| 50 | 0.24079 | -2.28295 | 108 | 0.14264 | 0.79354 | | | |
| 51 | 0.22589 | -2.35643 | 109 | 0.15843 | 0.76675 | | | |
| 52 | 0.2111 | -2.43255 | 110 | 0.17455 | 0.74258 | | | |
| 53 | 0.19644 | -2.51232 | 111 | 0.19092 | 0.72083 | | | |
| 54 | 0.18193 | -2.59624 | 112 | 0.20751 | 0.70104 | | | |
| 55 | 0.16758 | -2.68571 | 113 | 0.22425 | 0.68323 | | | |
| 56 | 0.15344 | -2.78153 | 114 | 0.24114 | 0.66697 | | | |
| 57 | 0.13953 | -2.88555 | 115 | 0.25813 | 0.65202 | | | |
| 58 | 0.12593 | -2.99938 | 116 | 0.27519 | 0.63819 | | | |

# Appendix D : One Support Position Optimization

## D.1 One Support Position without Considering Aerodynamic Load

```
function optimizationone

clc;clear;close;
l=0.6; % l is the length of the morphing part;
m=601;
x=linspace(0,l,m);% define the vector x;
x1=x;
A(m,m)=0;
B(m,m)=0;
y=-0.2693*x.^5+0.808*x.^4-0.9696*x.^3+0.5818*x.^2;
% y is the target morphing shape of the skin;
EI=23.333;
% I=bh^3/12=0.5*0.002^3/12; b is the span of the skin,h is thickness of the skin;
% E is the elastic modulus of the aluminum; E=7e+010N_m2;
M=3*y./(x.^3);  % M is P/EI at location x;
for i=1:m
for j=1:m
   if i>=j
      A(i,j)=1/2*M(i).*x(i).*x1(j).^2-1/6*M(i).*x1(j).^3;
   else
      A(i,j)=1/3*M(i).*x(i).^3+0.5*M(i).*x(i).^2.*(x1(j)-x(i));
   end
end
end
% A is the matrix,which row i is the y coordinate of the morphing shape at position x(i);
for i=1:m
B(i,:)=A(i,:)-y;
end
% B=A-y calculate the difference between target shape and morphing shape;
S=std(B,1,2);   % standard deviation of the B;
[~,p]=min(S);
% p is sequence number of the support position x which have minimum standard deviation
of curve difference;
P=3*y(p)/x(p)^3*EI;  % calculate the load on the location x(p);

fprintf('The optimize position x=%8.6fm\n',x(p));   % print the value of x(p);
fprintf('The force at x position is F=%8.6fN\n',P);
[MaxDeflection,q]=max(A(p,:)-y); % print the maxdeflection of the skin
fprintf('The maximum difference position is %8.6f\nm',x(q));
fprintf('The maximum difference between achieved deflected shape and target shape
is %8.6f\nm',MaxDifference);
figure(1)
plot(x,y,x,A(p,:));% plot the target shape and achieved morphing shape;
xlabel('x');ylabel('target shape and achieved morphing shape');
figure(2)
plot(x,A(p,:)-y); % plot the differences between target shape and achieved morphing shape;
xlabel('x');ylabel('Difference between target shape and achieved morphing shape');
```

## D.2 : One Support Position Optimization Considering Aerodynamic Load

```
% one support position with aerodynamic load
function optimization1
clc; clear; close;
l=0.6;  % l is the length of the morphing part;
EI=23.333;
% I=bh^3/12=0.5*0.002^3/12; b is the span of the skin; h is thickness of the skin;
% E is the elastic modulus of the aluminum; E=7e+010N_m2;
m=input('Input m here:');  % the number of position of the beam;
x=linspace(0,l,m); % define the vector x;
x1=x;
A(m,m)=0;
B(m,m)=0;
w0=4927.3;  % Define the tapered distributed aerodynamic loads, unit N/m;
y=-0.2693*x.^5+0.808*x.^4-0.9696*x.^3+0.5818*x.^2;
% define the equation of the beam;
y1=w0/EI/l*(l^3*x1.^2/12-x1.^5/120-l^2*x1.^3/12+l*x1.^4/24);
% y1 define the deformation of aerodynamic load apply on the skin;
M=3*(y-y1)./(x1.^3);  % M define P/EI at position x1;
Torque=M.*EI.*y; % calculate the torque at the root of the beam;
Bendingmoment=M.*EI.*x; % calculate the bending moment at the root of the beam;
for i=1:m
for j=1:m
   if i>=j
      A(i,j)=0.5*M(i)*x(i)*x1(j).^2-1/6*M(i)*x1(j).^3+y1(j);
   else
      A(i,j)=1/3*M(i)*x(i)^3+0.5*M(i)*x(i)^2.*(x1(j)-x(i))+y1(j);
   end
end
end
% A is the matrix,which row i is the y coordinate of the morphing shape at position x(i);
for i=1:m
B(i,:)=A(i,:)-y;
end
% B=A-y calculate the differences of target shape with morphing shape;
S=std(B,1,2);
% Standard deviation of the B;
[~,p]=min(S);  % p is sequence number of the x, with smallest S;
Position=l/(m-1)*(p-1)  % P is the optimized position of x;
fprintf('The optimal position is %8.6fm;\n',Position);
fprintf('The torque at the root of the beam %8.6fN*m;\n',Torque(p));
fprintf('The bending moment at the root of the beam is %8.6fN*m;\n',Bendingmoment(p));
[Maxdeflection,q]=max(A(p,:)-y); % q is sequence number of the maxdeflection position;
fprintf('Maxdeflection is %8.6fm\n',Maxdeflection);
Max_Def_position=l/(m-1)*(q-1) % Max_position is the position with maximum difference.
fprintf('The maximum different position %8.6fm;\n',Max_Def_position);
figure(1)
plot(x,y,x,A(p,:));% plot the target shape and achieved morphing shape;
xlabel('x');ylabel('Target shape and achieved morphing shape');
figure(2)
plot(x,A(p,:)-y);% plot the differences between target shape and achieved morphing shape;

xlabel('x');ylabel('Differences between target shape and achieved morphing shape');
```

# Appendix E Direct Search Method

## E.1 : Three Support Positions Optimization

```
% with aerodynamic load
function optimization3
clc; clear; close;
m=input('Input m here:');
l=0.6;
x=linspace(0,l,m);
N=combntns(2:m,3);
k=nchoosek(m-1,3);
% I=bh^3/12=0.5*0.002^3/12; b is the spanwise of the skin, h is thickness;
% E=7e+010N_m2
EI=23.333;
w0=5000;
A(k,m)=0;
B(k,m)=0;
T(k,1)=0;
y=-0.2693*x.^5+0.808*x.^4-0.9696*x.^3+0.5818*x.^2;
y1=w0/EI/l*(l^3*x.^2/12-x.^5/120-l^2*x.^3/12+l*x.^4/24);
for i=1:k
Y=[6*(y(N(i,1))-y1(N(i,1)));6*(y(N(i,2))-y1(N(i,2)));6*(y(N(i,3))-y1(N(i,3)))];
X=[2*x(N(i,1))^3,3*x(N(i,2))*x(N(i,1))^2-x(N(i,1))^3,3*x(N(i,3))*x(N(i,1))^2-
x(N(i,1)).^3;
3*x(N(i,1))^2.*x(N(i,2))-x(N(i,1)).^3,2*x(N(i,2)).^3,3*x(N(i,2)).^2*x(N(i,3))-
x(N(i,2)).^3;
3*x(N(i,1))^2*x(N(i,3))-x(N(i,1)).^3,3*x(N(i,2)).^2*x(N(i,3))-
x(N(i,2)).^3,2*x(N(i,3)).^3];
    M=X\Y;
    T(i)=(M(1)*y(N(i,1))+M(2)*y(N(i,2))+M(3)*y(N(i,3)))*EI;
    for j=1:m
    if j<=N(i,1)
A(i,j)=0.5*(M(1)*x(N(i,1))+M(2)*x(N(i,2))+M(3)*x(N(i,3)))*x(j)^2-
1/6*(M(1)+M(2)+M(3))*x(j)^3+y1(j);
    elseif j<=N(i,2)
A(i,j)=1/3*M(1)*x(N(i,1))^3+0.5*M(1)*x(N(i,1))^2*(x(j)-
x(N(i,1)))+0.5*(M(2)*x(N(i,2))+M(3)*x(N(i,3)))*x(j).^2-
1/6*(M(2)+M(3))*x(j).^3+y1(j);
    elseif j<=N(i,3)
A(i,j)=1/3*M(1)*x(N(i,1))^3+0.5*M(1)*x(N(i,1))^2*(x(j)-
x(N(i,1)))+1/3*M(2)*x(N(i,2))^3+0.5*M(2)*x(N(i,2))^2*(x(j)-
x(N(i,2)))+0.5*M(3)*x(N(i,3))*x(j)^2-1/6*M(3)*x(j)^3+y1(j);
    else
A(i,j)=1/3*M(1)*x(N(i,1))^3+0.5*M(1)*x(N(i,1))^2*(x(j)-
x(N(i,1)))+1/3*M(2)*x(N(i,2))^3+0.5*M(2)*x(N(i,2))^2*(x(j)-
x(N(i,2)))+1/3*M(3)*x(N(i,3))^3+0.5*M(3)*x(N(i,3))^2*(x(j)-x(N(i,3)))+y1(j);
    end
    end
end
```

```
for i=1:k
B(i,:)=A(i,:)-y;
end
S=std(B,1,2);  % calculate the standard deviation
[~,p]=min(S);
T(p)
P=0.001+(l-0.001)/(m-1)*(N(p,:)-1)
[u,q]=max(A(p,:)-y)
Q=0.001+(l-0.001)/(m-1)*(q-1)
figure(1)
plot(x,A(p,:),x,y);xlabel('x');ylabel('y');
figure(2)
plot(x,A(p,:)-y);xlabel('x');ylabel('difference between target shape and
achieved morphing shape;');
```

## E.2 Four Support Positions Optimization

```
% with aerodynamic load
function optimization4
clc; clear; close;
m=input('Input m here:');
l=0.6;
x=linspace(0.01,l,m);
N=combntns(2:m,4);
k=nchoosek(m-1,4);
% I=bh^3/12=0.5*0.002^3/12; b is the spanwise of the skin, h is thickness;
% E=7e+010N_m2
EI=23.333;
w0=5000;
A(k,m)=0;
B(k,m)=0;
y=-0.2693*x.^5+0.808*x.^4-0.9696*x.^3+0.5818*x.^2;
y1=w0/EI/l*(l^3*x.^2/12-x.^5/120-l^2*x.^3/12+l*x.^4/24);
T(k,1)=0;
BendingMoment(k,1)=0;
for i=1:k
Y=[6*(y(N(i,1))-y1(N(i,1)));6*(y(N(i,2))-y1(N(i,2)));6*(y(N(i,3))-
y1(N(i,3)));6*(y(N(i,4))-y1(N(i,4)))];
X=[2*x(N(i,1))^3,3*x(N(i,2))*x(N(i,1))^2-x(N(i,1))^3,3*x(N(i,3))*x(N(i,1))^2-
x(N(i,1)).^3,3*x(N(i,4))*x(N(i,1))^2-x(N(i,1))^3;
3*x(N(i,1))^2.*x(N(i,2))-x(N(i,1)).^3,2*x(N(i,2)).^3,3*x(N(i,2)).^2*x(N(i,3))-
x(N(i,2)).^3,3*x(N(i,4))*x(N(i,2))^2-x(N(i,2))^3;
3*x(N(i,1))^2*x(N(i,3))-x(N(i,1)).^3,3*x(N(i,2)).^2*x(N(i,3))-
x(N(i,2)).^3,2*x(N(i,3)).^3,3*x(N(i,4))*x(N(i,3))^2-x(N(i,3))^3;
3*x(N(i,1))^2*x(N(i,4))-x(N(i,1))^3,3*x(N(i,2))^2*x(N(i,4))-
x(N(i,2))^3,3*x(N(i,3))^2*x(N(i,4))-x(N(i,3))^3,2*x(N(i,4))^3];
    M=X\Y;
    T(i)=(M(1)*y(N(i,1))+M(2)*y(N(i,2))+M(3)*y(N(i,3))+M(4)*y(N(i,4)))*EI;
BendingMoment(i)=(M(1)*x(N(i,1))+M(2)*x(N(i,2))+M(3)*x(N(i,3))+M(4)*x(N(i,4)))
*EI-0.0838*EI;
    for j=1:m
    if j<=N(i,1)
A(i,j)=0.5*(M(1)*x(N(i,1))+M(2)*x(N(i,2))+M(3)*x(N(i,3))+M(4)*x(N(i,4)))*x(j)^
2-1/6*(M(1)+M(2)+M(3)+M(4))*x(j)^3+y1(j);
    elseif j<=N(i,2)
A(i,j)=1/3*M(1)*x(N(i,1))^3+0.5*M(1)*x(N(i,1))^2*(x(j)-
x(N(i,1)))+0.5*(M(2)*x(N(i,2))+M(3)*x(N(i,3))+M(4)*x(N(i,4)))*x(j)^2-
1/6*(M(2)+M(3)+M(4))*x(j).^3+y1(j);
    elseif j<=N(i,3)
A(i,j)=1/3*M(1)*x(N(i,1))^3+0.5*M(1)*x(N(i,1))^2*(x(j)-
x(N(i,1)))+1/3*M(2)*x(N(i,2))^3+0.5*M(2)*x(N(i,2))^2*(x(j)-
x(N(i,2)))+0.5*(M(3)*x(N(i,3))+M(4)*x(N(i,4)))*x(j)^2-
1/6*(M(3)+M(4))*x(j)^3+y1(j);
    elseif j<=N(i,4)
A(i,j)=1/3*M(1)*x(N(i,1))^3+0.5*M(1)*x(N(i,1))^2*(x(j)-
x(N(i,1)))+1/3*M(2)*x(N(i,2))^3+0.5*M(2)*x(N(i,2))^2*(x(j)-
```

```
x(N(i,2)))+1/3*M(3)*x(N(i,3))^3+0.5*M(3)*x(N(i,3))^2*(x(j)-
x(N(i,3)))+0.5*M(4)*x(N(i,4))*x(j)^2-1/6*M(4)*x(j)^3+y1(j);
    else
A(i,j)=1/3*M(1)*x(N(i,1))^3+0.5*M(1)*x(N(i,1))^2*(x(j)-
x(N(i,1)))+1/3*M(2)*x(N(i,2))^3+0.5*M(2)*x(N(i,2))^2*(x(j)-
x(N(i,2)))+1/3*M(3)*x(N(i,3))^3+0.5*M(3)*x(N(i,3))^2*(x(j)-
x(N(i,3)))+1/3*M(4)*x(N(i,4))^3+0.5*M(4)*x(N(i,4))^2*(x(j)-x(N(i,4)))+y1(j);
    end
    end
end
% calculate the standard deviation
for i=1:k
B(i,:)=A(i,:)-y;
end
S=std(B,1,2);
[~,p]=min(S);
T(p)
P=0.01+(l-0.01)/(m-1)*(N(p,:)-1)
[Maxdeflection,q]=max(A(p,:)-y)
Q=0.01+(l-0.01)/(m-1)*(q-1)
%[n1,p1]=min(BendingMoment)
%N(p1,:)
figure(1)
plot(x,y,x,A(p,:));xlabel('x');ylabel('y');
figure(2)
plot(x,A(p,:)-y);xlabel('x');ylabel('Differences between target shape and
achieved morphing shape;');
```

## E.3 Five Support Positions Optimization

```
% with aerodynamic load
function optimization5
clc;clear;close;
m=input('Input m here:');
l=0.6;
x=linspace(0.01,l,m);
N=combntns(2:m,5);
k=nchoosek(m-1,5);
% I=bh^3/12=0.5*0.002^3/12; b is the spanwise of the skin, h is thickness;
% E=7e+010N_m2
EI=23.333;
w0=5000;
A(k,m)=0;
B(k,m)=0;
T(k,1)=0;
y=-0.2693*x.^5+0.808*x.^4-0.9696*x.^3+0.5818*x.^2;
y1=w0/EI/l*(l^3*x.^2/12-x.^5/120-l^2*x.^3/12+l*x.^4/24);
for i=1:k
Y=[6*(y(N(i,1))-y1(N(i,1)));6*(y(N(i,2))-y1(N(i,2)));6*(y(N(i,3))-
y1(N(i,3)));6*(y(N(i,4))-y1(N(i,4)));6*(y(N(i,5))-y1(N(i,5)))];
X=[2*x(N(i,1))^3,3*x(N(i,2))*x(N(i,1))^2-x(N(i,1))^3,3*x(N(i,3))*x(N(i,1))^2-
x(N(i,1))^3,3*x(N(i,4))*x(N(i,1))^2-x(N(i,1))^3,3*x(N(i,5))*x(N(i,1))^2-
x(N(i,1))^3;
3*x(N(i,1))^2*x(N(i,2))-x(N(i,1))^3,2*x(N(i,2))^3,3*x(N(i,2))^2*x(N(i,3))-
x(N(i,2))^3,3*x(N(i,4))*x(N(i,2))^2-x(N(i,2))^3,3*x(N(i,5))*x(N(i,2))^2-
x(N(i,2))^3;
3*x(N(i,1))^2*x(N(i,3))-x(N(i,1))^3,3*x(N(i,2))^2*x(N(i,3))-
x(N(i,2)).^3,2*x(N(i,3))^3,3*x(N(i,4))*x(N(i,3))^2-
x(N(i,3))^3,3*x(N(i,5))*x(N(i,3))^2-x(N(i,3))^3;
3*x(N(i,1))^2*x(N(i,4))-x(N(i,1))^3,3*x(N(i,2))^2*x(N(i,4))-
x(N(i,2))^3,3*x(N(i,3))^2*x(N(i,4))-
x(N(i,3))^3,2*x(N(i,4))^3,3*x(N(i,5))*x(N(i,4))^2-x(N(i,4))^3;
3*x(N(i,1))^2*x(N(i,5))-x(N(i,1))^3,3*x(N(i,2))^2*x(N(i,5))-
x(N(i,2))^3,3*x(N(i,3))^2*x(N(i,5))-x(N(i,3))^3,3*x(N(i,4))^2*x(N(i,5))-
x(N(i,4))^3,2*x(N(i,5))^3];
    M=X\Y;
T(i)=(M(1)*y(N(i,1))+M(2)*y(N(i,2))+M(3)*y(N(i,3))+M(4)*y(N(i,4))+M(5)*y(N(i,5
)))*EI;
    for j=1:m
    if j<=N(i,1)

A(i,j)=0.5*(M(1)*x(N(i,1))+M(2)*x(N(i,2))+M(3)*x(N(i,3))+M(4)*x(N(i,4))+M(5)*x
(N(i,5)))*x(j)^2-1/6*(M(1)+M(2)+M(3)+M(4)+M(5))*x(j)^3+y1(j);
    elseif j<=N(i,2)
```

```
A(i,j)=1/3*M(1)*x(N(i,1))^3+0.5*M(1)*x(N(i,1))^2*(x(j)-
x(N(i,1)))+0.5*(M(2)*x(N(i,2))+M(3)*x(N(i,3))+M(4)*x(N(i,4))+M(5)*x(N(i,5)))*x
(j)^2-1/6*(M(2)+M(3)+M(4)+M(5))*x(j)^3+y1(j);
    elseif j<=N(i,3)
A(i,j)=1/3*M(1)*x(N(i,1))^3+0.5*M(1)*x(N(i,1))^2*(x(j)-
x(N(i,1)))+1/3*M(2)*x(N(i,2))^3+0.5*M(2)*x(N(i,2))^2*(x(j)-
x(N(i,2)))+0.5*(M(3)*x(N(i,3))+M(4)*x(N(i,4))+M(5)*x(N(i,5)))*x(j)^2-
1/6*(M(3)+M(4)+M(5))*x(j)^3+y1(j);
    elseif j<=N(i,4)
A(i,j)=1/3*M(1)*x(N(i,1))^3+0.5*M(1)*x(N(i,1))^2*(x(j)-
x(N(i,1)))+1/3*M(2)*x(N(i,2))^3+0.5*M(2)*x(N(i,2))^2*(x(j)-
x(N(i,2)))+1/3*M(3)*x(N(i,3))^3+0.5*M(3)*x(N(i,3))^2*(x(j)-
x(N(i,3)))+0.5*(M(4)*x(N(i,4))+M(5)*x(N(i,5)))*x(j)^2-
1/6*(M(4)+M(5))*x(j)^3+y1(j);
    elseif j<=N(i,5)
A(i,j)=1/3*M(1)*x(N(i,1))^3+0.5*M(1)*x(N(i,1))^2*(x(j)-
x(N(i,1)))+1/3*M(2)*x(N(i,2))^3+0.5*M(2)*x(N(i,2))^2*(x(j)-
x(N(i,2)))+1/3*M(3)*x(N(i,3))^3+0.5*M(3)*x(N(i,3))^2*(x(j)-
x(N(i,3)))+1/3*M(4)*x(N(i,4))^3+0.5*M(4)*x(N(i,4))^2*(x(j)-
x(N(i,4)))+0.5*M(5)*x(N(i,5))*x(j)^2-1/6*M(5)*x(j)^3+y1(j);
    else
A(i,j)=1/3*M(1)*x(N(i,1))^3+0.5*M(1)*x(N(i,1))^2*(x(j)-
x(N(i,1)))+1/3*M(2)*x(N(i,2))^3+0.5*M(2)*x(N(i,2))^2*(x(j)-
x(N(i,2)))+1/3*M(3)*x(N(i,3))^3+0.5*M(3)*x(N(i,3))^2*(x(j)-
x(N(i,3)))+1/3*M(4)*x(N(i,4))^3+0.5*M(4)*x(N(i,4))^2*(x(j)-
x(N(i,4)))+1/3*M(5)*x(N(i,5))^3+0.5*M(5)*x(N(i,5))^2*(x(j)-x(N(i,5)));
    end
    end
end
% calculate the standard deviation
for i=1:k
B(i,:)=A(i,:)-y;
end
S=std(B,1,2);
[~,p]=min(S);
T(p)
P=0.01+(l-0.01)/(m-1)*(N(p,:)-1)
[Maxdeflection,q]=max(A(p,:)-y)
Q=0.01+(l-0.01)/(m-1)*(q-1)
figure(1)
plot(x,y,x,A(p,:));xlabel('x');ylabel('y');
figure(2)
plot(x,A(p,:)-y);xlabel('x');ylabel('difference between target shape and
achieved morphing shape');
```

# Appendix F MATLAB Function m File for One, Three, Four and Five Loads with Aerodynamic Loads used in ‘Optimization Tool’.

## F.1 One Load with Aerodynamic Loads

```
function f=myopt1(p)
m=101;
l=0.6;
x=linspace(0,l,m);
EI=23.333;
% I=bh^3/12=0.5*0.002^3/12; b is the span of the skin, h is thickness of the skin;
% E is the elastic modulus of the aluminum; E=7e+010N_m2;
w0=4927.3; % w0 is the tapered distributed aerodynamic load;
y=-0.2693*x.^5+0.808*x.^4-0.9696*x.^3+0.5818*x.^2;
% y is the target shape of the morphing flap;
y1=w0/EI/l*(l^3*x.^2/12-x.^5/120-l^2*x.^3/12+l*x.^4/24);
% y1 is the morphing shape under aerodynamic load without support;
P=-0.2693*p.^5+0.808*p.^4-0.9696*p.^3+0.5818*p.^2;
% P is the target deflection at position p;
P1=w0/EI/l*(l^3*p.^2/12-p.^5/120-l^2*p.^3/12+l*p.^4/24);
% P1 is the morphing shape under aerodynamic load without support at position p;
   M=3*(P-P1)/(p^3);
   f1=(1/2*M*p.*x.^2-1/6*M.*x.^3).*(0<x & x<=p)+...
     (1/3*M*p^3+0.5*M.*p.^2.*(x-p)).*(p<x & x<=l)+y1;
% f1 is the achieved deflected shape;
f=std(f1-y,1,2);
% f is the standard deviation of the difference between achieved shape and target shape;
figure(1)
plot(x,f1,x,y);
% plot the target shape and difference along x direction;
xlabel('x');ylabel('Target shape and achieved morphing shape');
figure(2)
plot(x,f1-y)
xlabel('x');ylabel('Differences between target shape and achieved morphing shape');
[maxdeflection,q]=max(f1-y)
```

## F.2 Three Loads with Aerodynamic Loads

```
function f=myopt3(p) %define the function name ‘myopt3’,and output f
m=101; % define the number of the vector x
l=0.6; % define the length of the morphing part
x=linspace(0,l,m);
EI=23.333;
% I=bh^3/12=0.5*0.002^3/12; b is the spanwise of the skin, h is thickness;
% E is the Young’s module, and E=7e+010N_m2
w0=4927.3;% w0 is the tapered distributed aerodynamic load at the middle of the chord, unit N/m;
y=-0.2693*x.^5+0.808*x.^4-0.9696*x.^3+0.5818*x.^2;
% y define the target shape;
y1=w0/EI/l*(l^3*x.^2/12-x.^5/120-l^2*x.^3/12+l*x.^4/24);
% y1 define the skin deflection under aerodynamic load;
P=-0.2693*p.^5+0.808*p.^4-0.9696*p.^3+0.5818*p.^2;
% P calculate the desired deflection at position p
P1=w0/EI/l*(l^3*p.^2/12-p.^5/120-l^2*p.^3/12+l*p.^4/24);
% P1 calculate the deflection under aerodynamic load;
```

```
     Y=[6*(P(1)-P1(1));6*(P(2)-P1(2));6*(P(3)-P1(3))];
     X=[2*p(1)^3,3*p(2)*p(1)^2-p(1)^3,3*p(3)*p(1)^2-p(1).^3;
        3*p(1)^2.*p(2)-p(1).^3,2*p(2).^3,3*p(2).^2*p(3)-p(2).^3;
        3*p(1)^2*p(3)-p(1).^3,3*p(2).^2*p(3)-p(2).^3,2*p(3).^3];
    M=X\Y;
% M calculated the P/EI at different position
f1=(0.5*(M(1)*p(1)+M(2)*p(2)+M(3)*p(3))*x.^2-1/6*(M(1)+M(2)+M(3))*x.^3).*(0<x &
x<p(1))+...
 (1/3*M(1)*p(1).^3+0.5*M(1)*p(1).^2*(x-p(1))+0.5*(M(2)*p(2)+M(3)*p(3))*x.^2-
1/6*(M(2)+M(3))*x.^3).*(p(1)<x & x<p(2))+...
     (1/3*M(1)*p(1)^3+0.5*M(1)*p(1)^2*(x-p(1))+1/3*M(2)*p(2)^3+0.5*M(2)*p(2)^2*(x-
p(2))+0.5*M(3)*p(3)*x.^2-1/6*M(3)*x.^3).*(p(2)<x & x<p(3))+...
     (1/3*M(1)*p(1)^3+0.5*M(1)*p(1)^2*(x-p(1))+1/3*M(2)*p(2)^3+0.5*M(2)*p(2)^2*(x-
p(2))+1/3*M(3)*p(3)^3+0.5*M(3)*p(3)^2*(x-p(3))).*(p(3)<x & x<=l)+y1;
% f1 define the achieved deflected shape
  f=std(f1-y,1,2);

% f defines the difference between the achieved deflected shape and desired
target shape, and calculates the standard deviation.
```

## F.3 Four Loads with Aerodynamic Loads

```
function f=myopt4(p)
l=0.6;
x=0:0.001:l;
EI=23.333;
w0=5000;
y=-0.2693*x.^5+0.808*x.^4-0.9696*x.^3+0.5818*x.^2;
y1=w0/EI/l*(l^3*x.^2/12-x.^5/120-l^2*x.^3/12+l*x.^4/24);
P=-0.2693*p.^5+0.808*p.^4-0.9696*p.^3+0.5818*p.^2;
P1=w0/EI/l*(l^3*p.^2/12-p.^5/120-l^2*p.^3/12+l*p.^4/24);
Y=[6*(P(1)-P1(1));6*(P(2)-P1(2));6*(P(3)-P1(3));6*(P(4)-P1(4))];
X=[2*p(1)^3,3*p(2)*p(1)^2-p(1)^3,3*p(3)*p(1)^2-p(1)^3,3*p(4)*p(1)^2-p(1)^3;
3*p(1)^2*p(2)-p(1)^3,2*p(2)^3,3*p(2)^2*p(3)-p(2)^3,3*p(4)*p(2)^2-p(2)^3;
3*p(1)^2*p(3)-p(1)^3,3*p(2)^2*p(3)-p(2)^3,2*p(3)^3,3*p(4)*p(3)^2-p(3)^3;
3*p(1)^2*p(4)-p(1)^3,3*p(2)^2*p(4)-p(2)^3,3*p(3)^2*p(4)-p(3)^3,2*p(4)^3];
    M=X\Y;
f1=(0.5*(M(1)*p(1)+M(2)*p(2)+M(3)*p(3)+M(4)*p(4))*x.^2-
1/6*(M(1)+M(2)+M(3)+M(4))*x.^3).*(0<x & x<=p(1))+...
(1/3*M(1)*p(1).^3+0.5*M(1)*p(1).^2*(x-
p(1))+0.5*(M(2)*p(2)+M(3)*p(3)+M(4)*p(4))*x.^2-
1/6*(M(2)+M(3)+M(4))*x.^3).*(p(1)<x & x<=p(2))+...
(1/3*M(1)*p(1)^3+0.5*M(1)*p(1)^2*(x-p(1))+1/3*M(2)*p(2)^3+0.5*M(2)*p(2)^2*(x-
p(2))+0.5*(M(3)*p(3)+M(4)*p(4))*x.^2-1/6*(M(3)+M(4))*x.^3).*(p(2)<x &
x<=p(3))+...
(1/3*M(1)*p(1)^3+0.5*M(1)*p(1)^2*(x-p(1))+1/3*M(2)*p(2)^3+0.5*M(2)*p(2)^2*(x-
p(2))+1/3*M(3)*p(3)^3+0.5*M(3)*p(3)^2*(x-p(3))+0.5*M(4)*p(4)*x.^2-
1/6*M(4)*x.^3).*(p(3)<x & x<=p(4))+...
(1/3*M(1)*p(1)^3+0.5*M(1)*p(1)^2*(x-p(1))+1/3*M(2)*p(2)^3+0.5*M(2)*p(2)^2*(x-
p(2))+1/3*M(3)*p(3)^3+0.5*M(3)*p(3)^2*(x-
p(3))+1/3*M(4)*p(4)^3+0.5*M(4)*p(4)^2*(x-p(4))).*(p(4)<x & x<=l)+y1;
  f=std(f1-y,1,2);
```

## F.4 Five Loads with Aerodynamic Loads

```
function f=myopt5(p)
l=0.6; % l is the length of the beam;
x=0:0.001:0.6; % x is the position on the beam;
EI=23.333;
% EI is the bending rigidity of the skin;
% I=bh^3/12=0.5*0.002^3/12; b is the spanwise of the skin, h is thickness;
% E=7e+010N_m2
w0=5000;% w0 is the tapered distributed load of the aerodynamic;
y=-0.2693*x.^5+0.808*x.^4-0.9696*x.^3+0.5818*x.^2;
% y is the equation of target shape of the morphing flap;
y1=w0/EI/l*(l^3*x.^2/12-x.^5/120-l^2*x.^3/12+l*x.^4/24);
% y1 is the deformation of the skin under tapered distributed aerodynamic load;
P=-0.2693*p.^5+0.808*p.^4-0.9696*p.^3+0.5818*p.^2;
P1=w0/EI/l*(l^3*p.^2/12-p.^5/120-l^2*p.^3/12+l*p.^4/24);
```

```
Y=[6*(P(1)-P1(1));6*(P(2)-P1(2));6*(P(3)-P1(3));6*(P(4)-P1(4));6*(P(5)-P1(5))];
X=[2*p(1)^3,3*p(2)*p(1)^2-p(1)^3,3*p(3)*p(1)^2-p(1)^3,3*p(4)*p(1)^2-
p(1)^3,3*p(5)*p(1)^2-p(1)^3;
3*p(1)^2*p(2)-p(1)^3,2*p(2)^3,3*p(2)^2*p(3)-p(2)^3,3*p(4)*p(2)^2-
p(2)^3,3*p(5)*p(2)^2-p(2)^3;
3*p(1)^2*p(3)-p(1)^3,3*p(2)^2*p(3)-p(2)^3,2*p(3)^3,3*p(4)*p(3)^2-
p(3)^3,3*p(5)*p(3)^2-p(3)^3;
3*p(1)^2*p(4)-p(1)^3,3*p(2)^2*p(4)-p(2)^3,3*p(3)^2*p(4)-
p(3)^3,2*p(4)^3,3*p(5)*p(4)^2-p(4)^3;
3*p(1)^2*p(5)-p(1)^3,3*p(2)^2*p(5)-p(2)^3,3*p(3)^2*p(5)-p(3)^3,3*p(4)^2*p(5)-
p(4)^3,2*p(5)^3];
    M=X\Y;
% M is P/6EI at location p;
f1=(0.5*(M(1)*p(1)+M(2)*p(2)+M(3)*p(3)+M(4)*p(4)+M(5)*p(5))*x.^2-
1/6*(M(1)+M(2)+M(3)+M(4)+M(5))*x.^3).*(0<x & x<=p(1))+...
(1/3*M(1)*p(1)^3+0.5*M(1)*p(1)^2*(x-
p(1))+0.5*(M(2)*p(2)+M(3)*p(3)+M(4)*p(4)+M(5)*p(5))*x.^2-
1/6*(M(2)+M(3)+M(4)+M(5))*x.^3).*(p(1)<x & x<=p(2))+...
(1/3*M(1)*p(1)^3+0.5*M(1)*p(1)^2*(x-p(1))+1/3*M(2)*p(2)^3+0.5*M(2)*p(2)^2*(x-
p(2))+0.5*(M(3)*p(3)+M(4)*p(4)+M(5)*p(5))*x.^2-
1/6*(M(3)+M(4)+M(5))*x.^3).*(p(2)<x & x<=p(3))+...
(1/3*M(1)*p(1)^3+0.5*M(1)*p(1)^2*(x-p(1))+1/3*M(2)*p(2)^3+0.5*M(2)*p(2)^2*(x-
p(2))+1/3*M(3)*p(3)^3+0.5*M(3)*p(3)^2*(x-p(3))+0.5*(M(4)*p(4)+M(5)*p(5))*x.^2-
1/6*(M(4)+M(5))*x.^3).*(p(3)<x & x<=p(4))+...
(1/3*M(1)*p(1)^3+0.5*M(1)*p(1)^2*(x-p(1))+1/3*M(2)*p(2)^3+0.5*M(2)*p(2)^2*(x-
p(2))+1/3*M(3)*p(3)^3+0.5*M(3)*p(3)^2*(x-
p(3))+1/3*M(4)*p(4)^3+0.5*M(4)*p(4)^2*(x-p(4))+0.5*M(5)*p(5)*x.^2-
1/6*M(5)*x.^3).*(p(4)<x & x<=p(5))+...
(1/3*M(1)*p(1)^3+0.5*M(1)*p(1)^2*(x-p(1))+1/3*M(2)*p(2)^3+0.5*M(2)*p(2)^2*(x-
p(2))+1/3*M(3)*p(3)^3+0.5*M(3)*p(3)^2*(x-
p(3))+1/3*M(4)*p(4)^3+0.5*M(4)*p(4)^2*(x-
p(4))+1/3*M(5)*p(5)^3+0.5*M(5)*p(5)^2*(x-p(5))).*(p(5)<x & x<=l)+y1;
% f1 is achieved deflected shape of the skin with 5 support positions.
figure(1)
plot(x,f1,x,y);xlabel('x');ylabel('y');
figure(2)
plot(x,f1-y);xlabel('x');ylabel('difference between target shape and achieved
morphing shape');
f=std(f1-y,1,2);

% calculate the standard deviation of the f1-y as an output of the function
```

# Appendix G : How to Import Points into CATIA

Firstly, Go to the address, where the CATIA is installed. For example, 'C:\Program Files (x86)\Dassault Systems\B20\intel_a\code\command', and find an excel file with the name of 'GSD_PointSplineLoftFromExcel'.

Secondly, get a backup of the file and save it. Now open the file. As you can see, there are several rows and columns of numbers that are grouped between 'StartCurve' and EndCurve'. Each row addressed one point. And each group of points that are located between a pair of 'StartCurve' and EndCurve' form a spline(one spline cross over the points of the group). Column A stand for x coordinate, Column B stands for y coordinate, Column C stands for z coordinate.

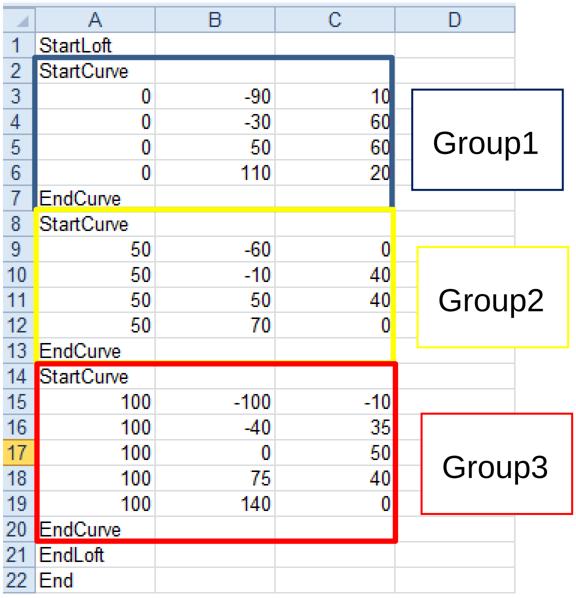

| | A | B | C | D |
|---|---|---|---|---|
| 1 | StartLoft | | | |
| 2 | StartCurve | | | |
| 3 | 0 | -90 | 10 | |
| 4 | 0 | -30 | 60 | |
| 5 | 0 | 50 | 60 | |
| 6 | 0 | 110 | 20 | |
| 7 | EndCurve | | | |
| 8 | StartCurve | | | |
| 9 | 50 | -60 | 0 | |
| 10 | 50 | -10 | 40 | |
| 11 | 50 | 50 | 40 | |
| 12 | 50 | 70 | 0 | |
| 13 | EndCurve | | | |
| 14 | StartCurve | | | |
| 15 | 100 | -100 | -10 | |
| 16 | 100 | -40 | 35 | |
| 17 | 100 | 0 | 50 | |
| 18 | 100 | 75 | 40 | |
| 19 | 100 | 140 | 0 | |
| 20 | EndCurve | | | |
| 21 | EndLoft | | | |
| 22 | End | | | |



Then delete the extra points coordinate and paste specified coordinate instead of them, Changed file is like below.

| | | |
|---|---|---|
| **StartLoft** | | |
| **StartCurve** | | |
| **1** | 0 | 0 |
| **0.99747721** | 0 | 0.00296703 |
| **…** | 0 | … |
| **0.99704469** | 0 | -0.00001975 |

| | | |
|---|---|---|
| **1** | 0 | 0 |
| **EndCurve** | | |
| **EndLoft** | | |
| **End** | | |

After changing the file, open CATIA and create a new part with your own wanted name. Now use alt+8 to run the macro in excel file.(Note that CATIA must be opened and a new part file must be created before this step.)

By running the macro, a window appears, choose 'feuil1.Main' and click on run button. Now another window appears, and there are 3 options, type'2' and click on ok, the points will be imported to CATIA and splines will be crossed over the points of each group.